GPCC AND GPCP PRECIPITATION PRODUCTS AND GRACE AND GRACE-FO TERRESTRIAL WATER STORAGE OBSERVATIONS FOR THE ASSESSMENT OF DROUGHT RECOVERY TIMES

A THESIS SUBMITTED TO
THE GRADUATE SCHOOL OF NATURAL AND APPLIED SCIENCES
OF
MIDDLE EAST TECHNICAL UNIVERSITY

BY

ÇAĞATAY ÇAKAN

IN PARTIAL FULFILLMENT OF THE REQUIREMENTS
FOR
THE DEGREE OF MASTER OF SCIENCE
IN
CIVIL ENGINEERING

OCTOBER 2024

Approval of the thesis:

GPCC AND GPCP PRECIPITATION PRODUCTS AND GRACE AND GRACE-FO TERRESTRIAL WATER STORAGE OBSERVATIONS FOR THE ASSESSMENT OF DROUGHT RECOVERY TIMES

submitted by **ÇAĞATAY ÇAKAN** in partial fulfillment of the requirements for the degree of **Master of Science** in **Civil Engineering, Middle East Technical University** by,

Prof. Dr. Naci Emre Altun
Dean, **Graduate School of Natural and Applied Sciences** ________________

Prof. Dr. Erdem Canbay
Head of the Department, **Civil Engineering** ________________

Prof. Dr. M. Tuğrul Yılmaz
Supervisor, **Civil Engineering, METU** ________________

Examining Committee Members:

Prof. Dr. İsmail Yücel
Civil Engineering, METU ________________

Prof. Dr. M. Tuğrul Yılmaz
Civil Engineering, METU ________________

Prof. Dr. Elçin Kentel Erdoğan
Civil Engineering, METU ________________

Assoc. Prof. Dr. Ali Ercan
Civil Engineering, METU ________________

Assoc Prof. Dr. Sertaç Oruç
Civil Engineering, Ankara Yıldırım Beyazıt Uni. ________________

Date: 23.10.2024

I hereby declare that all information in this document has been obtained and presented in accordance with academic rules and ethical conduct. I also declare that, as required by these rules and conduct, I have fully cited and referenced all material and results that are not original to this work.

Name Last name : Çağatay Çakan

Signature :

ABSTRACT

GPCC AND GPCP PRECIPITATION PRODUCTS AND GRACE AND GRACE-FO TERRESTRIAL WATER STORAGE OBSERVATIONS FOR THE ASSESSMENT OF DROUGHT RECOVERY TIMES

Çakan, Çağatay
Master of Science, Civil Engineering
Supervisor : Prof. Dr. M. Tuğrul Yılmaz

October 2024, 94 pages

Accurate precipitation observations are essential for understanding hydrological processes. Most precipitation products rely on station-based observations, necessitating additional independent data for validation. This study evaluates the accuracy of the Global Precipitation Climatology Center (GPCC) and Global Precipitation Climatology Project (GPCP) precipitation products by estimating hydrological drought recovery time (DRT) from terrestrial water storage anomalies (TWSA) and precipitation observations across five Köppen-Geiger climate zones. Precipitation datasets (GPCC Full Data Monthly Product v2022 and GPCP v3.2) and TWSA datasets (JPL mascon and G3P) from Gravity Recovery and Climate Experiment (GRACE) and GRACE Follow-On (GRACE-FO) satellite missions were used for DRT estimates. Two methods, storage deficit and required precipitation amount, were applied to calculate DRT. Results show GPCC and GPCP provide similar mean DRTs and consistencies. DRT estimations using G3P (12.1) is 2.8 months less than JPL mascon (14.9). Conversely, G3P exhibited 4.0% higher consistency than JPL mascon. The equatorial zone showed the lowest mean DRT and highest consistency, while the polar zone showed the highest mean DRT and lowest consistency. These findings offer the information required for precipitation and TWSA product accuracy by investigating hydrological drought, which aids in comprehending meteorological and hydrological processes.

Keywords: GPCC, GPCP, GRACE, GRACE-FO, Drought Recovery Time

ÖZ

KURAKLIKTAN KURTULMA SÜRESİ İÇİN GPCP VE GPCC YAĞIŞ ÜRÜNLERİ VE GRACE VE GRACE-FO KARASAL SU DEPOLAMA GÖZLEMLERİ

Çakan, Çağatay
Yüksek Lisans, İnşaat Mühendisliği
Tez Yöneticisi: Prof. Dr. M. Tuğrul Yılmaz

Ekim 2024, 94 sayfa

Hassas yağış gözlemleri, hidrolojik süreçlerin anlaşılması için gereklidir. Çoğu yağış ürünü, istasyon tabanlı gözlemlere dayanmakta olup, doğrulama için ek bağımsız verilere ihtiyaç duyar. Bu çalışma, beş farklı Köppen-Geiger iklim bölgesinde karasal su depolama anomalileri (TWSA) ve yağış gözlemlerinden hidrolojik kuraklık toparlanma süresi (DRT) tahmin ederek Global Precipitation Climatology Center (GPCC) ve Global Precipitation Climatology Project (GPCP) yağış ürünlerinin doğruluğunu değerlendirmektedir. DRT tahminleri için yağış veri setleri (GPCC Full Data Monthly Product v2022 ve GPCP v3.2) ile Gravity Recovery and Climate Experiment (GRACE) ve GRACE Follow-On (GRACE-FO) uydu görevlerinden elde edilen TWSA veri setleri (JPL mascon ve G3P) kullanılmıştır. İki yöntem, depolama açığı ve gereken yağış miktarı, DRT hesaplamaları için uygulanmıştır. Sonuçlar, GPCC ve GPCP ürünlerinin benzer ortalama DRT tahminleri ve tutarlılıklar sağladığını göstermektedir. G3P kullanılarak yapılan DRT tahminleri (12.1), JPL mascon ürününe (14.9) kıyasla 2.8 ay daha azdır. Buna karşılık, G3P, JPL mascon ürüne göre %4.0 daha yüksek bir tutarlılık sergilemiştir. Ekvatoral bölge en düşük ortalama DRT ve en yüksek tutarlılığı gösterirken, polar bölge en yüksek ortalama DRT ve en düşük tutarlılığı göstermiştir. Bu bulgular, meteorolojik ve hidrolojik süreçlerin anlaşılmasına katkı sağlayan hidrolojik kuraklık araştırmaları yoluyla yağış ve TWSA ürünlerinin doğruluğu için gerekli bilgileri sunmaktadır.

Anahtar Kelimeler: GPCC, GPCP, GRACE, GRACE-FO, Kuraklıktan Kurtulma Süresi

To my family,

ACKNOWLEDGMENTS

This thesis represents a milestone in my academic career. It would not have been possible without the support, guidance, and encouragement of many individuals and group members.

I would like to express my deepest gratitude to my supervisor, Prof. Dr. Mustafa Tuğrul Yılmaz, for his continuous guidance, support, patience, and immense knowledge. His guidance helped me throughout the research and writing of this thesis. Looking back, I am glad I chose this field, and I would like to thank him for that as well.

I would like to extend my special thanks to Dr. Elmas Sinem İnce van der Wal for her support on this project topic. Her guidance has been crucial in shaping my academic journey.

I would also like to thank my office mates Ali Cem Çatal, Ali Serkan Bayar, Ali Ulvi Galip Şenocak, Aysu Arık, Beril Aydın, Berkin Gümüş, Numan Burak Barkış, and Ruhi Deniz Yalçın for our informative and enjoyable conversations. Their support played a crucial role in helping me overcome various challenges.

I would like to express my heartfelt gratitude to my friends, Barış Öztaş, Ilgın Başara, Semin Atasoy, and Yiğit Yusuf Çolak (Numerical Guys), for their unwavering friendship. Although we are now in different places, I will always cherish our conversations at Mesire.

I would like to express my deepest gratitude to İrem Bayın for her unwavering support and encouragement throughout my life. Her help with every challenge I've faced has been invaluable.

Finally, and most importantly, I would like to thank my family for their unconditional love and support. I am grateful to my mother, Rukiye Çakan, for always encouraging me and wanting to help me pursue through challenging and lengthy tasks; to my father, Selahattin Çakan, who has endless faith in me for the things I want to achieve; and to my grandmother, Hayriş, for being a constant source of support on the other end of the phone whenever I faced difficulties.

TABLE OF CONTENTS

CHAPTERS

APPENDICES

LIST OF TABLES

TABLES

LIST OF FIGURES

FIGURES

LIST OF ABBREVIATIONS

ABBREVIATIONS

cdPA	Cumulative Detrended Precipitation Anomaly
CLIMAT	Monthly Climate Reports
CWC	Canopy Surface Water Storage
cP	Cumulative Precipitation
cPA	Cumulative Precipitation Anomaly
DLR	German Aerospace Center
DRT	Drought Recovery Time
dTWSA	Deviation of Storage
ERPA	Estimated Required Precipitation Amount
ESA	European Space Agency
ET	Evapotranspiration
G3P	Global Gravity-based Groundwater Project
GDAP	GEWEX Data and Assessment Panel (GDAP
GEWEX	Global Water and Energy Experiment
GFZ	German Research Center for Geosciences
GPCC	Global Precipitation Climatology Center
GPCC FDM	Global Precipitation Climatology Center Full Data Monthly Product
GPCP	Global Precipitation Climatology Project
GRACE	Gravity Recovery and Climate Experiment
GRACE-FO	Gravity Recovery and Climate Experiment Follow On
GTS	Global Telecommunication Systems
GW	Groundwater Storage
JPL	Jet Propulsion Laboratory
mascons	Mass Concentration blocks
NASA	National Aeronautics and Space Administration

P	Precipitation
R	Runoff
SE	Standard Error
SH	Spherical Harmonics
SM	Soil Moisture Content in the Soil Layers
SPEI	Standardized Precipitation Evapotranspiration Index
SPI	Standardized Precipitation Index
SRI	Standardized Runoff Index
SSI	Standardized Streamflow Index
SWE	Snow Depth Water Equivalent
SYNOP	Synoptic Weather Reports
TWS	Terrestrial Water Storage
TWSA	Terrestrial Water Storage Anomaly
WMO	World Meteorological Organization
WCRP	World Climate Research Program

LIST OF SYMBOLS

SYMBOLS

ρ	Correlation Coefficient
β_0	Intercept in Regression Coefficient
β_1	Slope in Regression Coefficient

CHAPTER 1

INTRODUCTION

A crucial component of the global water cycle is precipitation, which provides fresh water to inland regions and thus enables vegetation to flourish. Terrestrial ecosystems and climate zones are defined by the average amounts of precipitation and the corresponding temporal distribution of rainfall events (Bayar et al., 2023; Lai et al., 2018). However, an abnormally high or low amount of precipitation can have disastrous effects on the biosphere, agriculture, and human societies. The monitoring of extreme events such as droughts (Barker et al., 2016; Lai et al., 2019; Wu et al., 2023; Xu et al., 2015) and floods (Belabid et al., 2019; Harris et al., 2007; Maggioni & Massari, 2018), as well as short, medium and long-term precipitation forecasts (Akbari Asanjan et al., 2018; Senocak et al., 2023) are a central objective of hydrometeorological research.

The most common method for monitoring precipitation is using in-situ rain gauge data (Barker et al., 2016; Wehbe et al., 2017; Wei et al., 2019). Nonetheless, gauge station distribution is frequently uneven and sparse, especially in complicated terrain where stations might not be accessible (Wang et al., 2017). In contrast, significant progress has been made with satellite-based precipitation products obtained from remote sensing devices, which offer a viable alternative to ground-based precipitation observations with varying spatiotemporal resolutions (Bai et al., 2019; Prakash et al., 2015; Wang et al., 2017; Wu et al., 2023). The Global Precipitation Climatology Center (GPCC) and Global Precipitation Climatology Project (GPCP) are two commonly used precipitation products with global coverage (Adler et al., 2003; Sun et al., 2018a). GPCC provides in-situ station precipitation observations, while GPCP offers blended observations, combining in-situ station and satellite data.

GPCC and GPCP precipitation products have often been evaluated against a variety of atmospheric reanalysis data as well as with one another (e.g., Prakash et al., 2015). There has been good agreement between GPCC and GPCP at regional sizes, especially in the tropics GPCP (Negrón Juárez et al., 2009; Sun et al., 2018b). Furthermore, a comparison of the GPCC and GPCP revealed consistency in the spatial distribution of the climatology of annual and seasonal rainfall across West Africa (Lamptey, 2008). Despite the regional similarities found, there are also distinct differences. In comparison to station-based precipitation data in China, GPCC performed better than GPCP (Wang et al., 2017). Additionally, GPCC indicated greater spatiotemporal representativeness of precipitation patterns in Iran (Darand & Khandu, 2020) and exhibited better performance in the Sahel region based on statistical error metrics (Ali et al., 2005). These studies generally compared precipitation products with in-situ measurements to assess their quality. Nevertheless, as both datasets rely on observations from in-situ stations, evaluating precipitation products against in-situ stations becomes inappropriate. Additionally, precipitation products may use other datasets to enhance their results, which can introduce bias when validating these products against one another. Therefore, using other independent variables (without precipitation) could be more effective for evaluating precipitation products. Consequently, independent evaluations, separate from in-situ station observations, may be necessary for products that rely on ground-based data, such as GPCC and GPCP.

Drought monitoring is essential because drought is one of the most devastating natural disasters, characterized by a significant decline in a region's water resources over an extended period. The effects of the drought might be catastrophic for human health, agriculture, irrigation, water supplies, and ecosystems (AghaKouchak et al., 2015; Ding et al., 2020; Mishra & Singh, 2010; Patz et al., 2014; Piao et al., 2010). The frequency, severity, and recovery time of droughts are defined by using drought indices, such as the standardized precipitation index (SPI, Mckee et al., 1993)), the standardized precipitation evapotranspiration index (SPEI, Vicente-Serrano et al., 2010), the standardized runoff index (SRI, Shukla & Wood, 2008), and the standardized streamflow index (SSI, Vicente-Serrano et al., 2012). SPI utilizes solely precipitation data to define drought characteristics, whereas SPEI depends on precipitation and evapotranspiration data. SSI utilizes the runoff data from the land surface, whereas SRI depends on streamflow in river channels (Lai et al., 2019). Meteorological droughts are caused by inadequate precipitation, while hydrological droughts arise from insufficient water storage (Behrangi et al., 2015; Keyantash & Dracup, 2002; Thomas et al., 2014). Complex hydrological models use precipitation data to determine hydrological drought using SSI and SRI (Lai et al., 2018; Madadgar & Moradkhani, 2014). As an alternative, without the need for complex hydrological models, the water storage deficiency might shed light on hydrological drought (Thomas et al., 2014). It solely relies on measurements of water stored on or below the ground and is used to estimate drought recovery time (DRT). Even the amount of precipitation needed to fill any storage deficiency may be predicted by combining precipitation and terrestrial water storage (TWS) observations (Singh et al., 2021).

The satellite mission Gravity Recovery and Climate Experiment (GRACE), conducted by the National Aeronautics and Space Administration (NASA) and the German Aerospace Center (DLR) from 2002 until 2017, enabled measurements of TWS (Springer et al., 2017). In order to extend the data record further up to the present, NASA and the German Research Center for Geosciences (GFZ) have been operating GRACE Follow-On (GRACE-FO), the successor to GRACE, since 2018. The measurement of irregularities in the orbits of two identical twin satellites trailing each other at a distance of approximately 200 km in a polar orbit, initially 490 km in altitude, yields terrestrial water storage anomalies (TWSA), which comprise all subsurface and surface water balance components (Wahr et al., 2004). The comparison of data obtained at different times allows for the computation of temporal changes in the Earth's gravity field. Variations in TWS are reflected in the remaining signal on monthly-to-interannual scales after atmospheric, oceanic, and geophysical factors have been subtracted. Spherical harmonic (SH) or mass concentration (mascons) are two different solutions includes the ready-to-use TWS data from the GRACE and GRACE-FO missions are provided. Hydrological model validation (Döll et al., 2024) and the relationship between interannual fluctuations in TWS and large-scale climate modes (Pfeffer et al., 2023) have both been accomplished using GRACE-based TWS. Assimilation of GRACE data into land-surface algorithms was even attempted (Eicker et al., 2014; Tangdamrongsub et al., 2021). Thus, GRACE and GRACE-FO datasets are currently the most frequently used in global TWS.

An independent evaluation of precipitation products by drought monitoring could be performed using GRACE and GRACE-FO TWS products as an alternative to evaluations using hydrological models (Beck et al., 2017; Gebrechorkos et al., 2024). The precipitation product assessment was conducted by drought monitoring using indices like SPI and SPEI in previous studies (Golian et al., 2019; Wei et al., 2019, 2021). However, in order to fully comprehend the utility of precipitation products, more independent evaluation studies utilizing critical parameters, such as TWS, that include all components of the surface and subsurface water balance are still required. This is particularly important for monitoring hydrological droughts since the spatial variability across different climate zones and globally has yet to be thoroughly explored.

The Köppen-Geiger Climate Classification system is extensively used for regional climate zonation by various disciplines, such as climate research, physical geography, hydrology, agriculture, biology, and education (Bayar et al., 2023; Kottek et al., 2006). It utilizes the temperature and precipitation datasets to define the limits of the climatic zones (Kottek et al., 2006).

The goal of this study is to independently assess and compare the GPCC and GPCP precipitation products by utilizing the GRACE and GRACE-FO dataset (e.g., G3P, which is spherical harmonics, and JPL mascon, which is mascon solutions) in perspective of evaluating drought characteristic. The evaluation of precipitation products using TWS products as an independent variable has not yet been conducted. The current study evaluates the applicability of the GPCC and GPCP precipitation products for global hydrological applications. The evaluation covers different climate zones, as described by the Köppen-Geiger classification. The evaluation was conducted by estimating DRT based on TWSA and needed precipitation amount. The comparative analysis in this study allows for a basis for comprehending the connection between hydrological drought and global precipitation products through DRT estimates.

CHAPTER 2

DATASET AND METHODOLOGY

The flow chart of this thesis are shown in Figure 2.1. First, the dTWSA and cdPA parameters were calculated to estimate DRT values. The calculation of dTWSA is explained in Section 2.3, while the calculation of cdPA is explained in Section 2.4. Then, the DRT values is calculated based on storage deficit method, described in Section 2.6.1. Also, the DRT values is calculated based on required precipitation amount method, described in Section 2.6.2. Then, the consistency of the DRT estimation methods is calculated, described in Section 2.7.1. Finally, the DRT estimations and consistency in DRT estimations presented for Köppen-Geiger Climate Classification, described in Section 2.8. Additionally, the effect of the area of the pixel is investigated for parameters (dTWSA and cdPA) and DRT estimations, described in Section 2.9.

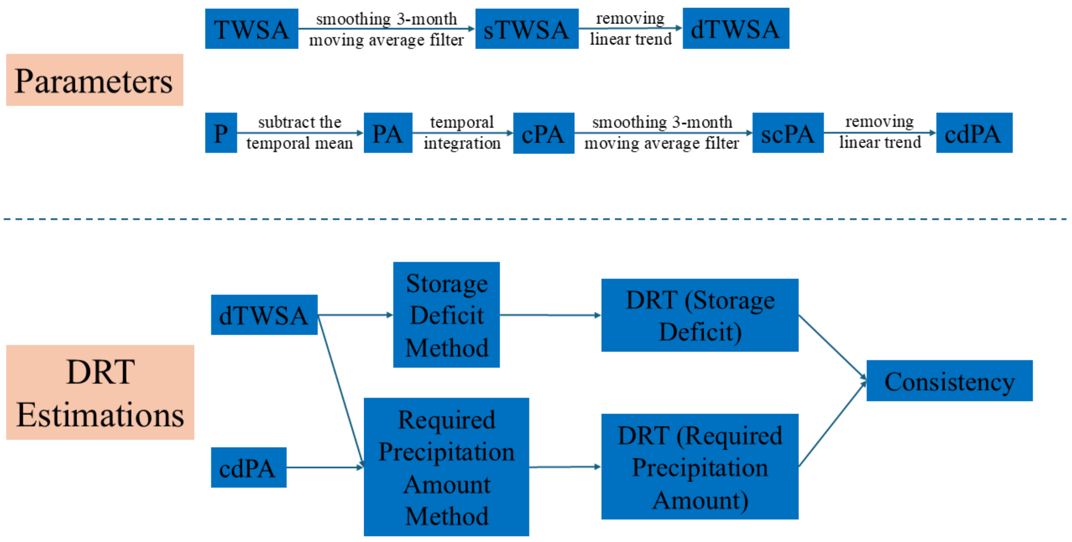

Figure 2.1. Flow chart of this thesis

2.1 Dataset

In this study, two distinct precipitation datasets (GPCC and GPCP) and two different TWS datasets (G3P and JPL mascon) were utilized. Detailed information regarding these datasets is provided in Table 2.1.

Table 2.1. Detailed information regarding the precipitation and TWS datasets

Type	Name	Spatial Resolution	Temporal Resolution	Spatial Coverage	Temporal Coverage
Precipitation	GPCC	0.5°	Monthly	90° N/S	1981-2020
Precipitation	GPCP	0.5°	Monthly	90° N/S	1979-present
TWS	G3P	0.5°	Monthly	90° N/S	2002-2020
TWS	JPL mascon	0.5°	Monthly	90° N/S	2002-present

2.1.1 GPCC and GPCP Precipitation

Although most precipitation products do not provide long-term global coverage for latitudes up to 90° N/S, GPCC and GPCP offer precipitation data for high latitudes. The GPCC was established by the World Meteorological Organization (WMO) in 1989 and combines monthly precipitation data over land from global telecommunication systems (GTS), synoptic weather reports (SYNOP), and monthly climate reports (CLIMAT). Various precipitation products with different spatiotemporal resolutions, including the Full Data Monthly Product (GPCC FDM), the Monitoring Product, and the First Guess Monthly Product, are provided by GPCC. Among these products, the GPCC FDM v2022 (Schneider et al., 2022) is suitable for water cycle studies (Schneider et al., 2014). For these reasons, it was utilized to investigate the relationship between precipitation and TWS for further analyses in this thesis. Monthly precipitation data with 0.5° spatial resolution is available from 1891 to 2020 for GPCC FDM product. It can be downloaded from the Deutscher Wetterdienst (German Meteorological Service) website (https://opendata.dwd.de/climate_environment/GPCC/html/fulldatamonthly_v2022_doi_download.html). The spatial distribution of the mean precipitation dataset obtained from GPCC was illustrated in Figure 2.2.

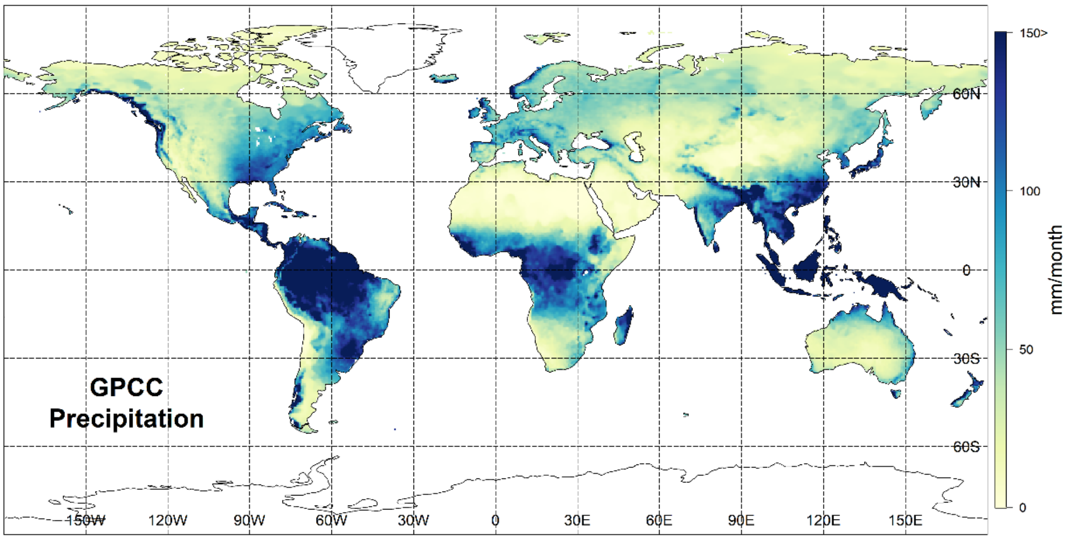

Figure 2.2. The spatial distribution of the temporal mean GPCC precipitation dataset from 2002 to 2020

The GPCP was managed by the World Climate Research Program (WCRP) under the Global Water and Energy Experiment (GEWEX) Data and Assessment Panel (GDAP) and blends gauge observation and satellite precipitation data to set up global precipitation estimates. The latest version of the GPCP precipitation product, GPCP v3.2 Satellite-Gauge (SG) Combined Data (Huffman et al., 2023), was used in this thesis. The GPCP v3.2 dataset provides monthly precipitation data with 0.5 spatial resolution from 1979 to the present. The spatial distribution of the mean precipitation dataset obtained from GPCC is illustrated in Figure 2.3. It is available from the Goddard Earth Sciences Data and Information Services Center (https://disc.gsfc.nasa.gov/datasets/GPCPMON_3.2/summary). Moreover, the time series of the mean precipitation dataset obtained from GPCC and GPCP are given in Figure 2.4.

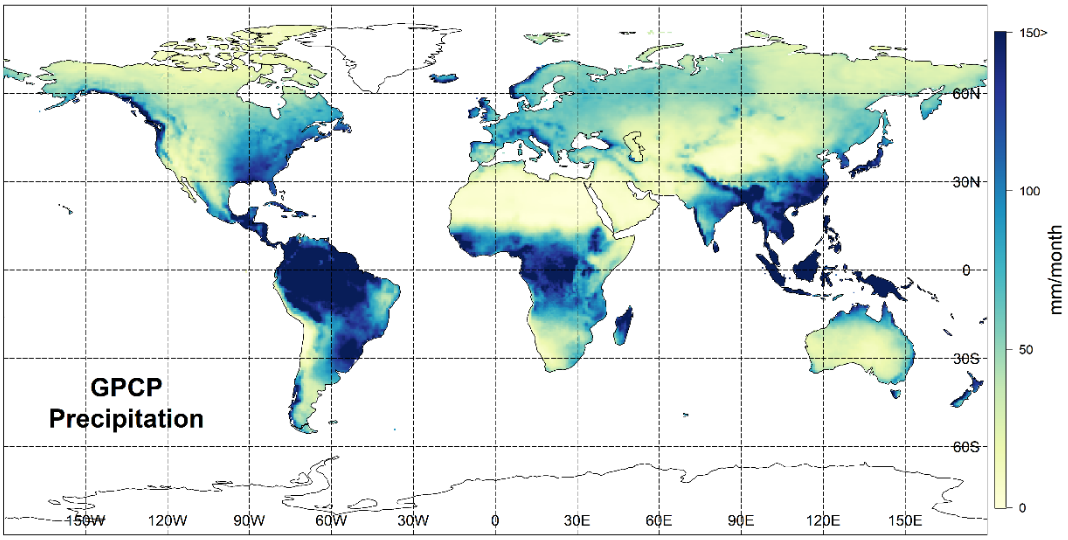

Figure 2.3. The spatial distribution of the temporal mean GPCP precipitation dataset from 2002 to 2020

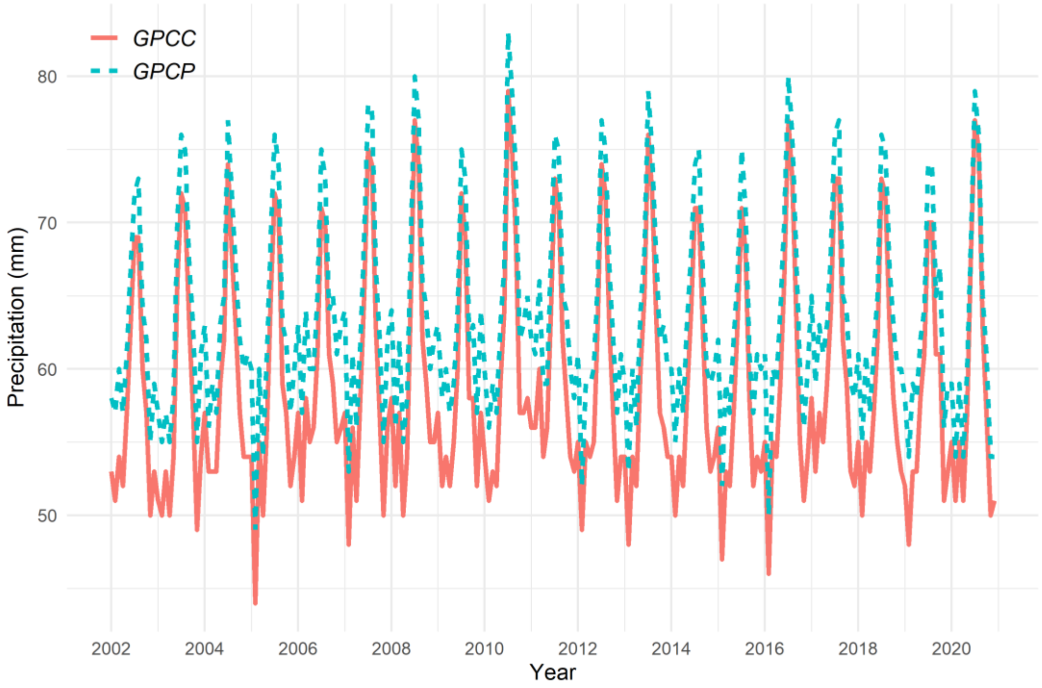

Figure 2.4. The time series of the global mean monthly precipitation dataset obtained from GPCC and GPCP

2.1.2 GRACE and GRACE TWS

GRACE and GRACE-FO measure the change in terrestrial water storage (TWS) by Earth's gravity field variations. The TWS data is available from GRACE and GRACE-FO spherical harmonics and mascon solutions. TWS anomalies are composed of the sum of the anomalies in snow, ice, surface water, soil moisture, and groundwater (Eq 2.1). In this study, the GRACE and GRACE-FO Level 3 products of G3P (spherical harmonics, Güntner et al., 2023) and JPL Release 6 (mascon, Watkins et al., 2015; Wiese et al., 2023) TWS products were utilized to estimate water storage deficit and examine the relationship between precipitation and TWS changes. The Level 3 products include all correction of the geophysical, smoothing and filtering the gravity field, and provide ready-to-use data as mass anomalies of water. Negative changes show mass losses, while positive changes show an increase in mass amount. Thus, it aids in our observation of the water flows and their temporal variations.

$$\Delta TWS = \Delta GW - \Delta SM - \Delta CWC - \Delta SWE \qquad (2.1)$$

where ΔTWS is the change in total water storage, ΔGW is the change in groundwater storage, ΔSM is the change in soil moisture content in soil layers, ΔSWE is the change in snow depth water equivalent, and ΔCWC is the change in canopy surface water storage.

The G3P dataset provides a monthly TWS dataset at a higher spatial resolution (0.5°) than the other spherical harmonic solutions (1.0°) from April 2002 to December 2020. The G3P TWS dataset (Güntner et al., 2023) is available from the GFZ Information System and Data Center (ftp://isdcftp.gfz-potsdam.de).

The monthly JPL mascon (from now on abbreviated as JPL) TWS dataset spans from April 2002 to the present at a spatial resolution of 0.5°, like G3P. The JPL TWS data (Watkins et al., 2015; Wiese et al., 2023) is acquired from the Virtual Directories of Earth Data CMR (https://cmr.earthdata.nasa.gov/virtual-directory/collections/C2536962485-POCLOUD/temporal/2002/04/16). The time series of the mean TWSA dataset obtained from G3P and JPL are demonstrated in Figure 2.5.

Because of the satellite battery issues, both G3P and JPL TWS datasets have missing monthly data, especially after 2011. The missing monthly data in the time series were filled with the average of previous and subsequent two months, an average of four months (Andrew et al., 2017; Long et al., 2015). Except for the missing data due to the satellite battery problems, a time gap between the GRACE and GRACE-FO missions is missing, spanning from July 2017 (the end of the GRACE mission) to May 2018 (the launch of the GRACE-FO mission). This time gap has been left missing.

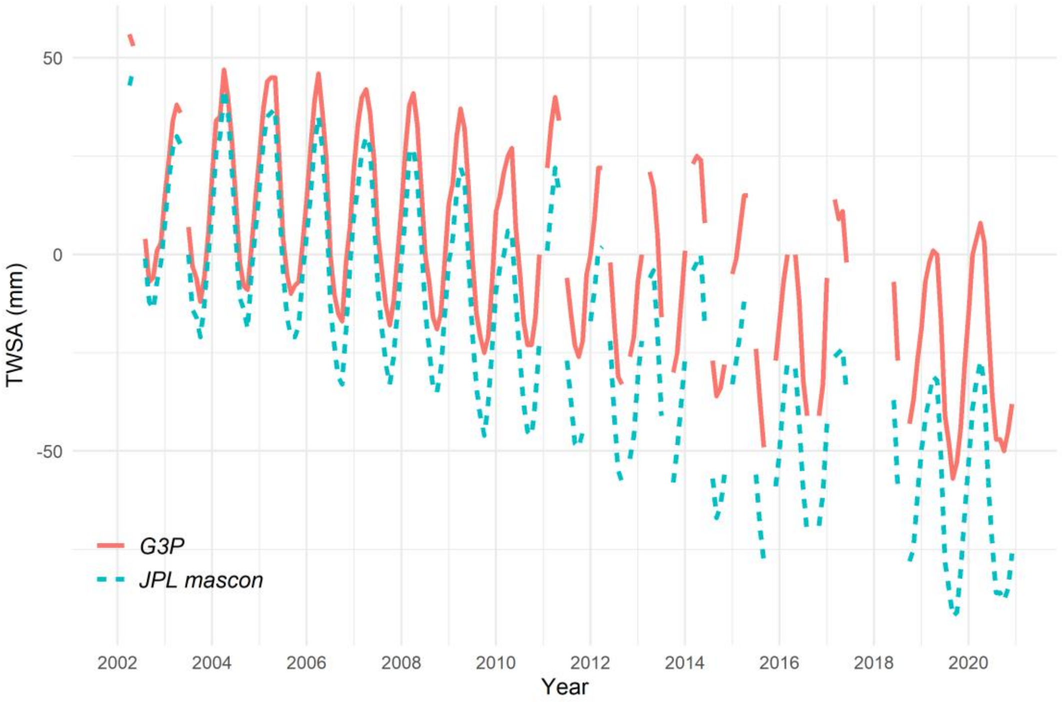

Figure 2.5. The time series of the global mean monthly TWSA dataset obtained from G3P and JPL

Both G3P and JPL have a baseline to calculate the anomalies. G3P TWS dataset represents anomalies relative to a long-term mean from April 2002 to December 2020. In contrast, the JPL TWS dataset utilizes a long-term mean from January 2004 to December 2009 as the baseline. The differences in TWSA time series, especially after 2010 (Figure 2.4), could arises from the baseline difference between TWSA products.

The baseline of the JPL TWSA should be matched with that of G3P TWSA to maintain consistency in the time series comparisons. (Humphrey et al., 2023; Monthly Mass Grids - Global Mascons (JPL RL06.1_v03) | Data Portal – GRACE Tellus, n.d.). Thus, the baseline of the JPL TWSA was changed from 2004-2009 to 2002-2020 in this study. First, the average for each grid point from April 2002 to December 2020 is calculated to align the baseline of the JPL TWSA (Eq. 2.2).

$$ref(TWSA)_{x,y} = \frac{1}{total\ month} \sum_{mb=1}^{total\ month} TWSA_{x,y,mb} \qquad (2.2)$$

where $ref(TWSA)_{x,y}$ is the reference value of TWSA, x and y refer to the horizontal and vertical grid locations over the study area, $TWSA_{x,y,mb}$ is the TWSA value, mb refers to the month since beginning of the analysis, and $total\ month$ is the total numbers of month in the analyses. Then, reference value is subtracted from each TWSA in the datasets to calculate the TWSA value according to the new baseline ($b(TWSA)$) as follows:

$$b(TWSA)_{x,y,mb} = TWSA_{x,y,mb} - ref(TWSA)_{x,y} \qquad (2.3)$$

2.2 Water Balance Equation

The water balance equation establishes a close relationship between TWS fluctuations and precipitation.

$$ds/dt = P - ET - R \qquad (2.4)$$

where ds/dt is the storage change over time, which is TWSA in this study, P is precipitation, ET is evapotranspiration, and R is streamflow, contains both surface and subsurface water. These values are expressed in millimeters of equivalent water height per month (mm/month).

Any change in storage over time (ds/dt) must be driven by water fluxes. These fluxes can be vertical, such as P or ET, occurring between the surface and the atmosphere. Alternatively, they can be horizontal, occurring at or below the Earth's surface, and are collectively referred to as R. Gravity missions directly observe TWSA relative to a long-term mean value. Thus, these observations can provide insights into water fluxes across various timescales.

In this thesis, the relationship between the combined ET + R fluxes and precipitation is assumed to be linear and stationary (Singh et al., 2021). Following this assumption, the possible variations in precipitation can be deduced by using the changes in TWSA. By comparing two storage measurements taken 30 days apart, the typical interval for GRACE solutions, quantitative information about the precipitation occurring during this time period can be derived.

2.3 Deviation of Storage (dTWSA)

Determining the timescales for drought recovery requires an understanding of the extent of water deficiencies. The variability in TWSA data can be used to infer these water deficiencies directly (Thomas et al., 2014). Long-term processes like groundwater extraction and/or glacier mass accumulation can affect variations in water storage. The TWSA data were detrended for each grid in order to reduce the influence of the long-term factors in this study. Eliminating the linear trend isolates the deviations from the long-term trend. These deviations are referred to as deviations of storage (dTWSA, Singh et al., 2021). The deviations represent the anomalies.

$$dTWSA_{x,y,mb} = TWSA_{x,y,mb} - trend(TWSA)_{x,y} \qquad (2.5)$$

where $dTWSA_{x,y,mb}$ is the deviation of storage, x and y refers to the horizontal and vertical grid locations over the study area, mb refers to the month since beginning of the analysis, $TWSA_{x,y,mb}$ is the TWSA value, and $trend(TWSA)_{x,y}$ is the linear trend of the TWSA, all given in mm equivalent water height per month (mm/month).

2.4 Cumulative Detrended Precipitation Anomaly (cdPA)

The precipitation anomalies (PA) were calculated by subtracting the temporal mean precipitation of the grid for the period between April 2002 and December 2020 (the reference period) from the precipitation.

$$PA_{x,y,mb} = P_{x,y,mb} - \overline{P_{x,y}} \tag{2.6}$$

where $PA_{x,y,mb}$is the precipitation anomaly value, *x* and *y* refer to the horizontal and vertical grid locations over the study area, *mb* refers to the month since beginning of the analysis, $P_{x,y,mb}$ is the precipitation value and $\overline{P_{x,y}}$ is the temporal mean precipitation value. To ensure compatibility between the precipitation data and TWSA, a temporal integration of the precipitation anomaly data is performed in this study, resulting in cumulative precipitation (cPA) data.

$$cPA_{x,y,mb} = PA_{x,ymb} + cPA_{x,y,mb-1} \tag{2.7}$$

where $cPA_{x,y,mb}$ is the cumulative precipitation anomaly value, *x* and *y* refer to the horizontal and vertical grid locations over the study area, *mb* refers to the month since beginning of the analysis. In this thesis, the cumulative precipitation anomalies (cPA) were smoothed using a 3-month moving average filter, applied with the filter function from the stats package in R, resulting in smoothed cumulative precipitation anomalies (scPA). (Singh et al., 2021). This procedure effectively reduced noise and short-term variations in the cPA. The scPA were then detrended to separate short-term fluctuations from long-term trends, resulting in the cumulative detrended precipitation anomalies (cdPA). This additional step reduced the long-term effects in precipitation patterns.

$$cdPA_{x,y,mb} = scPA_{x,y,mb} - trend(scPA)_{x,y} \tag{2.8}$$

where $cdPA_{x,y,mb}$ is the cumulative detrended precipitation anomaly value, *x* and *y* refer to the horizontal and vertical grid locations over the study area, *mb* refers to the month since beginning of the analysis, $scPA_{x,y,t}$ is the smoothed cumulative precipitation anomaly value $trend(scPA)_{x,y}$ is the trend of the smoothed cumulative precipitation anomaly, all given in mm equivalent water height per month (mm/month).

2.5 Relationship between cdPA and dTWSA

The amount of precipitation required to balance a water storage deficit can be estimated using the water balance equation, with the assumption of stationary and linear relationship between ET+R flux and precipitation. By establishing a direct connection between changes in TWSA and precipitation dynamics, this method provides an invaluable tool for comprehending water resources management. To estimate the amount of precipitation needed based on water deficiency, a linear relationship between cdPA and dTWSA was constructed as follows:

$$cdPA_{x,y,mb} = \beta_{0_{x,y}} + \beta_{1_{x,y}} * dTWSA_{x,y,mb} + \varepsilon \qquad (2.9)$$

where $\beta_{0_{x,y}}$ is the intercept, x and y refer to the horizontal and vertical grid locations over the study area, $\beta_{1_{x,y}}$ is the slope, and ε represents the residual errors of the fit. The cdPA and dTWSA are both in mm/month.

Given that cdPA and dTWSA are measured in the same units, a β_1 value of 1 indicates that cdPA is equal to dTWSA and variations in precipitation is same as the differences in storage. In contrast, a β1 value greater than 1 suggests that a portion of local precipitation is immediately lost through processes like evapotranspiration (ET) and runoff (R), without contributing to local storage. This implies that the decrease in precipitation amount can be attributed to other hydrological processes (e.g., ET and R) and is only partially reflected in the variability of storage data in these regions. Regions where β_1 is less than 1 imply that the storage deficit can be addressed with less precipitation than is actually required. In other words, there needs to be either further input from outside that coincides with local rain events, which would cause an underestimation of the amount of precipitation needed based only on storage fluctuations (Singh et al., 2021).

Based on the research conducted by Singh et al. (2021), we have computed the correlation coefficient ($\rho_{x,y}$) between cdPA and dTWSA and the maximum drought length for each pixel (globe, spatial resolution of 0.5°, 259200 pixels) using 19 years of monthly data (i.e., from 2002 to 2020), in addition to regression analyses (i.e., β_0 and β_1). In this case, a positive correlation between cdPA and dTWSA is anticipated, meaning that increases (decreases) in storage changes should result from positive (negative) precipitation anomalies. If storage change increases (decreases) in the presence of a negative (positive) precipitation anomaly, this indicates a weak or no linear relationship between cdPA and dTWSA. Correspondingly, in the study of Singh et al. (2021), regions with a weak or no linear association between the two variables (i.e., $\rho < 0$, $\beta_1 < 1$, and maximum drought period < 5 months) were removed from the global analyses since these regions were considered as being unsuitable for the further analysis. A considerable linear relationship may still exist in some pixels with β_1 values slightly less than 1, although sampling mistakes may result in fluctuations around 1, and random variability may also lead some pixels to exhibit marginal differences. Therefore, while Singh et al. (2021) masked out regions where β_1 was less than 1, this thesis applies a t-test for statistical significance to determine the threshold for β_1. The lm function in R was used to calculate p-value, which shows the significance threshold of $\beta 1$ values. Figure A1 illustrates the spatial distributions of the p-values of the β_1 for each TWS-precipitation product. The insignificant β_1 values (p-value>0.05) were excluded in this thesis along with regions with maximum drought length < 5 months. The masked-out criteria used to classify regions based on their suitability for further analysis are listed in Table 2.2.

Table 2.2. Masked-out Criteria used in the present study

Criteria Number	Criteria in this study	Singh et al. (2021)
1	-	$\rho < 0$
2	p-value of $\beta_1 > 0.05$	$\beta1 < 1$
3	maximum drought length < 5 months	maximum drought length < 5 months

2.6 DRT Estimations

TWSA datasets from G3P and JPL and precipitation datasets from GPCC and GPCC will be utilized in DRT estimations. We quantify DRT using two different estimation methods, closely adhering to the methodology provided by Singh et al. (2021), described in Section 2.10. Using solely on GRACE and GRACE-FO TWSA dataset, the first approach, relied on storage deficit, estimates DRT as the length of TWSA residuals from its climatology. The second approach uses the required precipitation amount, which is determined by combining the precipitation and TWSA datasets. According to this method, a drought is assumed to end when the absolute required precipitation amount (Section 2.6.2) exceeds the precipitation observations. Thus, the precipitation (GPCC and GPCP) and the TWSA (G3P and JPL) products and two DRT estimation methods (storage deficit and required precipitation amount) will be utilized in further analyses for various climate zones as defined by the Köppen-Geiger climate classification. The details of the DRT estimations are explained in Table 2.3. Precipitation products (GPCC and GPCP) are used in DRT-1, DRT-2, DRT-3, and DRT-4 for excluding regions, with exclusion criteria provided in Table 2.2.

Table 2.3. The details of the DRT estimations

Estimation No.	TWSA Product	Precipitation Product	Estimation Method
DRT-1	G3P	- / GPCP (excluding regions)	Storage Deficit
DRT-2	G3P	- / GPCC (excluding regions)	Storage Deficit
DRT-3	JPL	- / GPCP (excluding regions)	Storage Deficit
DRT-4	JPL	- / GPCC (excluding regions)	Storage Deficit
DRT-5	G3P	GPCP	Required Precipitation Amount
DRT-6	G3P	GPCC	Required Precipitation Amount
DRT-7	JPL	GPCP	Required Precipitation Amount
DRT-8	JPL	GPCC	Required Precipitation Amount

2.6.1 DRT Estimation based on Storage Deficit

Drought features can be better understood by examining how TWSA deviates from its climatology. A reference point by averaging the TWSA values for each month over the course of the time series is established in order to compute this deviation. For instance, a reference point for February would be calculated by the average of all February TWSA values in the dataset. The climatology for that particular month was reflected by this average monthly TWSA.

$$\overline{TWSA_{x,y,m}} = \frac{1}{total\ year} \sum_{yy=1}^{total\ year} TWSA_{x,y,m,yy} \qquad (2.10)$$

where $\overline{TWSA_{x,y,m}}$ is the mean TWSA value, *x* and *y* refer to the horizontal and vertical grid locations over the study area, *m* refers the month, $TWSA_{x,y,m,yy}$ is the

TWSA, yy refers to the year, and $total\ year$ is the total number of year of the datasets. Then, the corresponding monthly climatology value was subtracted from each TWSA data point to determine the deviation of each TWSA data point from the climatology, resulting in residuals.

$$dTWSA_{x,y,m,yy} = TWSA_{x,y,m,yy} - \overline{TWSA_{x,y,m}} \qquad (2.11)$$

where $dTWSA_{x,y,m,yy}$ is the deviation of the TWSA value x and y refer to the horizontal and vertical grid locations over the study area, m refers to the month, and yy refers to the year.

Deficits in water storage are indicated by negative residuals of TWSA from its climatology (Thomas et al., 2014). Long-term below-average water storage periods were identified as drought occurrences when persistent negative residuals persisted for more than three consecutive months (Singh et al., 2021). If these periods lasted less than three consecutive months, the negative residuals were not considered a drought (Singh et al., 2021). However, if a new phase of negative residuals began within a month after a prior drought recovery, it was regarded as a continuation of the same drought (Singh et al., 2021). This approach ensured a consistent record of drought events over time, allowing to create a comprehensive inventory of drought recovery periods for each grid point. DRT estimations were derived from the storage deficit method. This method examined the duration of negative residuals (indicating lower-than-usual storage values) of dTWSA at each grid and time, providing insights into the patterns and severity of drought occurrences over time (Detailed information about the differences in between this thesis and Singh et al. (2021) are given in Section 2.10).

2.6.2 DRT Estimation based on Required Precipitation Amount

Drought characteristics are also investigated by observing precipitation amount. The cdPA can be used to analyze each grid's drought characteristics. For this purpose, the second method, DRT estimation based on the required precipitation amount, is employed for this purpose. The linear relationship between dTWSA and cdPA (Eq. 2-9) yields the required precipitation amount to fill the storage deficit. The cdPA terms gives the required precipitation amount, while dTWSA is the storage deficiency. The climatology of precipitation was used to calculate the absolute required precipitation amount in this study. A reference point by averaging the precipitation values for each month throughout the time series is established in order to compute the absolute required precipitation amount from both precipitation products (GPCC and GPCP) using the time series from April 2002 to December 2020. For instance, a reference point for February was calculated by the average of all February precipitation values in the dataset. The climatology for that particular month was reflected by this average monthly precipitation.

$$\overline{P_{x,y,m}} = \frac{1}{total\ year} \sum_{yy=1}^{total\ year} P_{x,y,m,yy} \qquad (2.12)$$

where $\overline{P_{x,y,m}}$ is the mean P value, x and y refer to the horizontal and vertical grid locations over the study area, m refers to the month, $P_{x,y,m,yy}$ is the P value, yy refers to the year, and $total\ year$ is the total number of year in the datasets. Then, the corresponding monthly climatology value was added to the estimated required precipitation amount, obtained from the linear relationship between cdPA and dTWSA, to calculate the absolute required precipitation amount for each grid.

where $dTWSA_{x,y,m,yy}$ is the deviation of the TWSA value x and y refer to the horizontal and vertical grid locations over the study area, m refers to the month, and yy refers to the year.

$$ARPA_{x,y,m,yy} = ERPA_{x,y,m,yy} + \overline{P_{x,y,m}} \qquad (2.13)$$

where $ARPA_{x,y,m,yy}$ is the absolute required precipitation amount, x and y refer to the horizontal and vertical grid locations over the study area, m refers to the month, and yy refers to the year, and $ERPA_{x,y,m,yy}$ is the estimated required precipitation amount. The duration over which the observed precipitation amount surpassed the absolute required precipitation amount for any given time and location was analyzed to estimate DRT (Singh et al., 2021). This method allows for an extensive evaluation of DRT dynamics across various locations and periods.

2.7 Accuracy Analysis

2.7.1 Consistency in DRT Estimations

By analyzing the differences in the timing acquired from both approaches, the consistency (degree of agreement) between the two DRT estimations was measured. Here, the consistency was defined as the absolute time difference between the two DRT estimation methods, as illustrated in Table 2.4. For instance, the region was classified as consistent category 1 if the absolute time difference between the two approaches was within two months. In contrast, if the absolute time difference between the two methods was more than nine months, the region was classified as consistency category 4 (i.e., very poor consistency). The consistency between the two methods was measured by comparing the absolute differences between the DRT estimates for each TWS-precipitation product. With this investigation, the dependability and robustness of the DRT estimations are better understood. Essentially, it assisted us in determining the degree to which the two approaches converged on comparable DRT values for the same areas. In general, DRT estimation values cannot be directly validated via ground observations, these drought related characteristics are only estimated utilizing ancillary observations like precipitation and TWS. Accordingly, in the absence of direct validation, consistency between different and independent methodologies may imply the real skill of these methodologies in estimation of DRT.

Table 2.4. Consistency Categories in DRT Estimations

Consistency category	Time difference (months)
1 (very good consistency)	1-2
2 (good consistency)	3-4
3 (poor consistency)	5-8
4 (very poor consistency	9+

2.7.2 Calculated Statistics

The degree of uncertainty related to the means of the datasets were measured by using standard deviation (SD) and standard error (SE). A lower SE value, which is frequently attained with less fluctuation in the data, denotes a more accurate estimate of the mean DRT across each pixel (Lee et al., 2015). For every pixel and climate zone, respectively, the values of SD and SE were computed individually using the following formulas:

$$SD_{x,y} = \sqrt{\frac{1}{n_{x,y}} \sum_{i=1}^{n_{x,y}} (DRT_{x,y,i} - \mu_{x,y})^2} \qquad (2.14)$$

where $DRT_{x,y,i}$ is the i-th DRT value in the dataset, x and y refer to the horizontal and vertical grid locations over the study area, $\mu_{x,y}$ is the mean DRT, and $n_{x,y}$ is the number of the DRT values.

$$SE_{x,y} = \frac{SD_{x,y}}{\sqrt{n_{x,y}}} \qquad (2.15)$$

where $SD_{x,y}$ is the standard deviation of DRT, x and y refer to the horizontal and vertical grid locations over the study area, and $n_{x,y}$ is the number of the DRT values.

To evaluate the degree of uncertainty surrounding the mean values of the datasets, confidence intervals (CIs) are utilized in addition to SD and SE (Altman & Bland, 2005; Curran-Everett, 2008; Lee et al., 2015). With a certain degree of confidence (in this study, 95%) CIs offer a range of values that are likely to contain the true population mean as follows:

$$CI_{x,y} = \mu_{x,y} \mp Z * SE_{x,y} \qquad (2.16)$$

where $\mu_{x,y}$ is the mean DRT, x and y refer to the horizontal and vertical grid locations over the study area, and SE is the standard error of DRT. Here, a normal distribution assumption is made with the selection Z = 1.96. However, the sensitivity of the results for this assumption and alternative t-distribution scenario results are not investigated in this thesis study. Overall, this normal distribution assumption would underestimate the uncertainty of mean DRT.

2.8 Köppen-Geiger Climate Classification

In this study, the Köppen-Geiger Climate Classification dataset was prepared by Rubel et al. (2017) and covers the years 1986–2010 at a spatial resolution of 0.083°. There exist 5 main climate zones and 31 subtypes included in the Köppen-Geiger Climate Classification was prepared by Rubel et al. (2017). Figure 2.6 illustrates the 31 subtypes, while Figure 2.7 depicts the 5 main climate zones. In this study, the Köppen-Geiger climate classification dataset (spatial resolution of 0.083°) was regridded to be consistent with TWS and precipitation data used in this study (spatial resolution of 0.5°) by utilizing bilinear interpolation. This thesis concentrated on the five main Köppen-Geiger climate categories, which are equatorial, arid, warm temperate, snow, and polar, as depicted in Figure 2.7. The Köppen-Geiger Climate Classification dataset utilized in the present study is acquired from https://koeppen-geiger.vu-wien.ac.at/present.htm. The detailed information for the subzones of Köppen-Geiger climate classification is shown in Table 2.5.

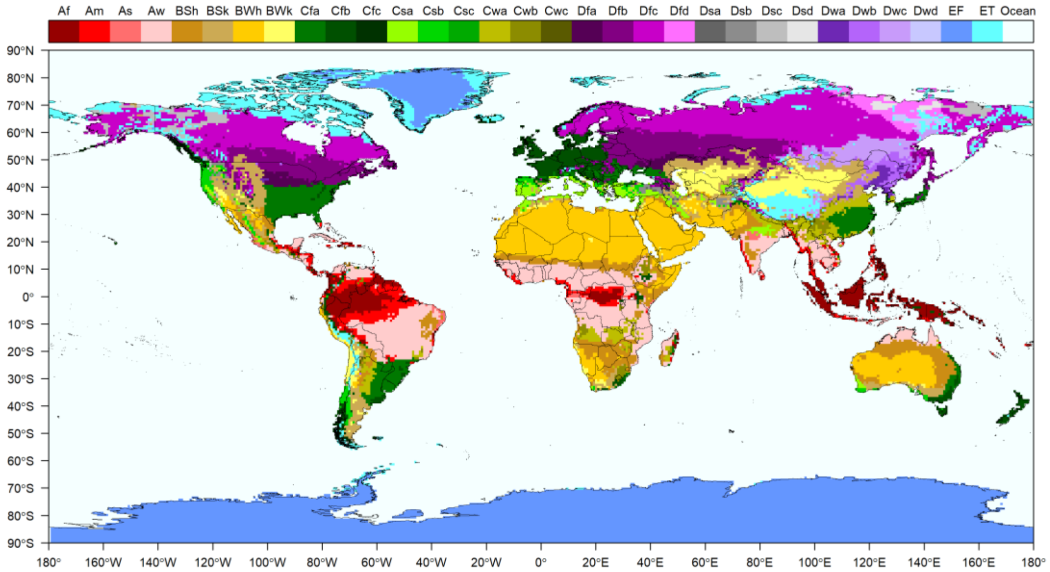

Figure 2.6. Köppen-Geiger Climate Classification (Rubel et al., 2017)

Table 2.5. Detailed Information for the Subzones of Köppen-Geiger Climate Classification (Rubel et al., 2017)

Main Climates	Precipitation	Temperature
A: equatorial	W: desert	h: hot arid
B: arid	S: steppe	k: cold arid
C: warm temperate	f: fully humid	a: hot summer
D: snow	s: summer dry	b: warm summer
E: polar	w: winter dry	c: cool summer
	m: moonsoonal	d: extremely continental
		F: polar frost
		T: polar tundrta

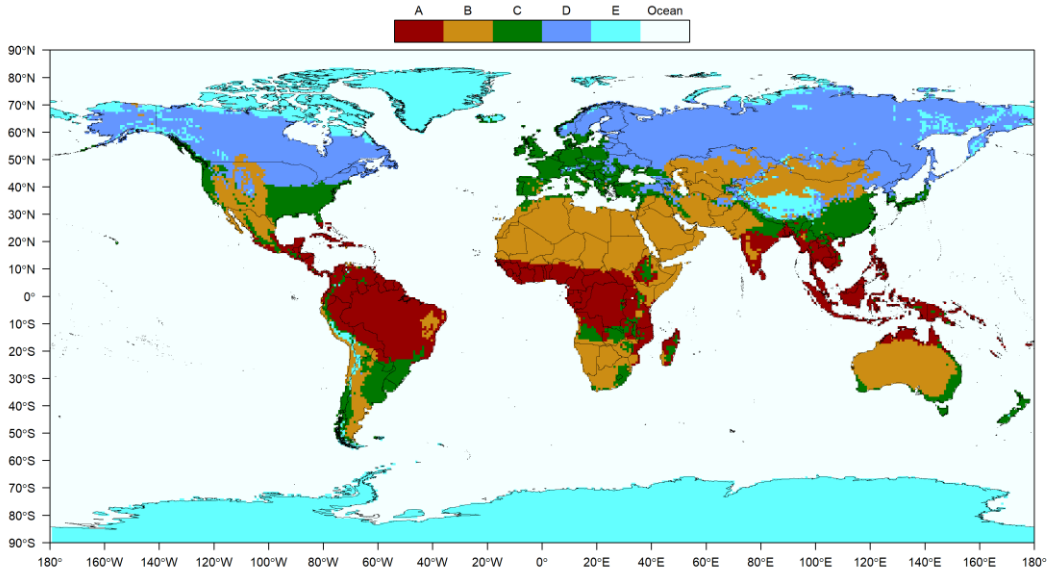

Figure 2.7. Köppen-Geiger Climate Classification (A, Equatorial; B, Arid; C, Warm temperate; D, Snow; and E, Polar Climate Zones) (Rubel et al., 2017)

2.9 Pixel Size Effect

This study utilized the gridded TWSA and precipitation datasets to estimate the mean DRT. The pixel sizes are constant across the datasets; however, the pixel sizes become smaller when moving from the equator to the poles. Area weights were calculated based on the area of the pixels and are shown in Figure 2.8. These area weights were used in the analysis to investigate whether the pixel size effect impacts the results. Here, the area weights are calculated by taking the ratio of the area of any pixel on the globe against the area of a pixel over equator. This implies the area weights would be near 1 around equator and near 0 around poles.

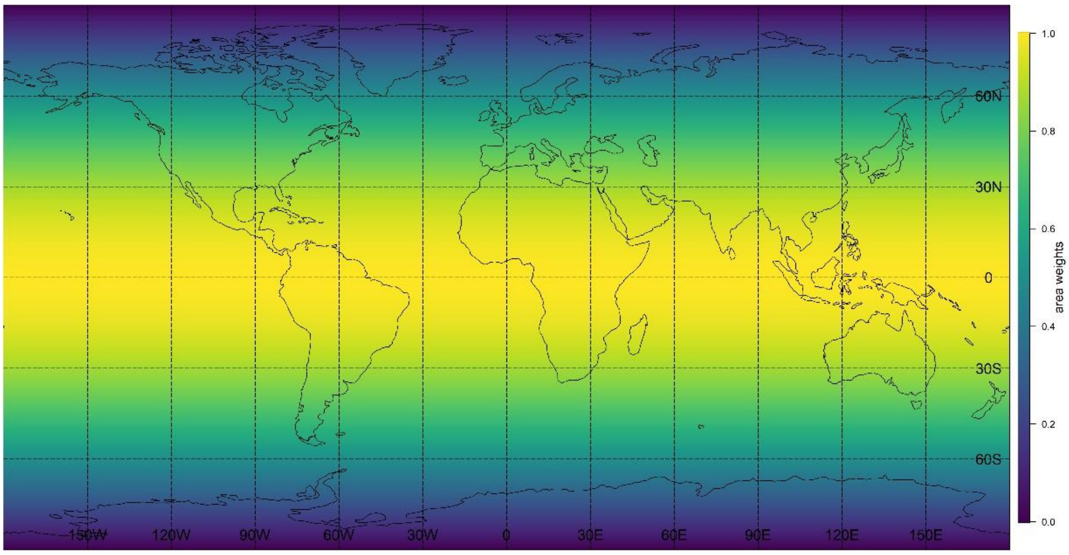

Figure 2.8. Area Weights of the Pixels

2.10 Difference from Previous Study

This study follows the methodology of Singh et al. (2021), but with some differences. Singh et al. (2021) used one TWSA dataset (JPL mascon) and one precipitation dataset (GPCP), while this study utilizes two TWSA datasets (G3P and JPL mascon) and two precipitation datasets (GPCC and GPCP). The spatial resolution of the JPL mascon, used by Singh et al. (2021), is 0.5°, which is the same resolution as the TWSA products used in this study. However, Singh et al. (2021) used the GPCP precipitation product with a spatial resolution of 2.5°, which was regridded using bilinear interpolation. In contrast, this study uses the updated GPCP precipitation product with a spatial resolution of 0.5°, and the GPCC product also has a spatial resolution of 0.5°. Thus, both datasets in this study have the same spatial resolution.

To calculate the cdPA in Singh et al. (2021), the precipitation anomaly was first obtained, then smoothed using a 3-month moving average, and the linear trend was removed. Finally, the detrended data was integrated over time to obtain the cdPA. Conversely, in this study, the precipitation data was first integrated over time to obtain cumulative precipitation data. The cumulative precipitation anomaly data was then derived, smoothed using a 3-month moving average, and the linear trend was removed to obtain the cdPA. The calculation procedure for this thesis was revised to first convert the units of the precipitation dataset into storage units. This change ensures consistency between precipitation and storage data, enabling a more similar process like GRACE.

Also, the exclusion criteria for β_1 in this study differ from those in the study of Singh et al. (2021). While Singh et al. (2021) excluded pixels if β_1 was less than 1, this study excludes pixels have insignificant β_1 values.

Singh et al. (2021) provided results for one global drought event in January 2016, whereas this study offers mean DRT estimations from different coupled products across five Köppen-Geiger climate zones and globally.

CHAPTER 3

RESULTS

3.1 Relationship between cdPA and dTWSA

Figure 3.1a shows the spatial distribution of correlation coefficients between dTWSA and cdPA for a selected data combination of dTWSA from G3P and cdPA from GPCP (hereafter referred to as G3P&GPCP). Since the G3P&GPCP coupled product has the highest global average correlation coefficient (0.31), the coupled product was chosen to display the actual values in the following figures. The correlation coefficients of the other coupled products are presented in Table 3.1. Additionally, the impact of pixel size was examined to understand how the correlation coefficient changes from the equator to the poles (Table 3.1). Our findings indicate that pixel sizes did not significantly affect the correlation coefficients, as the difference in the mean correlation coefficient whether or not the pixel size effect was considered, is 0.05. High correlations were observed over Australia (0.55), South America (0.46) and south Africa (ρ>0.47), regions with significant fluctuations in water storage (See Appendix B) and dense in situ observation networks (Figure C1). Compared to the other areas (~10% of grids in the non-polar regions), polar regions (~70% of grids in the polar regions) had higher negative correlations, where the reduction in water storage occurs both during and after the melting season without any direct association with the incoming precipitation. From October/November onwards, temperatures are usually below 0°C and any precipitation accumulates on the surface as the snowpack. From March/April onwards, temperatures are sufficiently high again that melting can occur at larger scales so that the TWS starts to drop again. Melting therefore results in lateral surface discharge of water and thereby a reduction of TWS. Similar negative correlations were observed in Central Asia and Northern Africa's arid regions, where water storage fluctuations are low (See Appendix B), and GRACE measurements are most likely driven by measurement noise. The overall measurement accuracy of GRACE (or GRACE measurement accuracy for short) slightly varies with latitude due to its polar orbit, resulting in more observations per unit area at the poles than at the equator each month. Additionally, there is a minor dependency on coastal proximity, as aliasing artifacts tend to be more pronounced near the sea compared to inland regions. Consequently, the relative accuracy of GRACE is primarily influenced by signal magnitudes: in regions with large signals (such as the Amazon), the signal-to-noise ratio (SNR) exceeds 1, allowing TWSvariations to be accurately observed. In contrast, in areas with smaller signals (such as deserts), the SNR is less than 1, meaning the GRACE data is predominantly noise.

Table 3.1. The Correlation Coefficients of Coupled Products with and without Pixel Size Effect

Coupled Product	Mean ρ without Pixel Size Effect	Mean ρ with Pixel Size Effect
G3P&GPCP	0.31	0.36
G3P&GPCC	0.28	0.34
JPL&GPCP	0.30	0.36
JPL&GPCC	0.28	0.34

Furthermore, the spatial distributions of ρ differences for the remaining combinations against the findings acquired for G3P&GPCP are illustrated in Figures 3.1b-d. Differences were observed in arid climate zones when swapping the TWS product from G3P to JPL (Figure 3.1c). These regions typically exhibit less fluctuations in TWS than non-arid regions, resulting in a low signal-to-noise ratio in GRACE and GRACE-FO observations (Figure B6). In such areas, processing preferences, such as the spatially variable a priori constraints (Watkins et al., 2015) applied in the mascon, have a greater effect. The standard deviation of the differences in Figure 3.1c (0.14) is smaller than that of the difference in Figure 3.1d (0.21). Thus, correlations are reduced by the switching of the precipitation product from GPCP to GPCC (Figures 3.1c and 3.1d) to a considerably greater extent in more regions, especially over locations with less dense in situ networks (Figure C1). Higher correlations obtained using GPCP as a precipitation product validate the additional value of satellite observations in areas that would otherwise lack data (e.g., the Congo Basin in central Africa). Nonetheless, several places where GPCC matches GRACE and GRACE-FO more closely than GPCP, indicating that systematic deficiencies in satellite data may also deteriorate the TWS-precipitation coupled product in some regions. Despite the differences mentioned above, precipitation and storage, as measured by satellite gravimetry, have an average correlation of 0.30. The significance threshold for the correlation is 0.14, based on the number of temporally available TWS data points. Therefore, an average correlation of 0.30 is considered both significant and substantial, suggesting that GRACE and GRACE-FO observations should be utilized more frequently in extensive hydrometeorological studies. This calculation includes all pixels, even those with negative correlations. Consequently, the average correlations remain above the significance threshold, even when pixels with negative correlations are included.

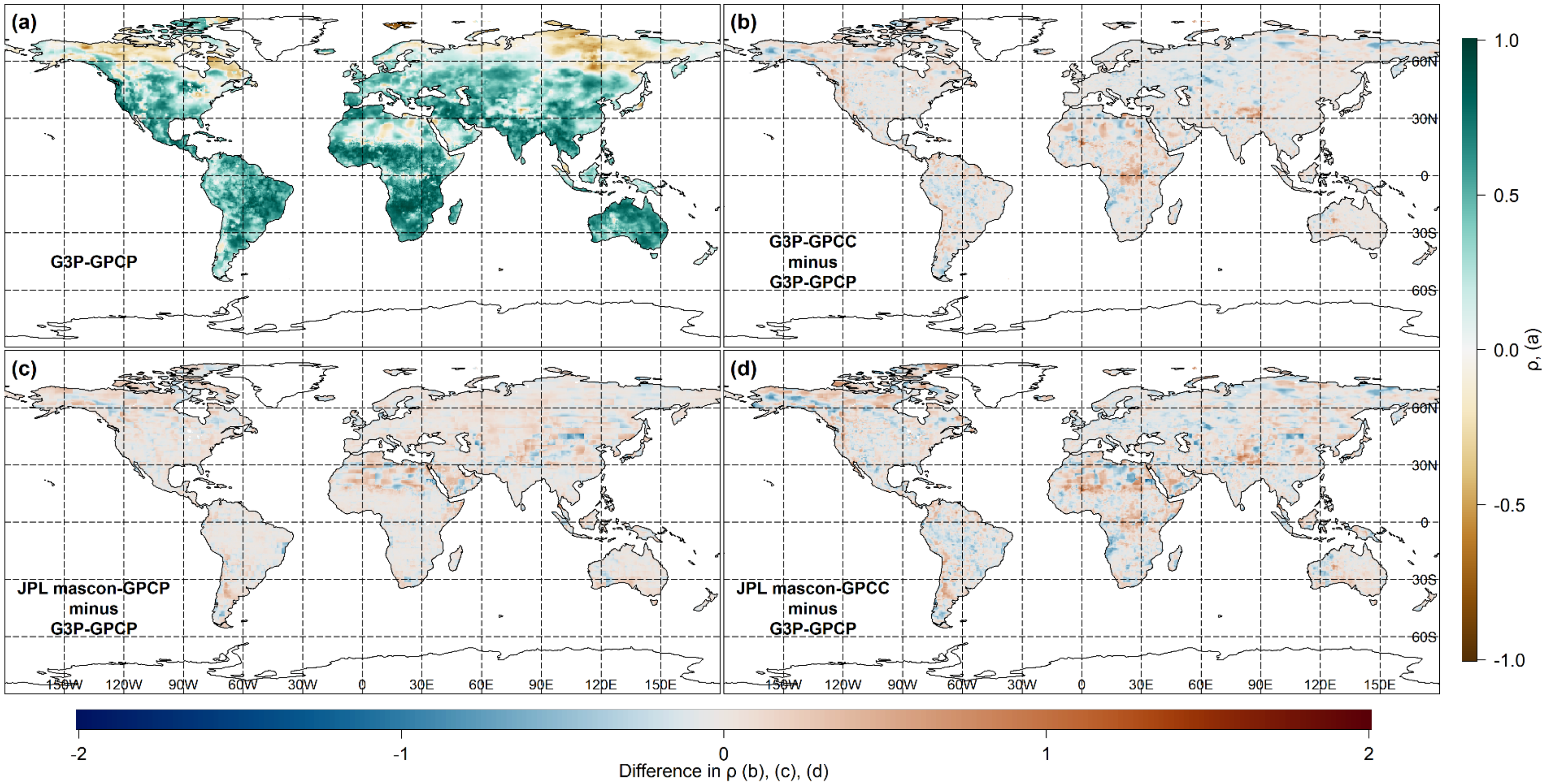

Figure 3.1. The spatial distributions of ρ between dTWSA and cdPA. (a) ρ obtained from G3P&GPCP. The differences in ρ obtained from (b) G3P&GPCC, (c) JPL&GPCP, (d) JPL&GPCC relative to G3P&GPCP.

Figure **Hata! Başvuru kaynağı bulunamadı.**a depicts the spatial distributions of β_1 (Eq. 2-8), larger than 0, for G3P&GPCP. The β_1 values were below 0 in the particular areas of North America, North Africa, and Northeastern Asia. The relationship between TWSA and precipitation is less dependable in these regions since factors other than precipitation likely affected TWSA values. The majority of regions having polar climates (i.e., Köppen-Geiger Climate Zone E) displayed β_1 values less than zero, suggesting a weak relationship between cdPA and dTWSA in these regions. A contrasting pattern was found between the arid zones, which was similar to the correlation coefficient analysis. The arid areas of North America (Zone B) exhibited a pattern more comparable to the arid regions in Australia. The percentage of excluded areas was higher in the arid regions in Africa than in Australia and North America. Also, the β_1 values were lower in the remaining arid areas of North Africa. Furthermore, the mean β_1 values of all coupled products are shown in Table 3.2. Similar to correlation analysis, the effect of the pixel area was investigated to get an idea of how the β_1 values change from the equator to the poles. The results, aligned with the correlation coefficient analysis, show that the pixel areas do not greatly impact the β_1 values, as minor differences, less than 6%, exist in the mean β_1 values whether or not the effect of the pixel areas was considered.

Table 3.2. The β_1 Values of Coupled Products with and without Pixel Size Effect

Coupled Product	Mean β_1 without Pixel Size Effect	Mean β_1 with Pixel Size Effect
G3P&GPCP	1.33	1.44
G3P&GPCC	1.27	1.38
JPL&GPCP	1.39	1.43
JPL&GPCC	1.34	1.39

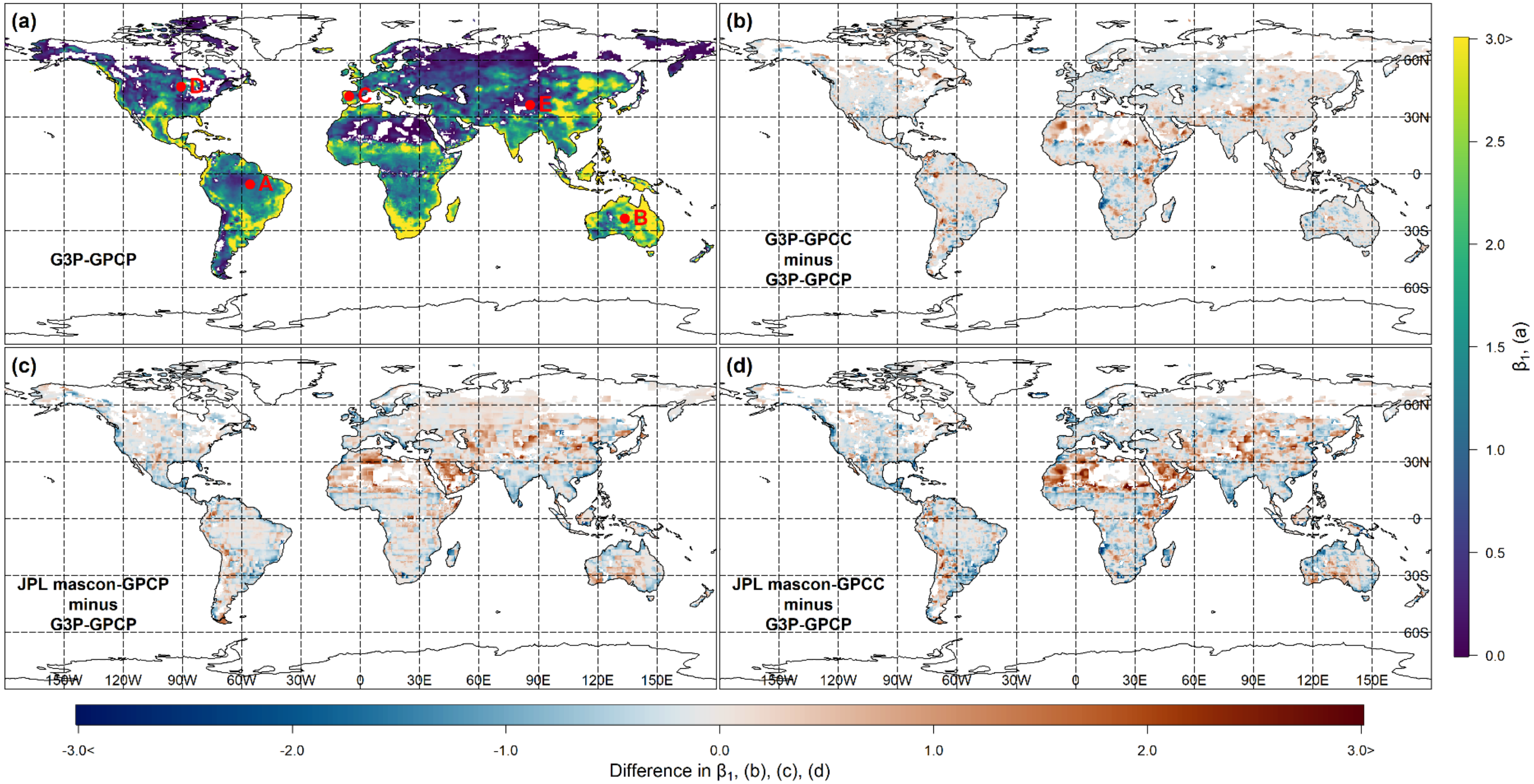

Figure 3.2. The spatial distributions of β_1 between dTWSA and cdPA. (a) β_1 obtained from G3P&GPCP. The differences in β_1 obtained from (b) G3P&GPCC, (c) JPL&GPCP, (d) JPL&GPCC relative to G3P&GPCP.

Moreover, the spatial distributions of β_1 differences for the remaining combinations against the findings acquired for G3P&GPCP are illustrated in Figures **Hata! Başvuru kaynağı bulunamadı.**b-d. When swapping the TWS product from G3P to JPL (Figure **Hata! Başvuru kaynağı bulunamadı.**c), the pixel area-weighted mean β_1 difference is -0.01. Thus, the β_1 values are mostly similar for the mascon solutions and for the spherical harmonics. Using the JPL instead of G3P revealed more locations with β_1 bigger than 3 in the warm temperate climate (Zone E) of Europe. Switching the precipitation product from GPCP to GPCC also showed a fairly similar effect, that the β_1 values were usually smaller for the in-situ observations than for the blended precipitation product. Also, JPL&GPCC showed the greatest overall decline in β_1 values against G3P&GPCP (-0.15). Specifically, in the snow zones of Asia and the arid zones of Australia, utilizing GPCP revealed more locations with β_1 closer to 1 than GPCC. This indicates that when utilizing GPCP as opposed to GPCC, there may be less need for extra variables to explain the relationship between precipitation anomalies and TWS variations in these regions.

3.2 The cdPA and dTWSA for Each Climate Zone

3.2.1 Equatorial Zone (A)

The time series of dTWSA obtained from both TWS products (G3P and JPL) are illustrated in Figure 3.3a for an example region in the Equatorial Zone (A) in Australia (55.75° W, 5.75° S, Figure **Hata! Başvuru kaynağı bulunamadı.**a). The time series of cdPA obtained from both precipitation products (GPCC and GPCP) are illustrated in Figure 3.3b for the same region. The dynamics of water availability and precipitation, as well as possible patterns of drought recovery, can be understood by using these visualizations to track and examine variations in water storage deviations and cdPA over time. The close agreement was found between the time series of G3P and JPL, and GPCC and GPCP, as well as between dTWSA and cdPA time series (average $\rho = 0.80$) for this region, as shown in Figure 3.3. The correlation coefficients between all products for the example region in the Equatorial Zone (A) are shown in Table 3.3. The regression coefficients between cdPA and dTWSA using different precipitation and TWSA products for the example region in the Equatorial Zone (A) are presented in Table 3.4.

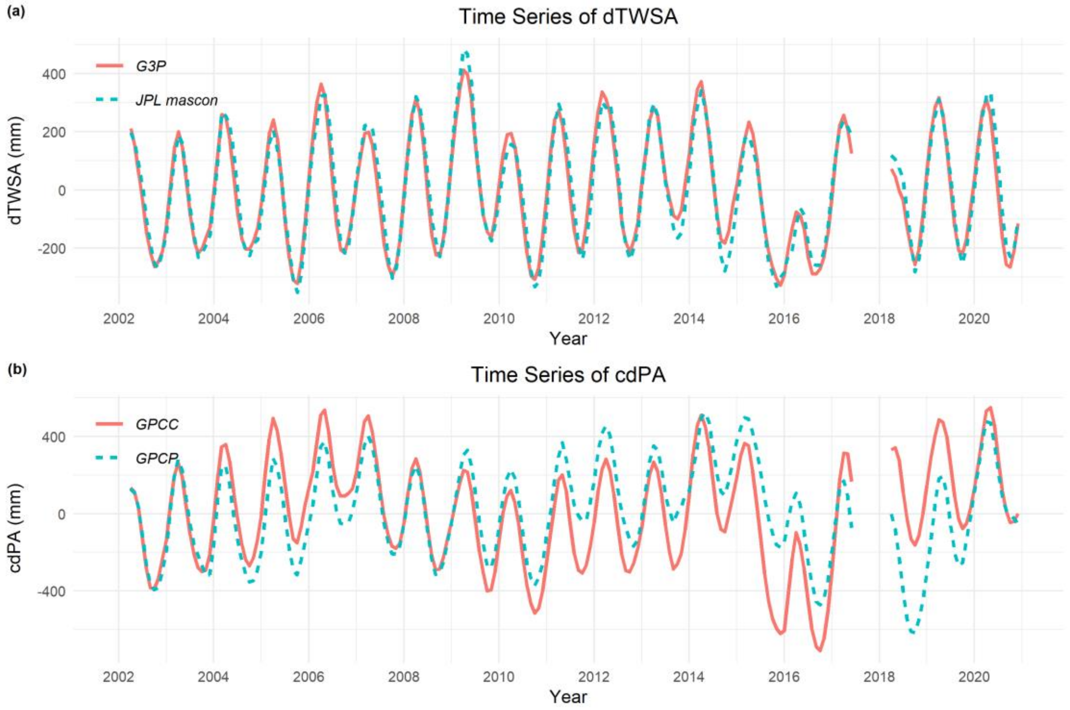

Figure 3.3. Time series of (a) dTWSA derived from both TWS products (G3P and JPL); and (b) cdPA derived from both precipitation products (GPCC and GPCP), each in an example region in the Equatorial zone (A) in South America (55.75° W, 5.75° S).

Table 3.3. Correlation Coefficient of All Products for an Example Region in the Equatorial Zone (A) in South America (55.75°W 5.75°S)

	G3P	JPL	GPCC	GPCP
G3P	-	0.98	0.81	0.79
JPL	0.98	-	0.81	0.77
GPCC	0.81	0.81	-	0.74
GPCP	0.79	0.77	0.74	-

Table 3.4. The β_1 values for Different Precipitation and TWSA Products for an Example Region in the Equatorial Zone (A) in South America (55.75°W 5.75°S)

Products	β_1 value
G3P&GPCP	1.02
G3P&GPCC	1.17
JPL&GPCP	0.98
JPL&GPCC	1.15

Based on the β_1 values in Table 3.4, which are around 1 for different products, the decrease in precipitation can be directly linked to the storage deficit for the example region in the Equatorial Zone (A) in South America (55.75°W, 5.75°S). This suggests that changes in precipitation closely correspond to variations in terrestrial water storage in this region.

3.2.2 Arid Zone (B)

The time series of dTWSA obtained from both TWS products (G3P and JPL) are illustrated in Figure 3.4a for an example region in the Arid Zone (B) in Australia (113.75° E, 23.75° S, Figure **Hata! Başvuru kaynağı bulunamadı.**a). The time series of cdPA obtained from both precipitation products (GPCC and GPCP) are illustrated in Figure 3.4b for the same region. The dynamics of water availability and precipitation, as well as possible patterns of drought recovery, can be understood by using these visualizations to track and examine variations in water storage deviations and cdPA over time. The close agreement was found between the time series of G3P and JPL, and GPCC and GPCP, as well as between dTWSA and cdPA time series (average $\rho = 0.65$) for this region, as shown in Figure 3.4. The correlation coefficients between all products for the example region in the Arid Zone (B) are shown in Table 3.5. The regression coefficients between cdPA and dTWSA using different precipitation and TWSA products for the example region in the Arid Zone (B) are presented in Table 3.6.

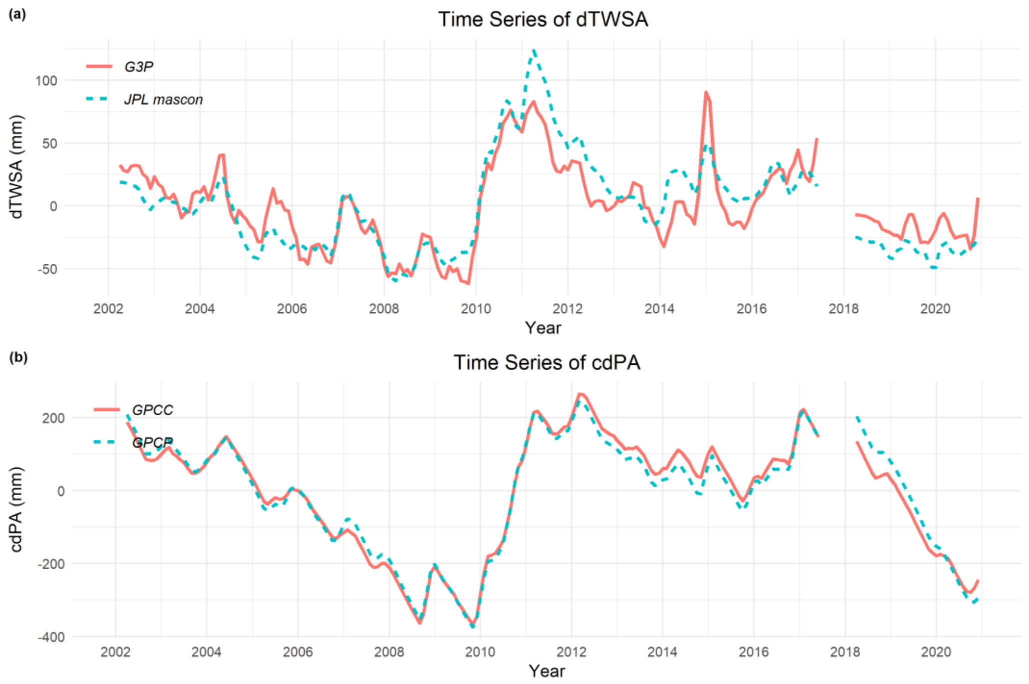

Figure 3.4. Time series of (a) dTWSA derived from both TWS products (G3P and JPL); and (b) cdPA derived from both precipitation products (GPCC and GPCP), each in an example region in the Arid zone (B) in Australia (113.75° E, 23.75° S)

Table 3.5. Correlation Coefficient of All Products for an Example Region in the Arid Zone (B) in Australia (133.75°E 23.75°S)

	G3P	JPL	GPCC	GPCP
G3P	-	0.88	0.67	0.66
JPL	0.88	-	0.65	0.60
GPCC	0.68	0.65	-	0.99
GPCP	0.66	0.60	0.99	-

Table 3.6. The β_1 values for Different Precipitation and TWSA Products for an Example Region in the Arid Zone (B) in Australia (133.75°E 23.75°S)

Products	β_1 value
G3P&GPCP	3.21
G3P&GPCC	3.34
JPL&GPCP	2.53
JPL&GPCC	2.77

Based on the β_1 values in Table 3.6, which are higher than 1 for different products, the decrease in precipitation can be attributed to other hydrological processes, such as ET and R, for the example region in the Arid Zone (B) in Australia (133.75°E, 23.75°S).

3.2.3 Warm Temperate Zone (C)

The time series of dTWSA obtained from both TWS products (G3P and JPL) are illustrated in Figure 3.5a for an example region in the Warm Temperate Zone (C) in Europe (5.75° W, 40.75° N). The time series of cdPA obtained from both precipitation products (GPCC and GPCP) are illustrated in Figure 3.5b for the same region. The dynamics of water availability and precipitation, as well as possible patterns of drought recovery, can be understood by using these visualizations to track and examine variations in water storage deviations and cdPA over time. The close agreement was found between the time series of G3P and JPL, and GPCC and GPCP, as well as between dTWSA and cdPA time series (average $\rho = 0.69$) for this region, as shown in Figure 3.5. The correlation coefficients between all products for the example region in the Warm Temperate Zone (C) are shown in Table 3.7. The regression coefficients between cdPA and dTWSA using different precipitation and TWSA products for the example region in the Warm Temperate Zone (C) are presented in Table 3.8.

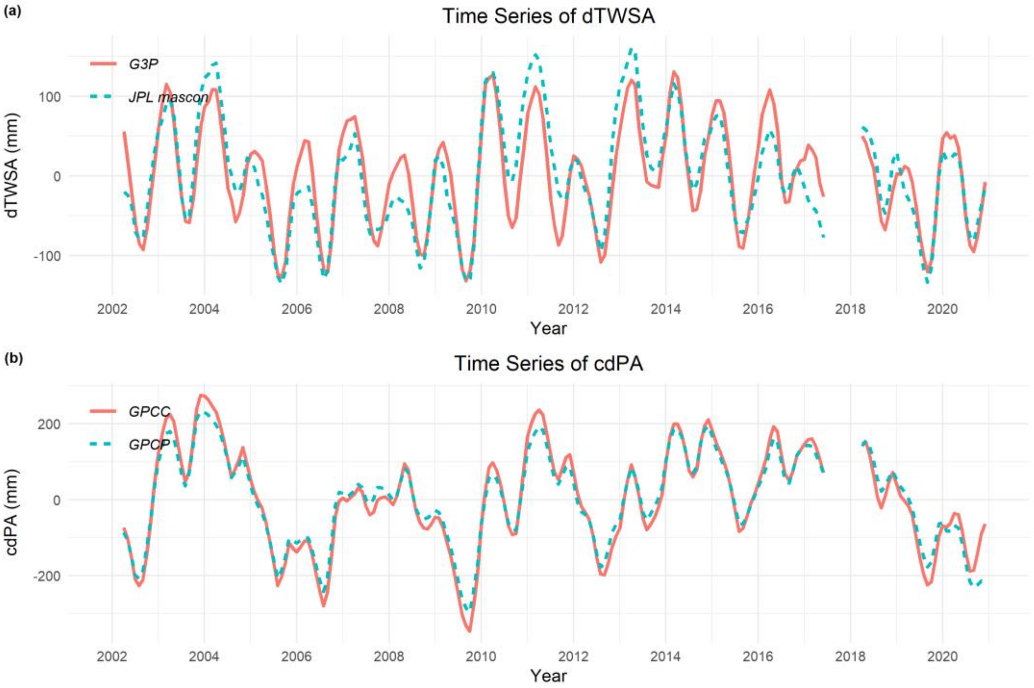

Figure 3.5. Time series of (a) dTWSA derived from both TWS products (G3P and JPL); and (b) cdPA derived from both precipitation products (GPCC and GPCP), each in an example region in the Warm Temperate Zone (C) in Europe (5.75° W, 40.75° S)

Table 3.7. Correlation Coefficient of All Products for an Example Region in the Warm Temperate Zone (C) in Europe (5.75° W, 40.75° S)

	G3P	JPL	GPCC	GPCP
G3P	-	0.89	0.69	0.66
JPL	0.89	-	0.72	0.69
GPCC	0.69	0.72	-	0.98

GPCP	0.66	0.69	0.98	-

Table 3.8. The β_1 values for Different Precipitation and TWSA Products for an Example Region in the Warm Temperate Zone (C) in Europe (5.75° W, 40.75° S)

Products	β_1 value
G3P&GPCP	3.21
G3P&GPCC	3.35
JPL&GPCP	2.53
JPL&GPCC	2.77

Based on the β_1 values in Table 3.8, which are higher than 1 for different products, the decrease in precipitation can be attributed to the other hydrological processes, such as ET and R, for the example region in the Warm Temperate Zone (C) in Europe (5.75° W, 40.75° N).

3.2.4 Snow Zone (D)

The time series of dTWSA obtained from both TWS products (G3P and JPL) are illustrated in Figure 3.6a for an example region in the Snow Zone (D) in North America (90.75° W, 45.75° N, Figure **Hata! Başvuru kaynağı bulunamadı.**a). The time series of cdPA obtained from both precipitation products (GPCC and GPCP) are illustrated in Figure 3.6b for the same region. The dynamics of water availability and precipitation, as well as possible patterns of drought recovery, can be understood by using these visualizations to track and examine variations in water storage deviations and cdPA over time. The close agreement was found between the time series of G3P and JPL, and GPCC and GPCP, as well as between dTWSA and cdPA time series (average ρ = 0.60) for this region, as shown in Figure 3.6. The correlation coefficients between all products for the example region in the Snow Zone (D) are shown in Table 3.9 The regression coefficients between cdPA and dTWSA using different precipitation and TWSA products for the example region in the Snow Zone (D) are presented in Table 3.10.

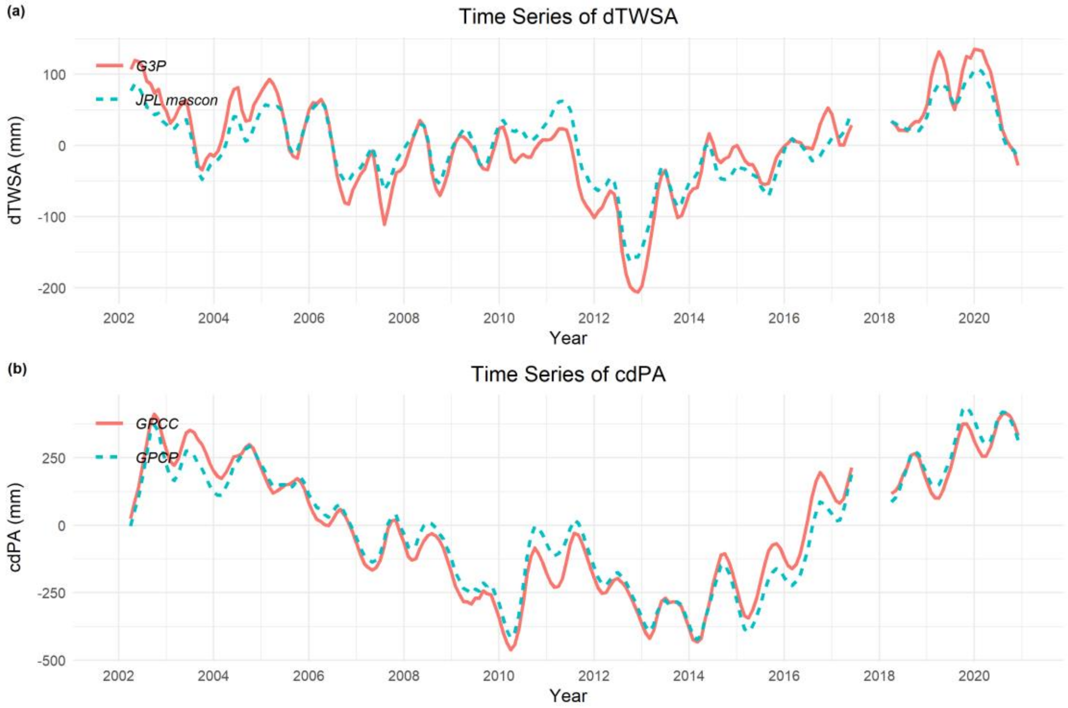

Figure 3.6. Time series of (a) dTWSA derived from both TWS products (G3P and JPL); and (b) cdPA derived from both precipitation products (GPCC and GPCP), each in an example region in the Snow Zone (D) in North America (90.75° W, 45.75° N)

Table 3.9. Correlation Coefficient of All Products for an Example Region in the Snow Zone (D) in North America (90.75° W, 45.75° N)

	G3P	JPL	GPCC	GPCP
G3P	-	0.95	0.63	0.65
JPL	0.95	-	0.53	0.60

GPCC	0.63	0.53	-	0.98
GPCP	0.65	0.60	0.98	-

Table 3.10. The β_1 values for Different Precipitation and TWSA Products for an Example Region in the Example Region in the Snow Zone (D) in North America (90.75° W, 45.75° N)

Products	β_1 value
G3P&GPCP	2.22
G3P&GPCC	2.23
JPL&GPCP	2.66
JPL&GPCC	2.44

Based on the β_1 values in Table 3.10, which are higher than 1 for different products, the decrease in precipitation can be attributed to other hydrological processes, such as ET and R, for the example region in the Snow Zone (D) in North America (90.75° W, 45.75° N).

3.2.5 Polar Zone (E)

The time series of dTWSA obtained from both TWS products (G3P and JPL) are illustrated in Figure 3.7a for an example region in the Polar Zone (E) in Asia (85.75° E, 36.25° N, Figure **Hata! Başvuru kaynağı bulunamadı.**a). The time series of cdPA obtained from both precipitation products (GPCC and GPCP) are illustrated in Figure 3.7b for the same region. The dynamics of water availability and precipitation, as well as possible patterns of drought recovery, can be understood by using these visualizations to track and examine variations in water storage deviations and cdPA over time. The mean correlation coefficient between the time series of G3P and JPL, and GPCC and GPCP, as well as dTWSA and cdPA for the example region in the Polar Zone (E) are shown in Table 3.11. The mean correlation coefficient between dTWSA and cdPA time series was found to be 0.42 for this region. The regression coefficients between cdPA and dTWSA using different precipitation and TWSA products for the example region in the Polar Zone (E) are presented in Table 3.12.

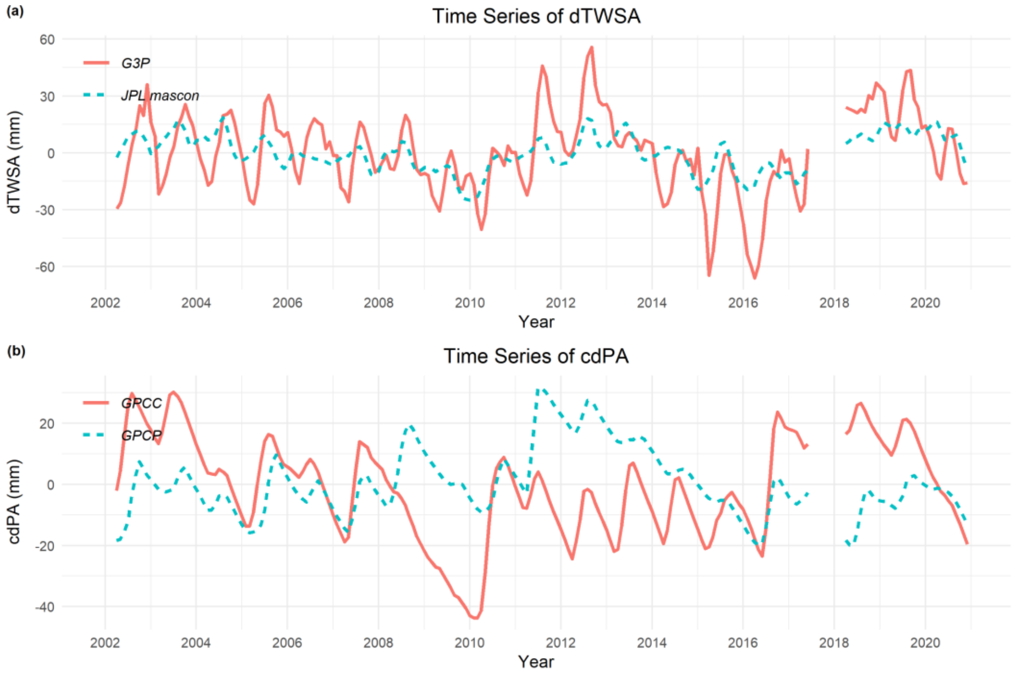

Figure 3.7. Time series of (a) dTWSA derived from both TWS products (G3P and JPL); and (b) cdPA derived from both precipitation products (GPCC and GPCP), each in an example region in the Polar Zone (E) in Asia (85.75° E, 36.25° N)

Table 3.11. Correlation Coefficient of All Products for an Example Region in the Polar Zone (E) in Asia (85.75° E, 36.25° N)

	G3P	JPL	GPCC	GPCP
G3P	-	0.62	0.48	0.48
JPL	0.62	-	0.55	0.17

GPCC	0.48	0.55	-	-0.12
GPCP	0.48	0.17	-0.12	-

Table 3.12. The β_1 values for Different Precipitation and TWSA Products for an Example Region in the Example Region in the Polar Zone (E) in Asia (85.75° E, 36.25° N)

Products	β_1 value
G3P&GPCP	0.25
G3P&GPCC	0.37
JPL&GPCP	0.20
JPL&GPCC	0.93

Based on the β_1 values in Table 3.12, which are less than 1 for all products except JPL & GPCC, the required precipitation amount may be underestimated when considering only storage fluctuations for the example region in the Polar Zone (E) in Asia (85.75° E, 36.25° N). For JPL&GPCC product, the variation in precipitation is almost equal to the variation in storage for this region.

3.3 Storage Deficit Amount

DRT estimation based on storage deficit was calculated using TWSA data for storage deficit amount. Figure **Hata! Başvuru kaynağı bulunamadı.**a illustrates the spatial distributions of mean storage deficit amount to calculate DRT estimations based on storage deficit method. Moreover, Figures **Hata! Başvuru kaynağı bulunamadı.**b-d demonstrate the spatial distribution of the differences between G3P&GPCC and

G3P&GPCP, JPL&GPCP, and JPL&GPCC, respectively. The mean storage deficit amount was the highest in the Equatorial (A) zone, exceeding 125 mm for the G3P & GPCC coupled products. In North Africa's Arid (B) zone, the mean storage deficit amount was the lowest, with less than 25 mm. When switching from G3P to JPL, the mean storage deficit amount marginally increased by 8 mm.

3.4 Required Precipitation Amount

DRT estimation based on required precipitation amount was calculated using both cdPA and TWSA data for necessary precipitation amount. Figure **Hata! Başvuru kaynağı bulunamadı.**a illustrates the spatial distributions of mean required precipitation amount to calculate DRT estimations based on required precipitation method. Moreover, Figures **Hata! Başvuru kaynağı bulunamadı.**b-d demonstrate the spatial distribution of the differences between G3P&GPCC and G3P&GPCP, JPL&GPCP, and JPL&GPCC, respectively. The mean required precipitation amount to fill the storage deficit was the highest in the Equatorial (A) zone, exceeding 500 mm for the G3P&GPCP coupled products. In North Africa's Arid (B) zone, the mean required precipitation amount was less than 100 mm, while in Australia's and North America's Arid (B) zones, it ranged between 100 and 200 mm for the G3P&GPCP coupled products. When switching from GPCP to GPCC, the required precipitation amount decreased marginally in South America, central Africa and south Asia on a global scale (3.2 mm). Similarly, when switching from G3P to JPL, the required precipitation amounts also marginally increased by 5 mm.

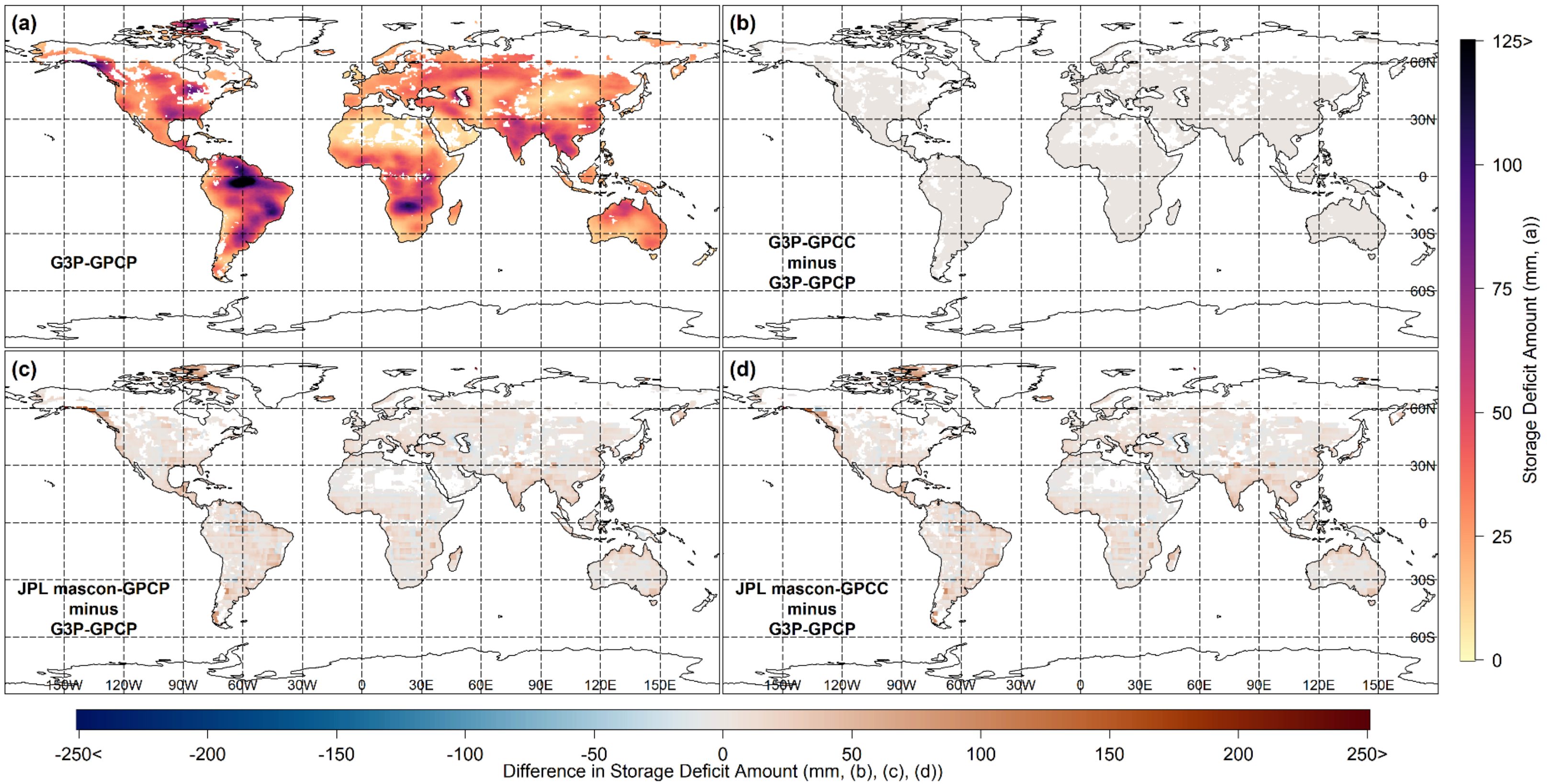

Figure 3.8. Display of mean storage deficit amount obtained from dTWSA. (a) DRT obtained from G3P&GPCP. The differences in DRT relative to G3P&GPCP for (b) G3P&GPCC, (c) JPL&GPCP, and (d) JPL&GPC

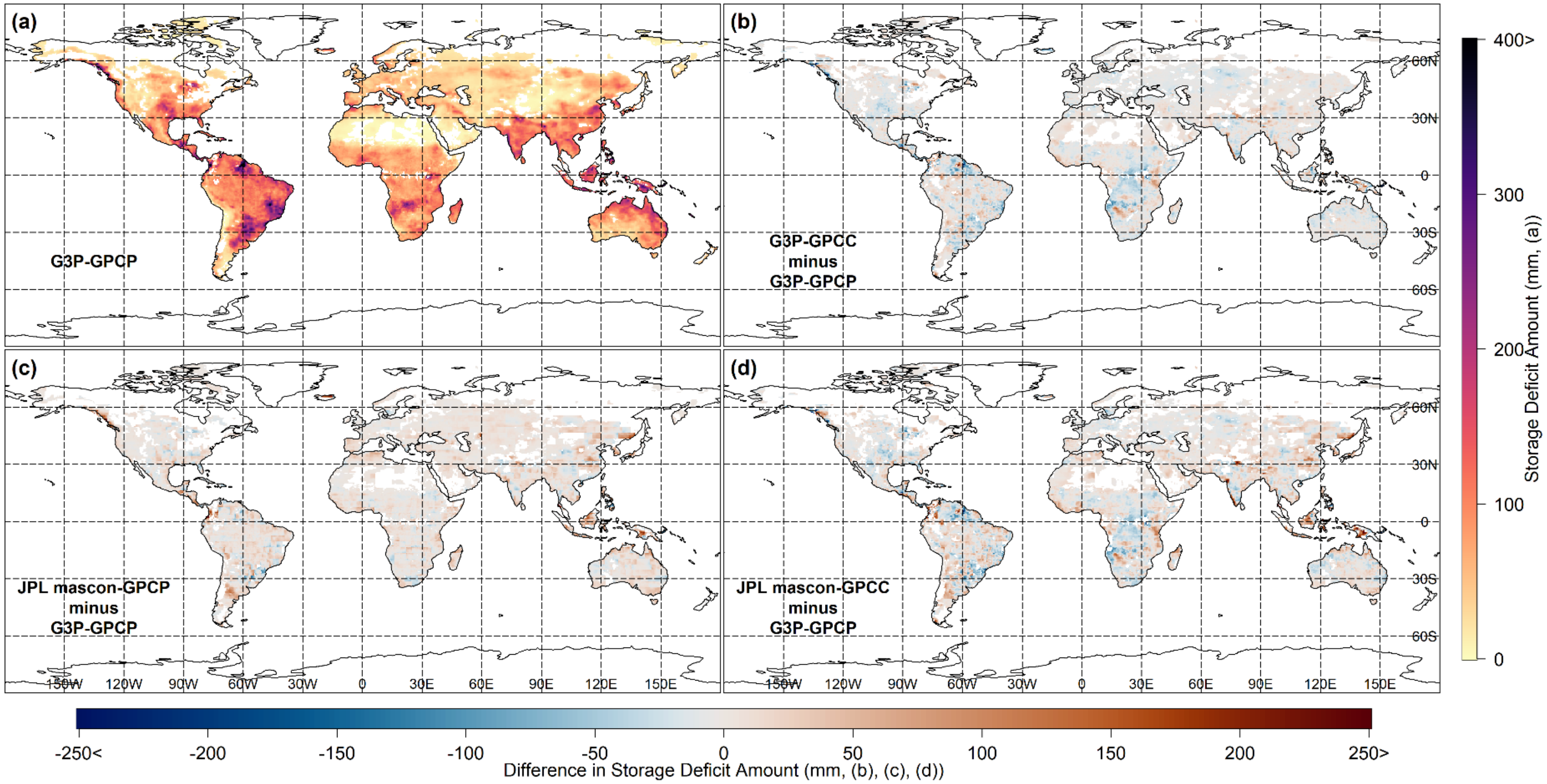

Figure 3.9. Display of mean required precipitation amount obtained from cdPA and dTWSA. (a) DRT obtained from G3P&GPCP. The differences in DRT relative to G3P&GPCP for (b) G3P&GPCC, (c) JPL&GPCP, and (d) JPL&GPCC

3.5 The Storage Deficit and Required Precipitation Amount for an Example Regions in Each Climate Zone

3.5.1 Equatorial Zone (A)

The storage deficit and required precipitation amount for an example region in the Equatorial zone (A) in South America (55.75° W, 5.75° S, Figure **Hata! Başvuru kaynağı bulunamadı.**a) are illustrated using both TWS products (G3P and JPL) and precipitation products (GPCC and GPCP) in Figure 3.10. Observed precipitation amount from corresponding precipitation product is also shown in Figure 3.10.

Figure 3.10a shows the storage deficit amount obtained from the G3P TWS product, the required precipitation amount from the G3P TWS and GPCP precipitation products, and the observed precipitation amount from the GPCP precipitation product, thereby illustrating results from the G3P&GPCP coupled products. Figures 3.10b-d present results obtained from the G3P&GPCC, JPL&GPCP, and JPL&GPCC coupled products, respectively.

For all coupled products, the maximum storage deficit amount was approximately 400 mm in April 2016 (Figure 3.10). The longest drought period for G3P was observed between October 2015 and May 2017 (Figure 3.10a and 3.10b), while for the longest drought period for JPL was observed between December 2014 and September 2016 (Figure 3.10c and 3.10d). The drought events between 2007 and 2008, as well as between mid-2015 and mid-2017, were continuous for the G3P product; however, they were not continuous for the JPL product. Other drought events were observed with both products.

Furthermore, the maximum observed precipitation amount for the GPCC was around 650 mm in March 2016 (Figure 3.10b and 3.10d), however, it was not observed for GPCP (350 mm). The maximum amount for the GPCP was around 550 mm in February 2005 (Figure 3.10a and 3.10c) and also it was observed for GPCC (Figure 3.10b and 3.10d).

(a) Using G3P&GPCP

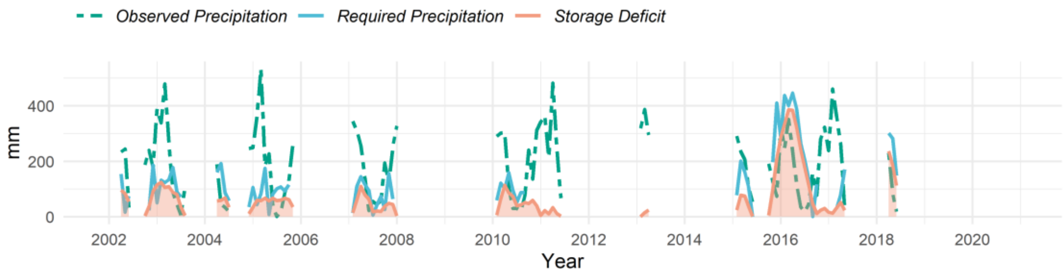

(b) Using G3P&GPCC

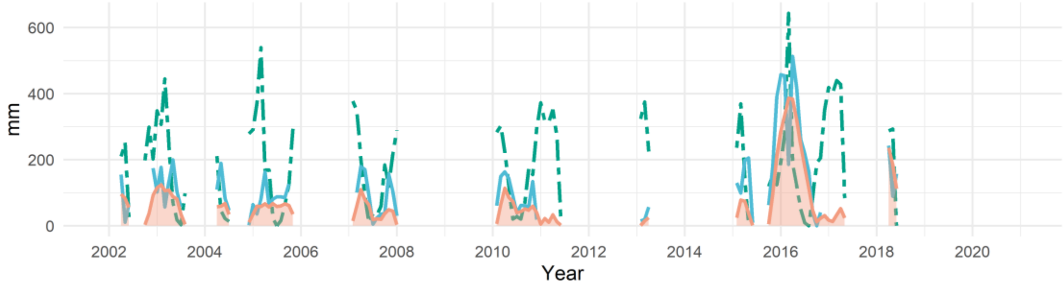

(c) Using JPL mascon&GPCP

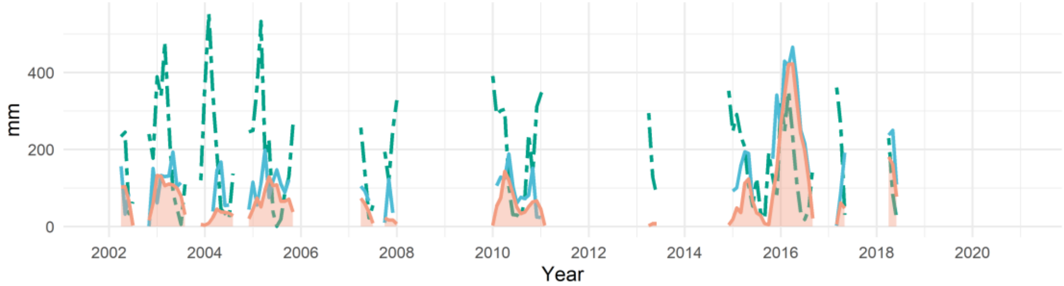

(d) Using JPL mascon&GPCC

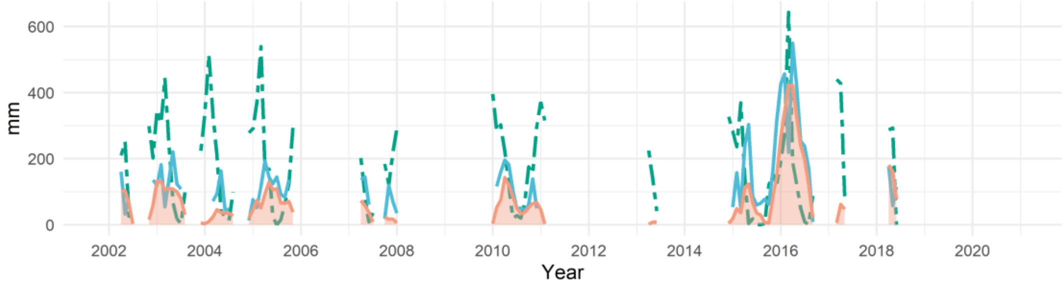

Figure 3.10. The time series of storage deficit amount, required precipitation amount, and observed precipitation amount using (a) obtained from G3P&GPCP, (b) G3P&GPCC, (c) JPL&GPCP, and (d) JPL&GPCC, each in an example region in the Equatorial zone (A) in South America (55.75° W, 5.75° S).

3.5.2 Arid Zone (B)

The storage deficit and required precipitation amount for an example region in the Arid Zone (B) in Australia (113.75° E, 23.75° S, Figure **Hata! Başvuru kaynağı bulunamadı.**a) are illustrated using both TWS products (G3P and JPL) and precipitation products (GPCC and GPCP) in Figure 3.11. Observed precipitation amount from corresponding precipitation product is also shown in Figure 3.11.

Figure 3.11a shows the storage deficit amount obtained from the G3P TWS product, the required precipitation amount from the G3P TWS and GPCP precipitation products, and the observed precipitation amount from the GPCP precipitation product, thereby illustrating results from the G3P&GPCP coupled products. Figures 3.11b-d present results obtained from the G3P&GPCC, JPL&GPCP, and JPL&GPCC coupled products, respectively.

The maximum storage deficit amount was approximately 60 mm and 70 mm in March 2008 for G3P and JPL, respectively (Figure 3.11). The longest drought period for G3P and JPL was observed between May 2007 and February 2010 (Figure 3.11). The drought was noted in 2013, mid-2013 and mid-2015 for the G3P TWS product, while no drought was observed using the JPL. Other drought events were observed with both products.

Furthermore, the maximum observed precipitation amount for the GPCC and GPCP was around 140 mm in November 2008 and February 2010 (Figure 3.11). In general, the observed precipitation from GPCC was aligned well with the observed precipitation from GPCP for this grid.

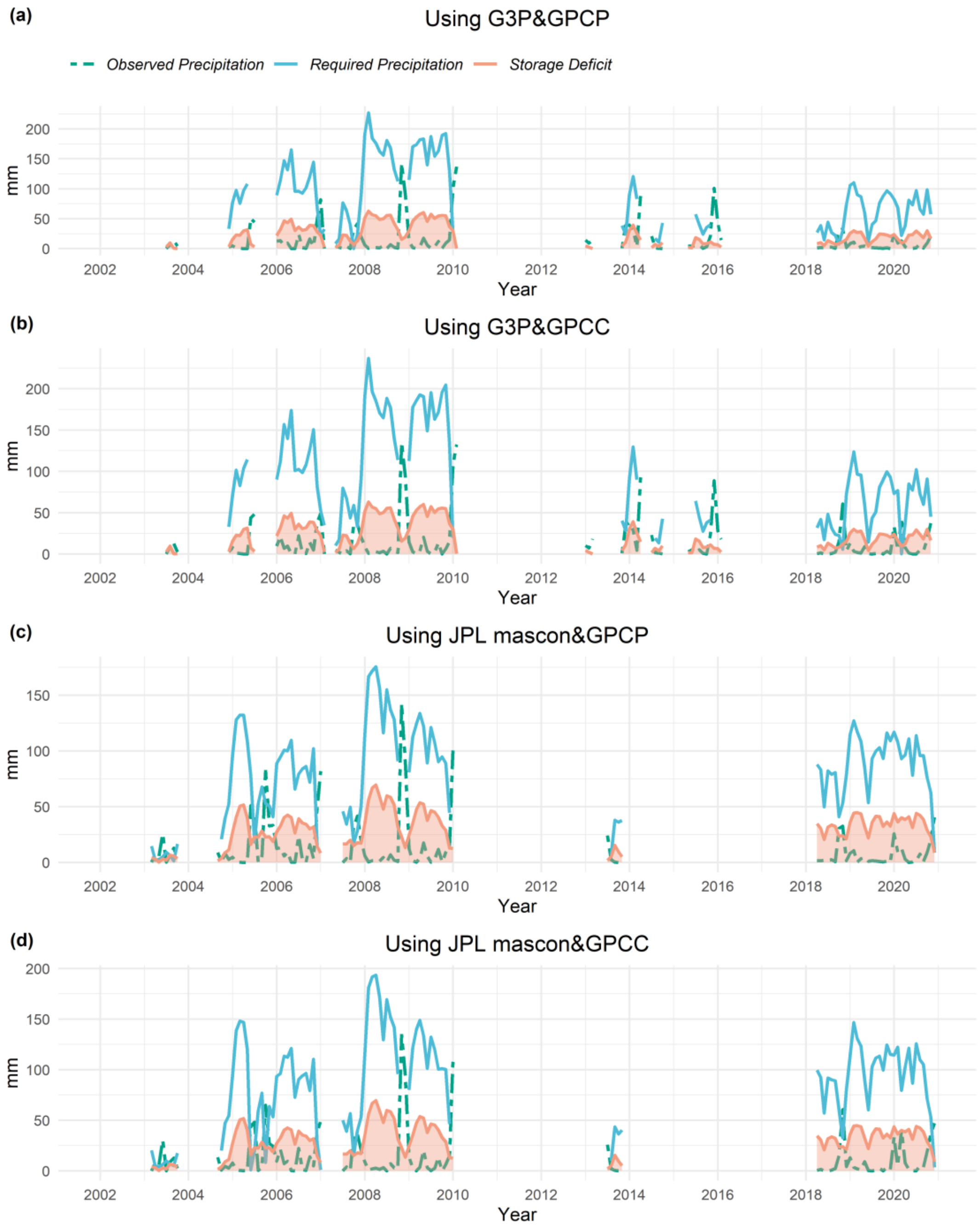

Figure 3.11. The time series of storage deficit amount, required precipitation amount, and observed precipitation amount using (a) obtained from G3P&GPCP, (b) G3P&GPCC, (c) JPL&GPCP, and (d) JPL&GPCC, each in an example region in the Arid Zone (B) in Australia (113.75° E, 23.75° S)

3.5.3 Warm Temperate Zone (C)

The storage deficit and required precipitation amount for an example region in the Warm Temperate Zone (C) in Europe (5.75° W, 40.75° N, Figure **Hata! Başvuru kaynağı bulunamadı.**a) are illustrated using both TWS products (G3P and JPL) and precipitation products (GPCC and GPCP) in Figure 3.12. Observed precipitation amount from corresponding precipitation product is also shown in Figure 3.12.

Figure 3.12a shows the storage deficit amount obtained from the G3P TWS product, the required precipitation amount from the G3P TWS and GPCP precipitation products, and the observed precipitation amount from the GPCP precipitation product, thereby illustrating results from the G3P&GPCP coupled products. Figures 3.12b-d present results obtained from the G3P&GPCC, JPL&GPCP, and JPL&GPCC coupled products, respectively.

The maximum storage deficit amount was approximately 80 mm in May 2012 for G3P (Figure 3.12a and 3.12b), while the maximum storage deficit amount was around 100 mm in May 2017 for the JPL (Figure 3.12c and 3.12d). The longest drought period was observed between December 2004 and September 2006 for G3P, while the longest drought was observed between December 2004 and December 2009 for JPL. Other drought events were observed with both products.

Furthermore, the maximum observed precipitation amount for the GPCC and GPCP was around 250 mm in October 2005 and December 2009 (Figure3.12). In general, the observed precipitation from GPCC was aligned well with the observed precipitation from GPCP for this grid.

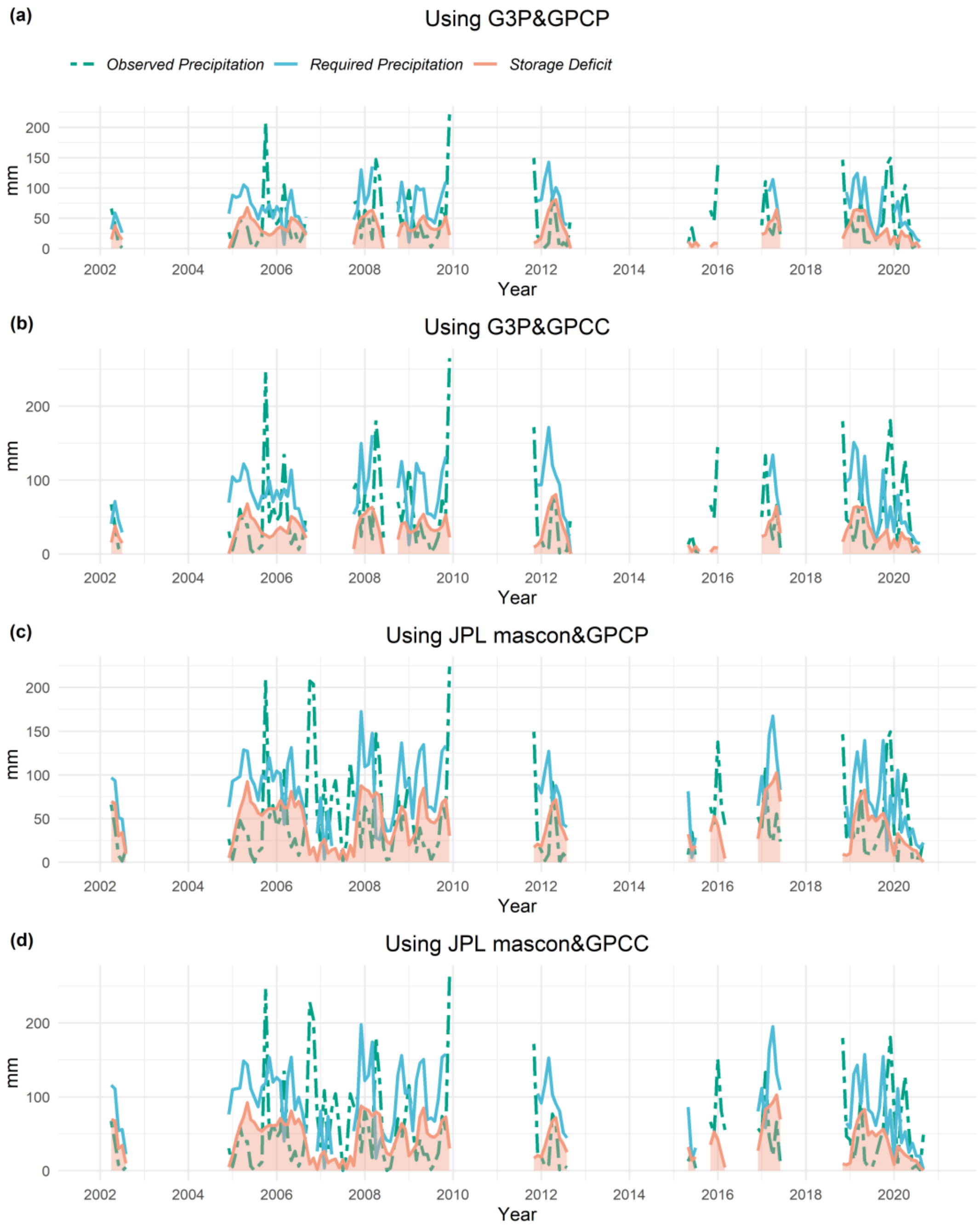

Figure 3.12. The time series of storage deficit amount, required precipitation amount, and observed precipitation amount using (a) obtained from G3P&GPCP, (b) G3P&GPCC, (c) JPL&GPCP, and (d) JPL&GPCC, each in an example region in the Warm Temperate Zone (C) in Europe (5.75° W, 40.75° N)

3.5.4 Snow Zone (D)

The storage deficit and required precipitation amount for an example region in the Snow Zone (D) in North America (90.75° W, 45.75° N, Figure **Hata! Başvuru kaynağı bulunamadı.**a) are illustrated using both TWS products (G3P and JPL) and precipitation products (GPCC and GPCP) in Figure 3.13. Observed precipitation amount from corresponding precipitation product is also shown in Figure 3.13.

Figure 3.13a shows the storage deficit amount obtained from the G3P TWS product, the required precipitation amount from the G3P TWS and GPCP precipitation products, and the observed precipitation amount from the GPCP precipitation product, thereby illustrating results from the G3P&GPCP coupled products. Figures 3.13b-d present results obtained from the G3P&GPCC, JPL&GPCP, and JPL&GPCC coupled products, respectively.

The maximum storage deficit amount was approximately 200 mm and 150 mm in December 2012 for G3P and JPL. respectively (Figure 3.13). The longest drought period was observed between May 2011 and July 2014 for G3P (Figure 3.13a and 3.13b), while the longest drought was observed between October 2011 and July 2016 for JPL (Figure 3.13c and 3.13d). Droughts were noted in 2010 and 2017 for the G3P TWS product, while no drought is observed using the JPL. Other drought events were observed with both products.

Furthermore, the maximum observed precipitation amount was around 200 mm in September 2010 for both GPCC and GPCP (Figure 3.13). In general, the observed precipitation from GPCC was aligned well with the observed precipitation from GPCP for this grid.

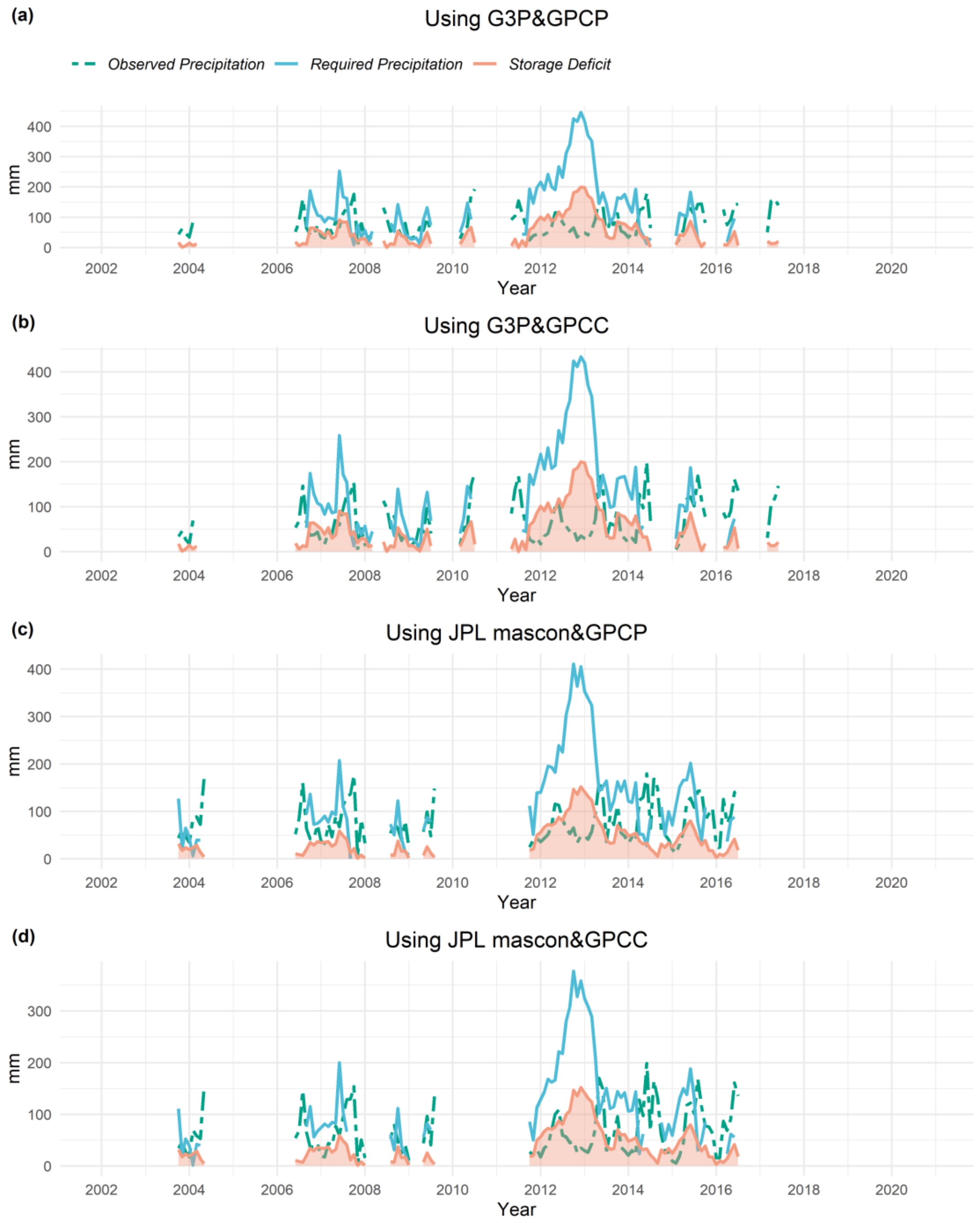

Figure 3.13. The time series of storage deficit amount, required precipitation amount, and observed precipitation amount using (a) obtained from G3P&GPCP, (b) G3P&GPCC, (c) JPL&GPCP, and (d) JPL&GPCC, each in an example region in the Snow Zone (D) in North America (90.75° W, 45.75° N)

3.5.5 Polar Zone (E)

The storage deficit and required precipitation amount for an example region in the Polar Zone (E) in Asia (85.75° E, 36.25° N, Figure **Hata! Başvuru kaynağı bulunamadı.**a) are illustrated using both TWS products (G3P and JPL) and precipitation products (GPCC and GPCP) in Figure 3.13. Observed precipitation amount from corresponding precipitation product was also shown in Figure 3.14.

Figure 3.14a shows the storage deficit amount obtained from the G3P TWS product, the required precipitation amount from the G3P TWS and GPCP precipitation products, and the observed precipitation amount from the GPCP precipitation product, thereby illustrating results from the G3P&GPCP coupled products. Figures 3.14b-d present results obtained from the G3P&GPCC, JPL&GPCP, and JPL&GPCC coupled products, respectively.

The maximum storage deficit amount was approximately 50 mm in June 2016 for G3P (Figures 3.14a and 3.14b), while the maximum storage deficit amount was around 20 mm in March 2010 for the JPL (Figures 3.14c and 3.14d). Also, there was a similar drought event (20 mm) in March 2010 for G3P (Figures 3.14a and 3.14b). The longest drought period was observed between June 2014 and March 2017 for G3P (Figures 3.14a and 3.14b), while the longest drought was observed between June 2014 and June 2017 for JPL (Figures 3.14c and 3.14d). The droughts were noted before mid-2005 and at the end of 2020 for the G3P TWS product, while no drought was observed using the JPL. In contrast, droughts were noted in 2006 and 2012 for the JPL TWS product, while no drought was observed using the G3P TWS product. Other drought events were observed with both products.

Furthermore, the maximum observed precipitation amount for the GPCP was around 15 mm in August 2016 (Figures 3.14a and 3.14c). The maximum amount for the GPCC was around 35 mm in June 2010 and August 2016 (Figures 3.14b and 3.14d). In general, the observed precipitation from GPCC was aligned well with the observed precipitation from GPCP for this grid.

(a) Using G3P&GPCP

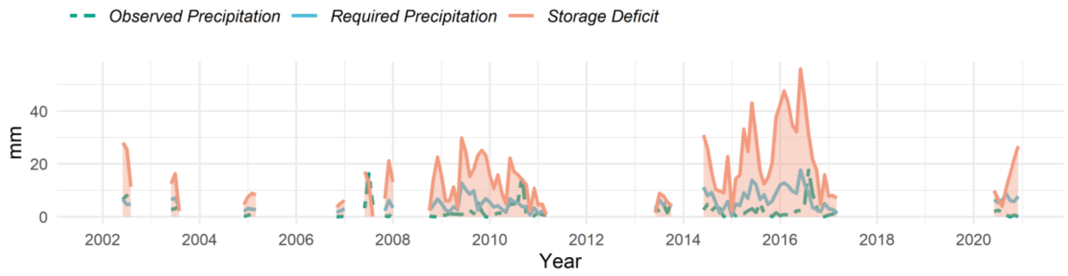

(b) Using G3P&GPCC

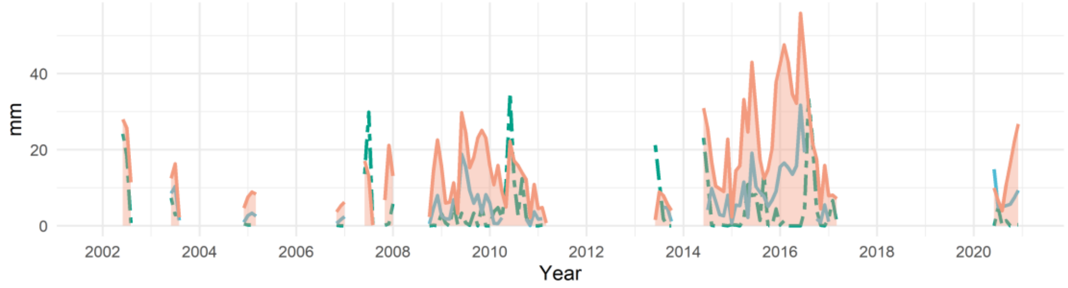

(c) Using JPL mascon&GPCP

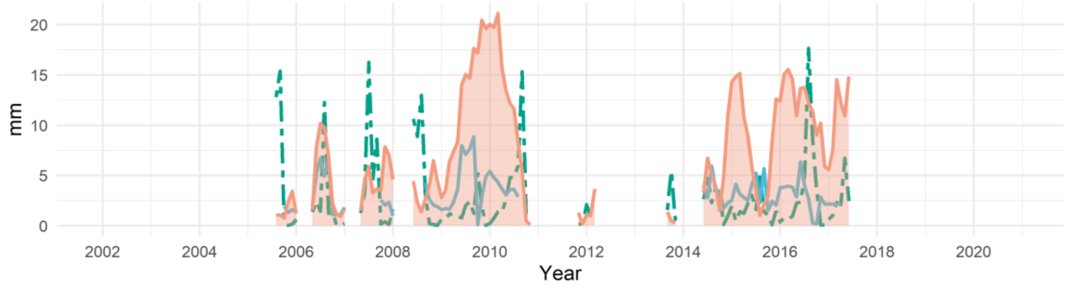

(d) Using JPL mascon&GPCC

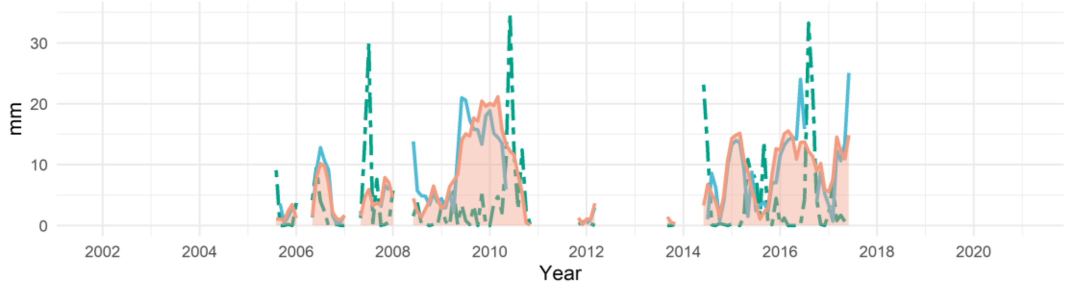

Figure 3.14. The time series of storage deficit amount, required precipitation amount, and observed precipitation amount using (a) obtained from G3P&GPCP, (b) G3P&GPCC, (c) JPL&GPCP, and (d) JPL&GPCC, each in an example region in the Polar Zone (E) in Asia (85.75° E, 36.25° N)

3.6 DRT Estimations

Figures **Hata! Başvuru kaynağı bulunamadı.**a and 3.16a demonstrate the spatial distributions of mean DRT estimations based on storage deficit and required precipitation amount methods using the G3P-GPCP coupled product, respectively. Additionally, Figures **Hata! Başvuru kaynağı bulunamadı.**b-d and 3.16b-d illustrate the spatial distribution of the differences between G3P & GPCC and G3P & GPCP, JPL & GPCP, and JPL & GPCC, respectively, for both approaches. Because the DRT estimations based on the storage deficit approach only used TWS products in the analysis, the mean DRT estimations for this method are the same in Figures **Hata! Başvuru kaynağı bulunamadı.**a and **Hata! Başvuru kaynağı bulunamadı.**b, as well as Figures **Hata! Başvuru kaynağı bulunamadı.**c and **Hata! Başvuru kaynağı bulunamadı.**d. The only purpose of using precipitation products in this method (Figure **Hata! Başvuru kaynağı bulunamadı.**) is the exclusion of the regions that are not suitable for the analysis (Table 2.2). Thus, the excluded regions are the only distinctions between G3P&GPCP and G3P&GPCC (Figure **Hata! Başvuru kaynağı bulunamadı.**b), as well as JPL&GPCP (Figure **Hata! Başvuru kaynağı bulunamadı.**c) and JPL&GPCC (Figure **Hata! Başvuru kaynağı bulunamadı.**d). Although precipitation products were integrated into DRT estimations based on the required precipitation amount method, the overall spatial patterns of mean DRT did not differ between G3P&GPCC and G3P&GPCP (Figure 3.16b) and between JPL&GPCP (Figure 3.16c) and JPL&GPCC (Figure 3.16d). The mean and spatial distributions of DRT estimations using both approaches were compatible with one another, as shown in Figures **Hata! Başvuru kaynağı bulunamadı.** and 3.16.

Furthermore, the mean DRT estimations based on storage deficit and required precipitation amount for all coupled products are shown in Table 3.13 and Table 3.14, respectively. Similar to correlation and regression analysis, the effect of the pixel area was investigated to get an idea of how the mean DRT estimations change from the equator to the poles. The results, aligned with the other pixel size analyses in this study, show that the pixel areas do not greatly impact the mean DRT estimations, as minor differences, 0.2 months, exist in the mean DRT estimations whether or not the effect of the pixel areas was considered.

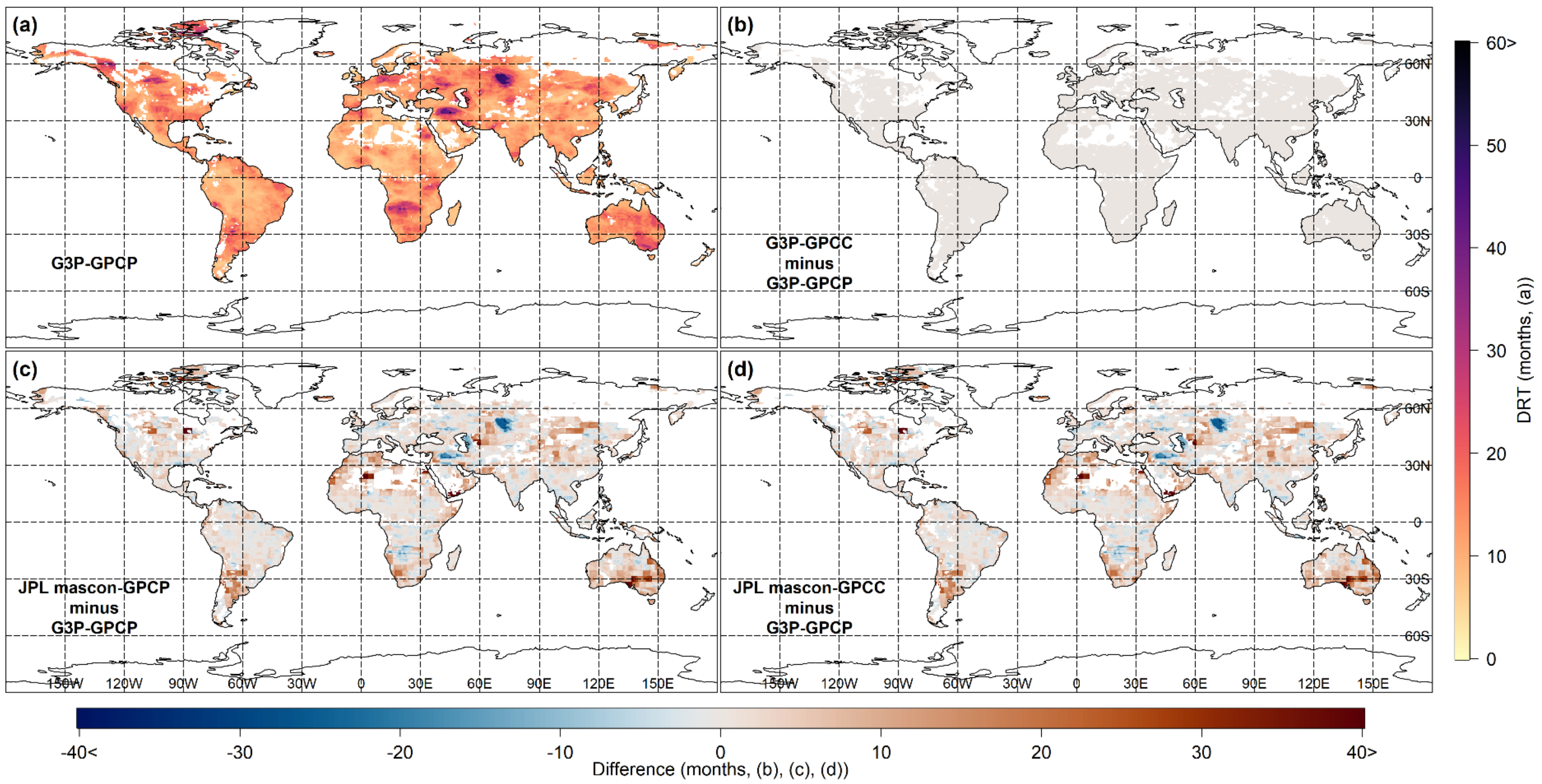

Figure 3.15. Display of mean DRT estimations based on storage deficit obtained from cdPA and dTWSA. (a) DRT obtained from G3P&GPCP. The differences in DRT relative to G3P&GPCP for (b) G3P&GPCC, (c) JPL&GPCP, and (d) JPL&GPCC

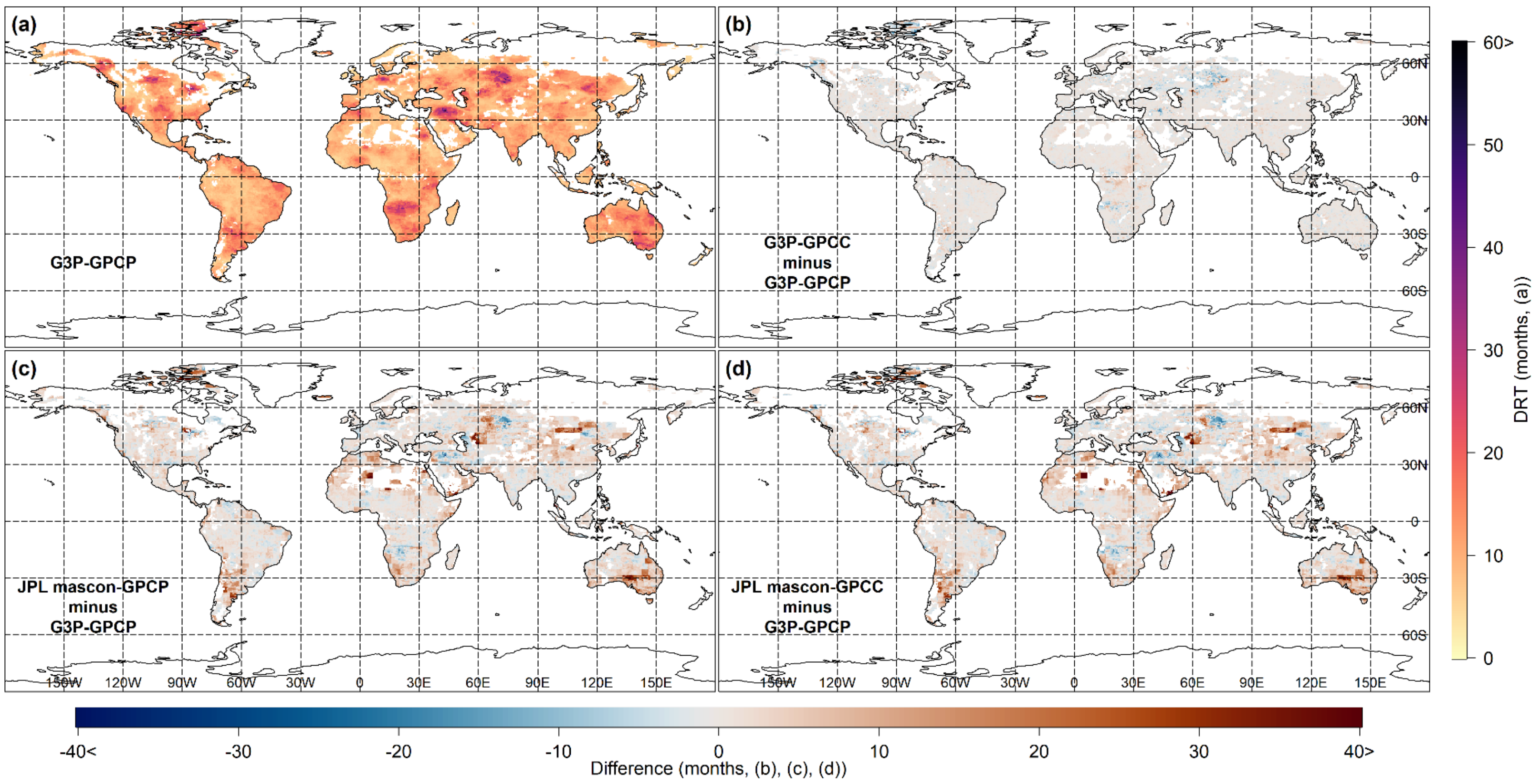

Figure 3.16. Display of mean DRT estimations based on required precipitation amount obtained from cdPA and dTWSA. (a) DRT obtained from G3P&GPCP. The differences in DRT relative to G3P&GPCP for (b) G3P&GPCC, (c) JPL&GPCP, and (d) JPL&GPCC

Table 3.13. The mean DRT Estimations based on Storage Deficit of Coupled Products with and without Pixel Size Effect

Coupled Product	Mean DRT without Pixel Size Effect	Mean DRT with Pixel Size Effect
G3P&GPCP	12.8	12.5
G3P&GPCC	12.7	12.5
JPL&GPCP	15.5	15.2
JPL&GPCC	15.4	15.1

Table 3.14. The mean DRT Estimations based on Required Precipitation Amount of Coupled Products with and without Pixel Size Effect

Coupled Product	Mean DRT without Pixel Size Effect	Mean DRT with Pixel Size Effect
G3P&GPCP	10.9	11.0
G3P&GPCC	10.8	10.9
JPL&GPCP	13.1	13.2
JPL&GPCC	13.0	13.1

The highest mean DRT (50-60 months) estimations based on the storage deficit approach were observed in Iran and Central Asia using G3P as TWS product and GPCC and GPCP as precipitation product, as shown in Figures **Hata! Başvuru kaynağı bulunamadı.**a and **Hata! Başvuru kaynağı bulunamadı.**b, respectively. Similarly, the highest mean DRT estimations were found in the same locations (Iran and Central Asia) for the required precipitation amount methods, as shown in Figures 3.16a and 3.16b, which used G3P as the TWS product and GPCC and GPCP as the precipitation product, respectively. The results of both DRT estimations, which used JPL as the TWS product with GPCC and GPCP as the precipitation product, showed that the regions with the highest mean DRT (50-60 months) were consistently observed in Iran, southeast Australia, central Asia, and north Africa, as depicted in Figures **Hata! Başvuru kaynağı bulunamadı.**c and **Hata! Başvuru kaynağı**

bulunamadı.d, as well as Figures 3.16c and 3.16d. Figures **Hata! Başvuru kaynağı bulunamadı.**a and 3.16a have a 0.75 spatial correlation, demonstrating a high level of spatial correlation between the two. The spatial correlations of the other coupled products were provided in Table 3.15.

Table 3.15. The spatial correlation of the DRT estimations based on both methods using all coupled products

Coupled Products	Spatial ρ of the DRT estimations based on both methods
G3P&GPCP	0.79
G3P&GPCC	0.78
JPL&GPCP	0.76
JPL&GPCC	0.77

Central and south Africa (~45 months), central and southern South America (~40 months), west and central North America (~40 months), eastern Australia (~35 months), east Asia (~30 months), and central Europe (~35 months) were found as the other regions that showed high DRT estimations based on both approaches and across all the product combinations. The current study's results, which are the regions with high DRT, are consistent with increasing worldwide aridity and drought areas since the mid-20th century, mostly due to widespread drying in eastern Australia and northern mid-latitude regions (Dai, 2011). Based on these approaches, the drought conditions in eastern Australia (~35 months) were more severe than in western Australia (~20 months). The results of the current study are consistent with earlier research that focused on tracking droughts in regions that have previously experienced prolonged, intense, multi-month drought events. These areas include central Europe, Iran, southeast Australia, central and western North America, and central South America, all of which have seen more severe droughts than other regions. Madadgar & Moradkhani (2014) observed droughts of varying intensities in the Colorado River Basin from 2001 to 2004, totaling 48 months of drought between 2000 and 2011. The current study's results indicate a mean DRT of approximately 30 months for the same region. The results of the current study (Figures **Hata! Başvuru kaynağı bulunamadı.**a and 3.16a) align with those of (Boergens et al., 2020), who found that Central Europe is prone to drought and required more than a year to recover from the extreme drought experienced during the summers of 2018 and 2019.

Moreover, when utilizing JPL, the mean DRT estimations derived from both approaches were higher than those obtained using G3P. In contrast, the choice of precipitation product (GPCC or GPCP) do not impact the overall spatial patterns of DRT estimates, as there is a close agreement between GPCC and GPCP regarding the spatial distributions of the mean DRT estimations for both TWS products (G3P and JPL), as shown in Figure 3.16. Standard error was used to assess the variability and uncertainty in the DRT estimations across the regions and datasets. Figures **Hata! Başvuru kaynağı bulunamadı.** and 3.18 illustrate the spatial distributions of the SE of DRT estimates, which were similar to the spatial distributions of the mean DRT estimates. The regions with the highest mean DRT also exhibited the highest SE. This indicates that regions experiencing more extended DRT periods showed greater variability in the DRT estimates.

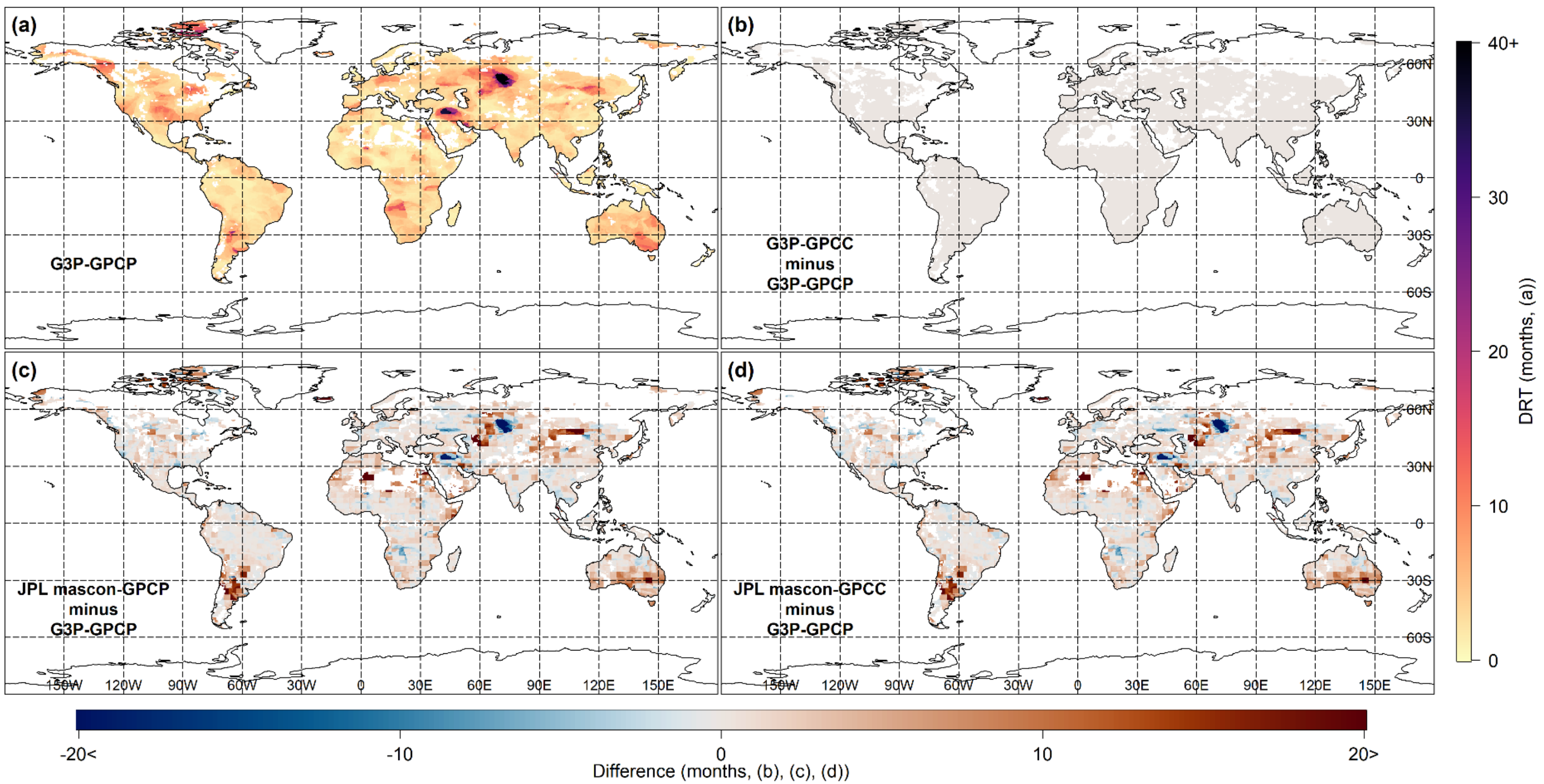

Figure 3.17. Display of the standard error of DRT estimations based on the storage deficit obtained from cdPA and dTWSA (a) Standard error obtained from G3P&GPCP. Differences in standard error relative to G3P&GPCP for (b) G3P&GPCC, (c) JPL-mascon&GPCP, and (d) JPL-mascon&GPCC

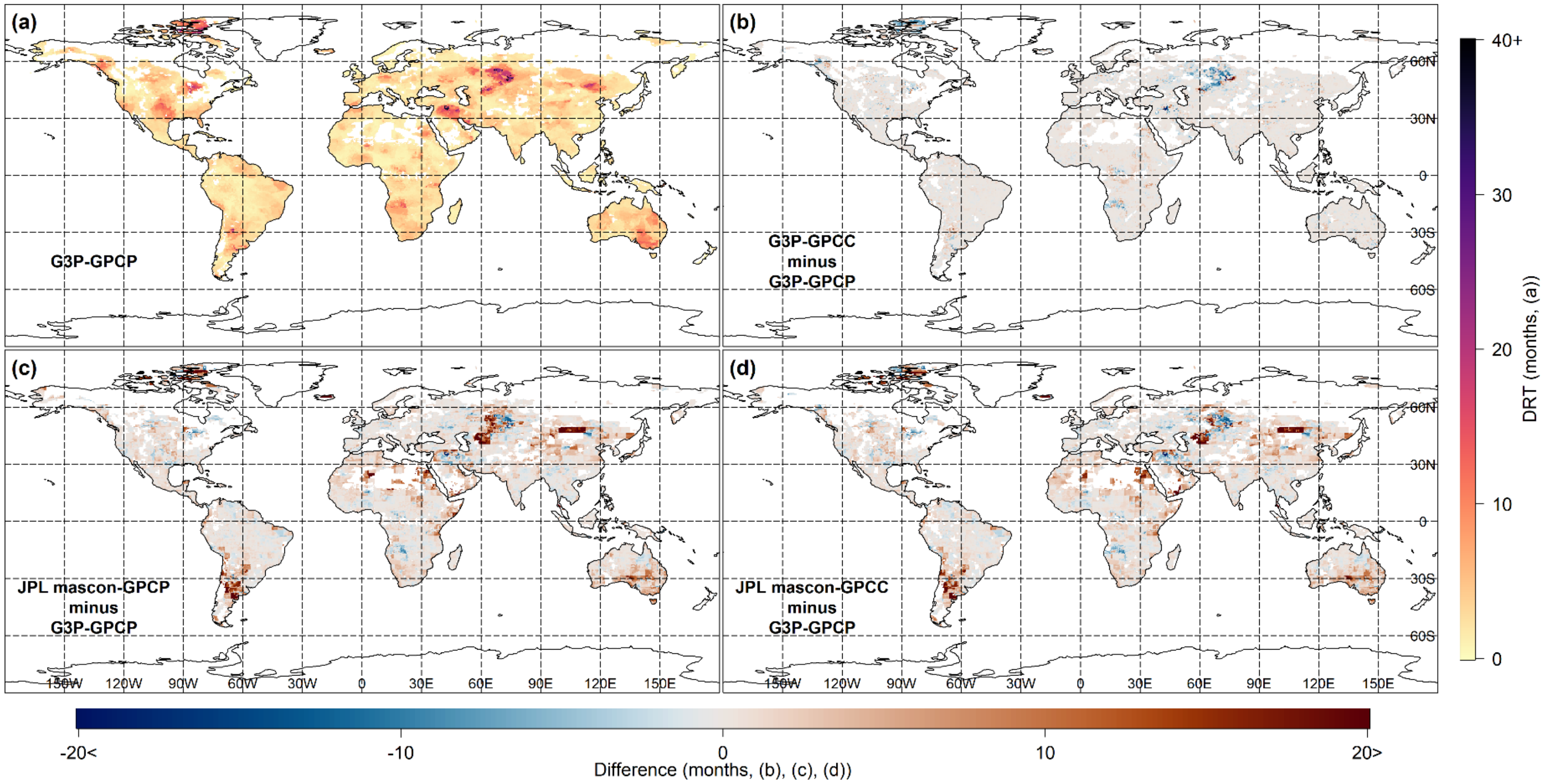

Figure 3.18. Display of the standard error of DRT estimations based on the required precipitation amount obtained from cdPA and dTWSA (a) Standard error obtained from G3P&GPCP. Differences in standard error relative to G3P&GPCP for (b) G3P&GPCC, (c) JPL-mascon&GPCP, and (d) JPL-mascon&GPCC

Figures 3.19a and 3.19b demonstrate the mean DRT estimations derived from storage deficit and required precipitation amounts, respectively, across the Köppen-Geiger main climate zones, utilizing all the TWS-precipitation coupled products. Variability in the mean DRT estimations is shown by error bars that represent the 95% confidence intervals for each zone and each TWS-precipitation coupled product. In each zone and each coupled product, the "n" values indicate the number of grids per coupled product. The highest mean DRT estimation was observed in the polar (E) zone for both DRT estimation methods, with 18.9 months for storage deficit and 16.1 months for required precipitation amount. Except for the polar (E) zone, the arid (B) zone showed the highest mean DRT estimation for both methods, with 15.0 months for storage deficit and 13.2 months for required precipitation amount. In contrast, the equatorial (A) zone showed the lowest mean DRT estimation for both methods, with 10.9 months for storage deficit and 9.8 months for required precipitation amount. Thus, these results are consistent with the earlier findings of Van Lanen et al. (2013), particularly for the regions that experience the least and most severe droughts. In the warm temperate (C) zone, the mean DRT derived from storage deficit and required precipitation amount was 14.0 months and 11.7 months, respectively; in the snow (D) zone, it was 14.8 months and 11.5 months, respectively. Specifically, the mean DRT estimations showed less than 0.2 months variability across all climate zones except the polar (E) zone, as evidenced by narrow 95% confidence intervals indicating low uncertainty. The highest differences between DRT estimations using G3P and JPL were 5.7 months for the Polar (E) zone and 3.8 months for the Arid (B) zone. In contrast, the differences in other zones are lower than those in the Polar (E) and Arid (B) zones. For all the TWS-precipitation coupled products, the SE for the DRT estimations derived from storage deficit and required precipitation amount throughout the Köppen-Geiger climatic zones are illustrated in Figures 3.20a and 3.20b, respectively. For both approaches, the highest SE was found in the polar (E) zone, while the lowest SE varied depending on the product. All climate zones, except the polar (E) zone, showed similar SE for GPCC and

GPCP. The SE obtained from estimations using G3P was marginally smaller than the SE obtained from estimations using JPL for both approaches.

(a) *DRT Based on Storage Deficit*

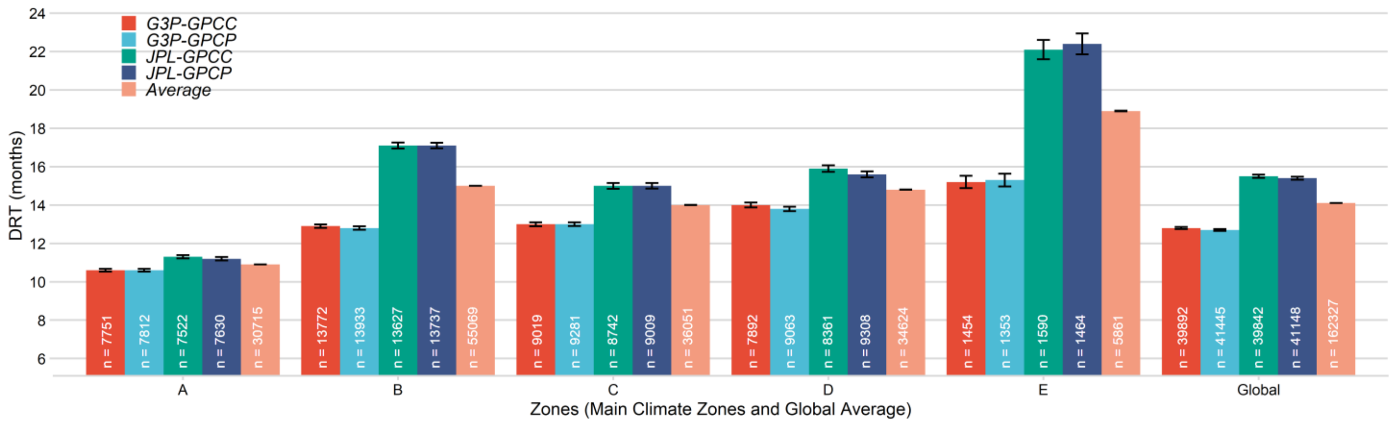

(b) *DRT Based on Required Precipitation Amount*

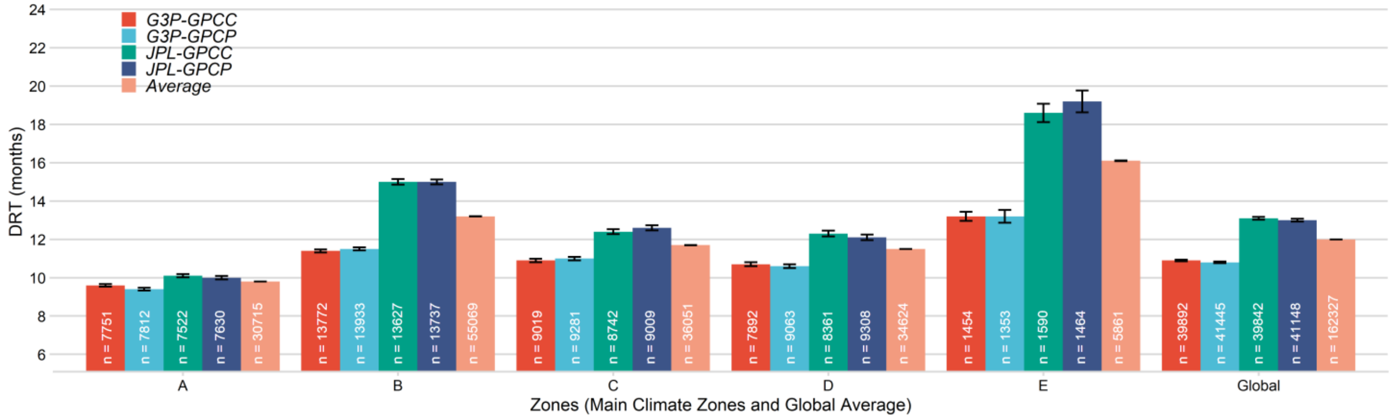

Figure 3.19. The means of DRT estimations based on (a) storage deficit and (b) required precipitation amount for the Köppen-Geiger main climate zones using all the TWS-precipitation coupled products. (A, Equatorial; B, Arid; C, Warm Temperate; D, Snow; and E, Polar Climate Zones).

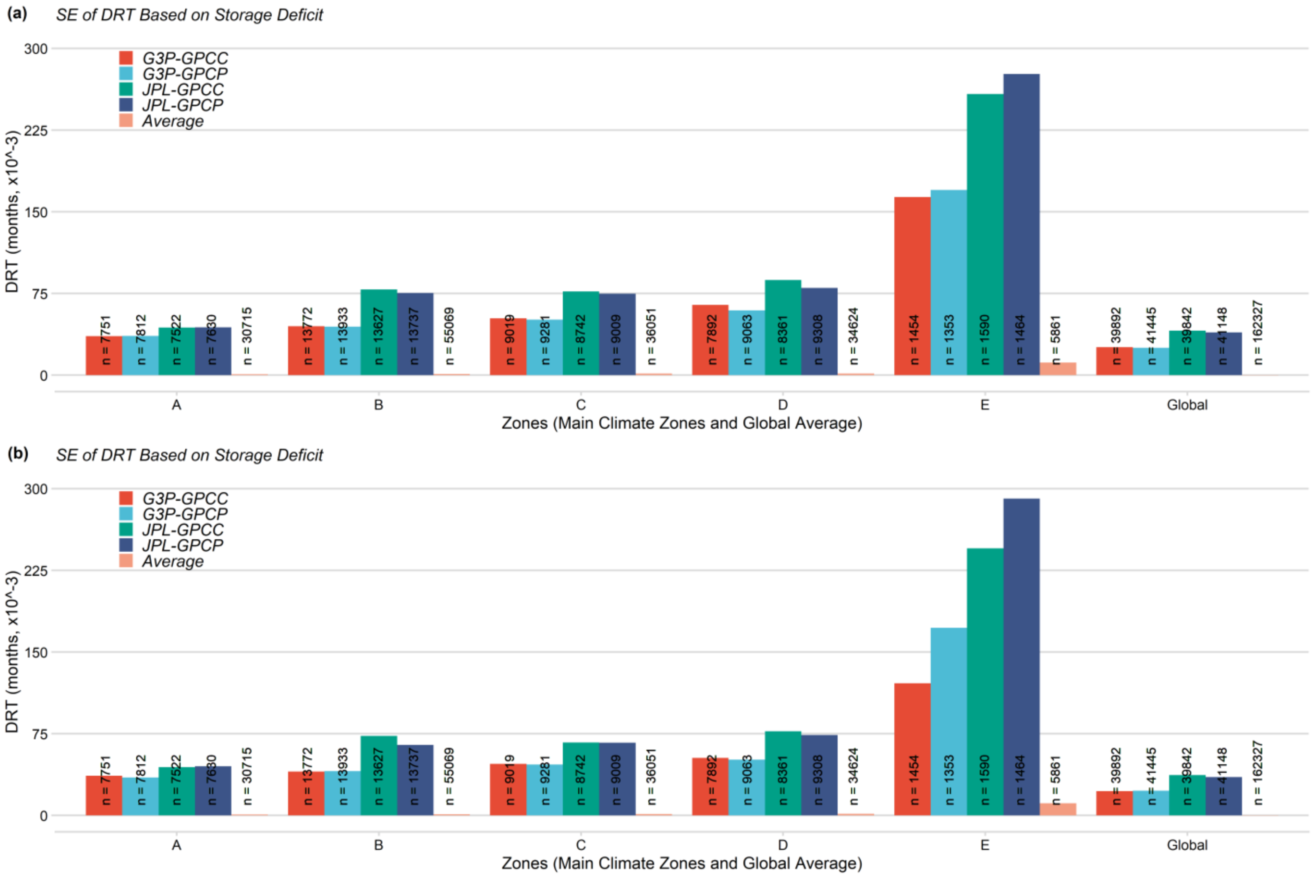

Figure 3.20. Standard error for average DRT estimations based on (a) storage deficit and (b) required precipitation amount for various climate zones from two different dTWSA (i.e., G3P and JPL-mascon) and two different cdPA (i.e., GPCP and GPCC) products calculated for Equatorial (A); Arid (B); Warm Temperates (C); Snow (D); and Polar (E) as given by the Köppen-Geiger classification

On a global average, the mean DRT estimation derived from the required precipitation amount was determined as 12.0 months, while the mean DRT estimation derived from the storage deficit was determined as 14.1 months. Regardless of precipitation products, the mean DRT estimations obtained from G3P (12.1 months) are consistently lower than those obtained from JPL (14.9 months) in each climate zone and the global average. In terms of precipitation products, DRT estimations derived from GPCC and GPCP show similar results (13.5 months) independent of TWS products across all climate zones and the global average. These results indicate a close agreement between GPCC and GPCP regarding DRT estimations and show that G3P-based DRT estimations are consistently lower than JPL-based DRT estimations in each climate zone and the global average.

3.7 Consistency in DRT Estimations

The spatial distributions of the consistency categories, described in Table 2.4, for the DRT estimation obtained from G3P&GPCP coupled products are illustrated in Figure 3.21a. Moreover, the spatial distributions of the differences in consistency categories for the DRT estimation obtained from G3P&GPCC, JPL&GPCP, and JPL&GPCC against G3P&GPCP are demonstrated in Figure 3.21b-d, respectively. The majority of regions were found to be in consistency category 1 (high agreement), with a mean absolute difference of 1.9 months between DRT estimations derived from the two approaches. Consistency results of all combinations of the products (Figure 3.21), including different TWS (G3P vs. JPL) and precipitation (GPCC vs. GPCP), showed similar spatial patterns. These similarities were also observed in the mean DRT estimation obtained from all coupled products. The regions in consistency category 4, where the time difference between DRT estimations is larger than 9 months, had the highest mean DRT estimations and the highest standard error of the mean DRT for both approaches, as expected (Table 3.16).

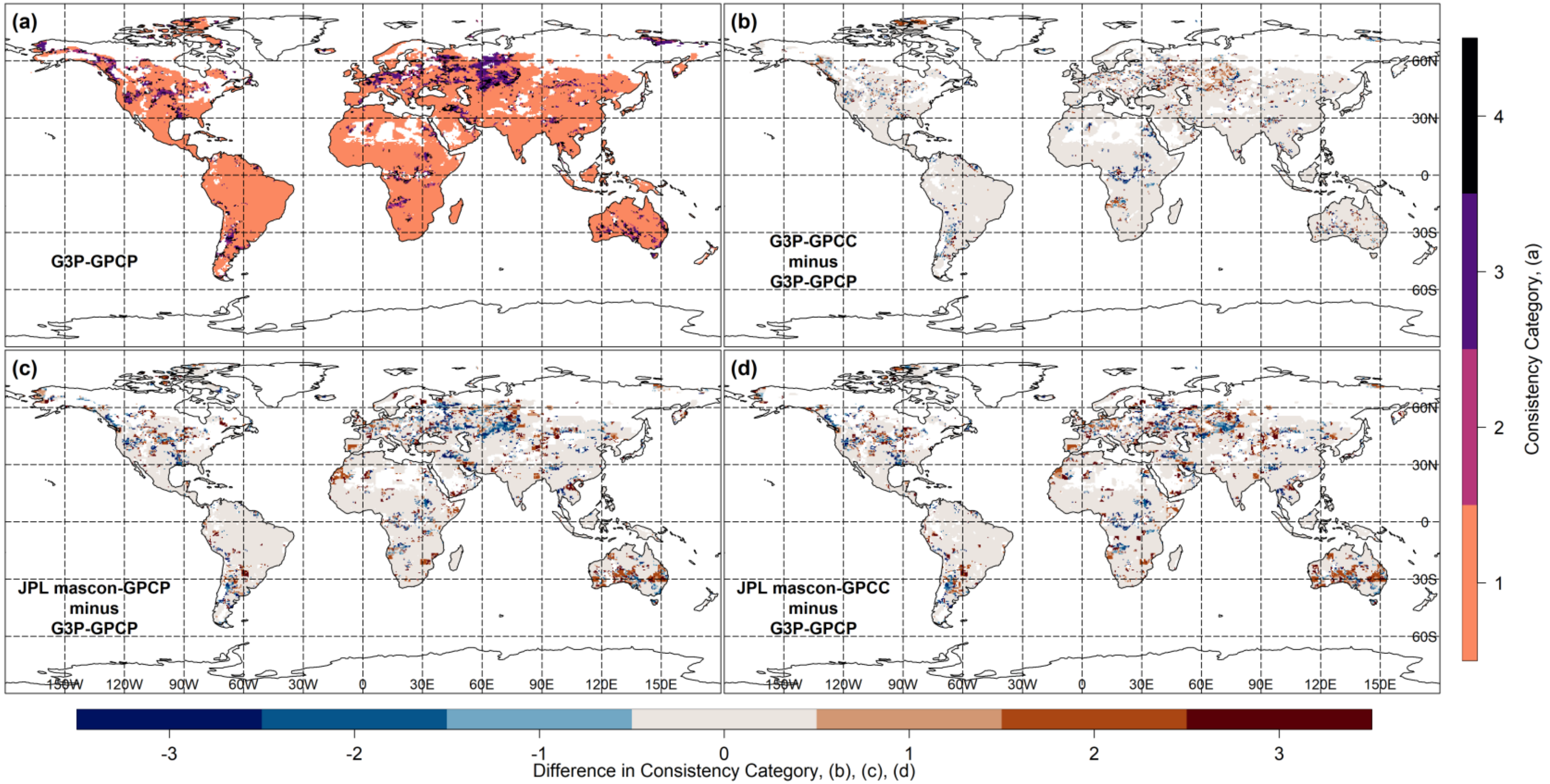

Figure 3.21. Display of the consistency in DRT estimations obtained from all TWS-precipitation coupled products (a) G3P-GPCC, (b) G3P-GPCP, (c) JPL-GPCC, (d) JPL-GPCP.

Table 3.16. Mean DRT and SE for the Consistency Categories

	Mean DRT (months)	Mean SE (months)
Category 1	12.6	4.1
Category 2	14.3	5.5
Category 3	17.2	7.7
Category 4	25.4	13.6

The consistency levels for the Köppen-Geiger climate zones utilizing all of the coupled products are displayed in Figure 3.22 as a percentage of consistency category 1 (time difference in DRT estimation of 1-2 months). With an average consistency of 98.4%, the equatorial (A) zone had the greatest, while the polar (E) zone had the lowest with an average consistency of 80.2%. On a global average, consistency category 1 was achieved by 89.6% of DRT estimations. The rate of consistency category 1 of DRT estimations obtained from G3P (90.7%) is higher than obtained from JPL (86.8%) across all the climate zones and the global average. In terms of the coupled products, the G3P&GPCP combination showed the highest consistency (91.0%), while JPL&GPCP displayed the lowest (86.4%).

The selection of the precipitation product (GPCC vs. GPCP) had a minor effect on consistency in DRT estimations with an average absolute difference of 0.3%, provided that the identical TWS product was utilized. In contrast, G3P had higher consistency in DRT estimation than JPL, with an average absolute difference of 4.0% when the same precipitation product was utilized. Climate zones also impacted consistencies in DRT estimations in addition to the selection of the products. The polar (E) zone had the highest difference between GPCC and GPCP, with a difference of 5.1%. In contrast, the arid (B, 0.2 months) zone and snow zone (E, 0.1 months) showed the lowest difference between the two, with a similar consistency in DRT estimations. Similarly, in the equatorial (A) zone, G3P and JPL showed the most similar consistency in DRT estimations, with a difference of 1.3%, while they displayed the largest difference (7.0%) in DRT estimation consistency in the arid (B) zone, and the polar (E) zone.

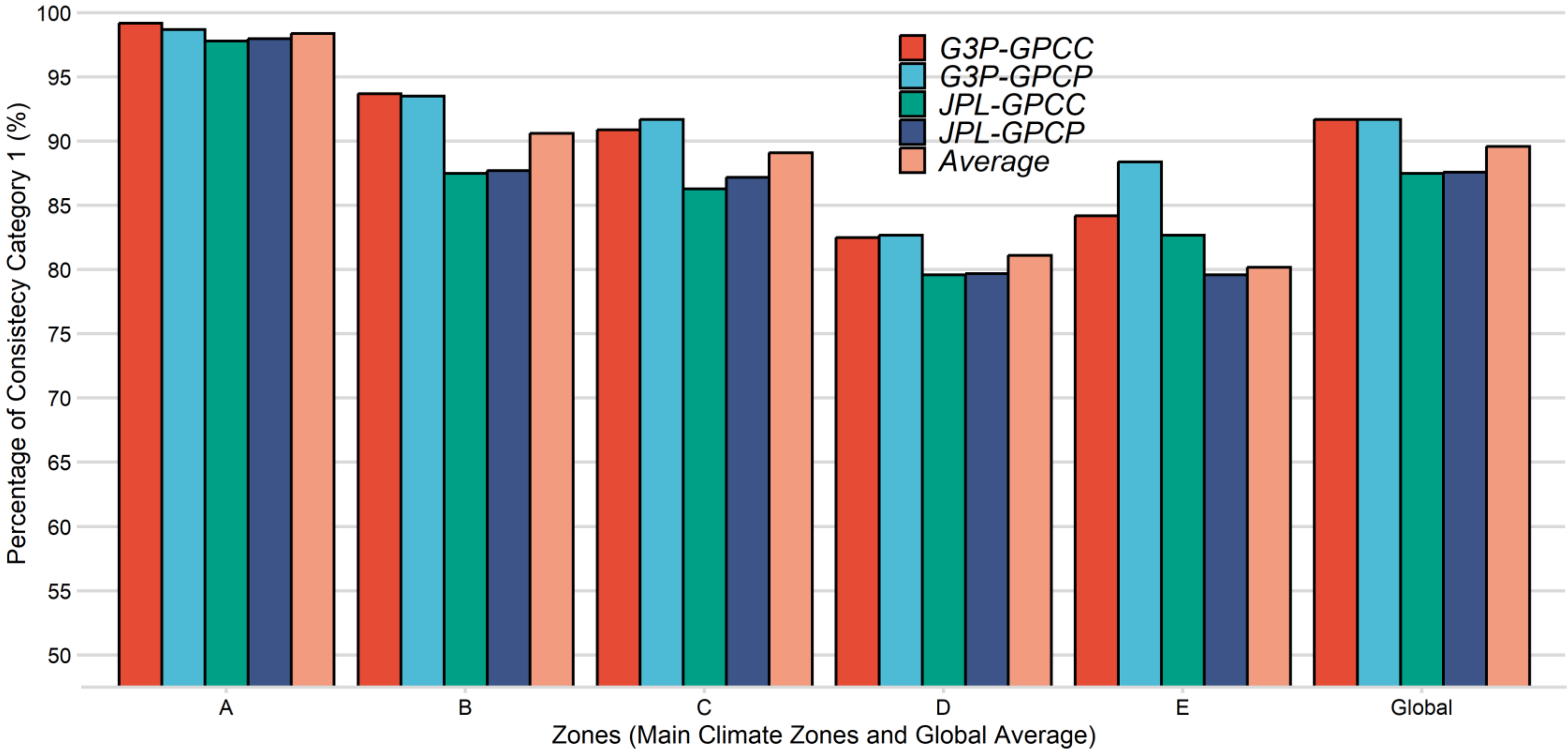

Figure 3.22. The percentage of DRT estimations whose consistency is category 1 for the Köppen-Geiger main climate zones using all the TWS-precipitation coupled products (A, Equatorial; B, Arid; C, Warm Temperate; D, Snow; and E, Polar Climate Zones)

CHAPTER 4

SUMMARY AND CONCLUSION

Satellite gravimetry measures monthly variations in TWS, which are closely related to the amount of precipitation that fell during that time frame. Thus, the innovative observing concept implemented with the GRACE and GRACE-FO missions offers a unique chance to verify precipitation products' long-term consistency. Based on the current analysis using TWS (G3P spherical harmonics and JPL) and precipitation (GPCC and GPCP) products, a generally high correlation between the two was found over semi-arid and even wetter climates, some parts of the equatorial, warm temperate and snow zones. On a global average, G3P and GPCP have the best correspondence. In general, correlation coefficients are not greatly affected by the choice of GRACE and GRACE-FO products, with the exception of arid regions with minimal storage fluctuations. However, when swapping precipitation products from GPCP to GPCC, correlation coefficients of cdPA and dTWSA change, especially in Africa and some parts of Central Asia, where there is a lack of in situ station coverage. In addition, the impact of satellite-based precipitation information in GPCP is relatively large because GPCC relies solely on in situ rain gauges, which have sparse coverage.

A new method of characterizing drought using the storage deficit is made possible by GRACE and GRACE-FO observations, which directly provide water storage anomalies. Thus, by directly observing the temporal evolution of the storage deficit, it is possible to determine the time needed to recover from a drought (Singh et al., 2021). This approach allows for the assessment of both the length and severity of a drought. It is observed that there is not much difference between the mean DRT estimations derived from GPCC and GPCP. On average, however, the mean DRT estimations across the Köppen-Geiger climate zones and the globe using JPL were 2.8 months longer than those using G3P. Furthermore, the findings demonstrate that the equatorial (A) zone had the lowest mean DRT estimation based on both methods, while the polar (E) zone had the highest for all TWS-precipitation combinations. In contrast, the consistency in DRT estimations using G3P was 4.0% higher than using JPL when the same precipitation product was utilized. Furthermore, for all TWS-precipitation combinations taken into consideration, the results showed that the equatorial (A) zone had the highest consistency in mean DRT estimations derived from both methods, whereas the polar (E) zone had the lowest consistency.

The close association between precipitation and TWS fluctuations highlights the potential utility of GRACE and GRACE-FO for hydrometeorological research, as demonstrated by the results of the current study. Its global coverage (albeit relatively low spatial resolution) makes it possible to assess various precipitation products from global atmospheric reanalysis and numerical weather prediction models, in addition to combinations of varying satellite and in situ observations (as done in this study). It can be expected that additional advancements in the quality of satellite gravimetry solutions for hydrological studies since studies on future satellite gravity missions and the use of more precise sensors are conducted by NASA and the European Space Agency (ESA).

Future studies can focus on the new satellite gravity missions conducted by NASA and ESA. These new missions are expected to have more precise sensors than GRACE and GRACE-FO. Additionally, other precipitation products, such as various blended products and reanalysis datasets, can be assessed from a hydrological drought perspective using these DRT estimation methods. Moreover, the subzone of Köppen-Geiger climate zones could be studied in the future for one coupled TWS-precipitation product.

REFERENCES

Adler, R. F., Huffman, G. J., Chang, A., Ferraro, R., Xie, P.-P., Janowiak, J., Rudolf, B., Schneider, U., Curtis, S., Bolvin, D., Gruber, A., Susskind, J., Arkin, P., And, ##, & Nelkin, E. (2003). *The Version-2 Global Precipitation Climatology Project (GPCP) Monthly Precipitation Analysis (1979-Present)*. http://precip.gsfc.nasa.gov

AghaKouchak, A., Farahmand, A., Melton, F. S., Teixeira, J., Anderson, M. C., Wardlow, B. D., & Hain, C. R. (2015). Remote sensing of drought: Progress, challenges and opportunities. In *Reviews of Geophysics* (Vol. 53, Issue 2, pp. 452–480). Blackwell Publishing Ltd. https://doi.org/10.1002/2014RG000456

Akbari Asanjan, A., Yang, T., Hsu, K., Sorooshian, S., Lin, J., & Peng, Q. (2018). Short-Term Precipitation Forecast Based on the PERSIANN System and LSTM Recurrent Neural Networks. *Journal of Geophysical Research: Atmospheres*, *123*(22), 12,543-12,563. https://doi.org/10.1029/2018JD028375

Ali, A., Diedhiou, A., & Lebel, T. (2005). *Rainfall Estimation in the Sahel. Part II: Evaluation of Rain Gauge Networks in the CILSS Countries and Objective Intercomparison of Rainfall Products*.

Bai, X., Wu, X., & Wang, P. (2019). Blending long-term satellite-based precipitation data with gauge observations for drought monitoring: Considering effects of different gauge densities. *Journal of Hydrology, 577*. https://doi.org/10.1016/j.jhydrol.2019.124007

Barker, L. J., Hannaford, J., Chiverton, A., & Svensson, C. (2016). From meteorological to hydrological drought using standardised indicators. *Hydrology and Earth System Sciences, 20*(6), 2483–2505. https://doi.org/10.5194/hess-20-2483-2016

Bayar, A. S., Yılmaz, M. T., Yücel, İ., & Dirmeyer, P. (2023). CMIP6 Earth System Models Project Greater Acceleration of Climate Zone Change Due To Stronger Warming Rates. *Earth's Future*, *11*(4). https://doi.org/10.1029/2022EF002972

Beck, H. E., Vergopolan, N., Pan, M., Levizzani, V., Van Dijk, A. I. J. M., Weedon, G. P., Brocca, L., Pappenberger, F., Huffman, G. J., & Wood, E. F. (2017). Global-scale evaluation of 22 precipitation datasets using gauge observations and hydrological modeling. *Hydrology and Earth System Sciences*, *21*(12), 6201–6217. https://doi.org/10.5194/hess-21-6201-2017

Behrangi, A., Nguyen, H., & Granger, S. (2015). Probabilistic seasonal prediction of meteorological drought using the bootstrap and multivariate information. *Journal of Applied Meteorology and Climatology*, *54*(7), 1510–1522. https://doi.org/10.1175/JAMC-D-14-0162.1

Belabid, N., Zhao, F., Brocca, L., Huang, Y., & Tan, Y. (2019). Near-real-time flood forecasting based on satellite precipitation products. *Remote Sensing*, *11*(3). https://doi.org/10.3390/rs11030252

Boergens, E., Güntner, A., Dobslaw, H., & Dahle, C. (2020). Quantifying the Central European Droughts in 2018 and 2019 With GRACE Follow-On. *Geophysical Research Letters*, *47*(14). https://doi.org/10.1029/2020GL087285

Dai, A. (2011). Drought under global warming: A review. In *Wiley Interdisciplinary Reviews: Climate Change* (Vol. 2, Issue 1, pp. 45–65). Wiley-Blackwell. https://doi.org/10.1002/wcc.81

Darand, M., & Khandu, K. (2020). Statistical evaluation of gridded precipitation datasets using rain gauge observations over Iran. *Journal of Arid Environments*, *178*. https://doi.org/10.1016/j.jaridenv.2020.104172

Ding, Y., Xu, J., Wang, X., Peng, X., & Cai, H. (2020). Spatial and temporal effects of drought on Chinese vegetation under different coverage levels.

Science of the Total Environment, *716*. https://doi.org/10.1016/j.scitotenv.2020.137166

Döll, P., Hasan, H. M. M., Schulze, K., Gerdener, H., Börger, L., Shadkam, S., Ackermann, S., Hosseini-Moghari, S.-M., Müller Schmied, H., Güntner, A., & Kusche, J. (2024). Leveraging multi-variable observations to reduce and quantify the output uncertainty of a global hydrological model: evaluation of three ensemble-based approaches for the Mississippi River basin. *Hydrology and Earth System Sciences*, *28*(10), 2259–2295. https://doi.org/10.5194/hess-28-2259-2024

Eicker, A., Schumacher, M., Kusche, J., Döll, P., & Schmied, H. M. (2014). Calibration/Data Assimilation Approach for Integrating GRACE Data into the WaterGAP Global Hydrology Model (WGHM) Using an Ensemble Kalman Filter: First Results. *Surveys in Geophysics*, *35*(6), 1285–1309. https://doi.org/10.1007/s10712-014-9309-8

Gebrechorkos, S. H., Leyland, J., Dadson, S. J., Cohen, S., Slater, L., Wortmann, M., Ashworth, P. J., Bennett, G. L., Boothroyd, R., Cloke, H., Delorme, P., Griffith, H., Hardy, R., Hawker, L., McLelland, S., Neal, J., Nicholas, A., Tatem, A. J., Vahidi, E., … Darby, S. E. (2024). Global-scale evaluation of precipitation datasets for hydrological modelling. *Hydrology and Earth System Sciences*, *28*(14), 3099–3118. https://doi.org/10.5194/hess-28-3099-2024

Golian, S., Javadian, M., & Behrangi, A. (2019). On the use of satellite, gauge, and reanalysis precipitation products for drought studies. *Environmental Research Letters*, *14*(7). https://doi.org/10.1088/1748-9326/ab2203

Harris, A., Rahman, S., Hossain, F., Yarborough, L., Bagtzoglou, A. C., & Easson, G. (2007). Satellite-based Flood Modeling Using TRMM-based Rainfall Products. *Sensors*, *7*, 3416–3427. http://gpm.gsfc.nasa.gov

Huffman, G. J., Adler, R. F., Behrangi, A., Bolvin, D. T., Nelkin, E. J., Guojun, G. U., & Ehsani, M. R. (2023). The New Version 3.2 Global Precipitation Climatology Project (GPCP) Monthly and Daily Precipitation Products. *Journal of Climate*, *36*(21), 7635–7655. https://doi.org/10.1175/JCLI-D-23-0123.1

Keyantash, J., & Dracup, J. A. (2002). *The Quantification of Drought: An Evaluation of Drought Indices*.

Kottek, M., Grieser, J., Beck, C., Rudolf, B., & Rubel, F. (2006). World map of the Köppen-Geiger climate classification updated. *Meteorologische Zeitschrift*, *15*(3), 259–263. https://doi.org/10.1127/0941-2948/2006/0130

Lai, C., Li, J., Wang, Z., Wu, X., Zeng, Z., Chen, X., Lian, Y., Yu, H., Wang, P., & Bai, X. (2018). Drought-induced reduction in net primary productivity across mainland China from 1982 to 2015. *Remote Sensing*, *10*(9). https://doi.org/10.3390/rs10091433

Lai, C., Zhong, R., Wang, Z., Wu, X., Chen, X., Wang, P., & Lian, Y. (2019). Monitoring hydrological drought using long-term satellite-based precipitation data. *Science of the Total Environment*, *649*, 1198–1208. https://doi.org/10.1016/j.scitotenv.2018.08.245

Lamptey, B. L. (2008). Comparison of gridded multisatellite rainfall estimates with gridded gauge rainfall over West Africa. *Journal of Applied Meteorology and Climatology*, *47*(1), 185–205. https://doi.org/10.1175/2007JAMC1586.1

Madadgar, S., & Moradkhani, H. (2014). Spatio-temporal drought forecasting within Bayesian networks. *Journal of Hydrology*, *512*, 134–146. https://doi.org/10.1016/j.jhydrol.2014.02.039

Maggioni, V., & Massari, C. (2018). On the performance of satellite precipitation products in riverine flood modeling: A review. In *Journal of Hydrology* (Vol. 558, pp. 214–224). Elsevier B.V. https://doi.org/10.1016/j.jhydrol.2018.01.039

Mckee, T. B., Doesken, N. J., & Kleist, J. (1993). THE RELATIONSHIP OF DROUGHT FREQUENCY AND DURATION TO TIME SCALES. In *Eighth Conference on Applied Climatology*.

Mishra, A. K., & Singh, V. P. (2010). A review of drought concepts. In *Journal of Hydrology* (Vol. 391, Issues 1–2, pp. 202–216). https://doi.org/10.1016/j.jhydrol.2010.07.012

Negrón Juárez, R. I., Li, W., Fernandes, K., & de Oliveira Cardoso, A. (2009). Comparison of precipitation data sets over the tropical South American and African continents. *Journal of Hydrometeorology*, *10*(1), 289–299. https://doi.org/10.1175/2008JHM1023.1

Patz, J. A., Frumkin, H., Holloway, T., Vimont, D. J., & Haines, A. (2014). Climate change: Challenges and opportunities for global health. *JAMA - Journal of the American Medical Association*, *312*(15), 1565–1580. https://doi.org/10.1001/jama.2014.13186

Pfeffer, J., Cazenave, A., Blazquez, A., Decharme, B., Munier, S., & Barnoud, A. (2023). Assessment of pluri-annual and decadal changes in terrestrial water storage predicted by global hydrological models in comparison with the GRACE satellite gravity mission. *Hydrology and Earth System Sciences*, *27*(20), 3743–3768. https://doi.org/10.5194/hess-27-3743-2023

Piao, S., Ciais, P., Huang, Y., Shen, Z., Peng, S., Li, J., Zhou, L., Liu, H., Ma, Y., Ding, Y., Friedlingstein, P., Liu, C., Tan, K., Yu, Y., Zhang, T., & Fang, J. (2010). The impacts of climate change on water resources and agriculture in China. In *Nature* (Vol. 467, Issue 7311, pp. 43–51). Nature Publishing Group. https://doi.org/10.1038/nature09364

Prakash, S., Gairola, R. M., & Mitra, A. K. (2015). Comparison of large-scale global land precipitation from multisatellite and reanalysis products with gauge-based GPCC data sets. *Theoretical and Applied Climatology*, *121*(1–2), 303–317. https://doi.org/10.1007/s00704-014-1245-5

Rubel, F., Brugger, K., Haslinger, K., & Auer, I. (2017). The climate of the European Alps: Shift of very high resolution Köppen-Geiger climate zones 1800-2100. *Meteorologische Zeitschrift*, *26*(2), 115–125. https://doi.org/10.1127/metz/2016/0816

Schneider, U., Becker, A., Finger, P., Meyer-Christoffer, A., Ziese, M., & Rudolf, B. (2014). GPCC's new land surface precipitation climatology based on quality-controlled in situ data and its role in quantifying the global water cycle. *Theoretical and Applied Climatology*, *115*(1–2), 15–40. https://doi.org/10.1007/s00704-013-0860-x

Schneider, U., Hänsel, S., Finger, P., Rustemeier, E., & Ziese, M. (2022). *GPCC Full Data Monthly Product Version 2022 at 0.5°: Monthly Land-Surface Precipitation from Rain-Gauges built on GTS-based and Historical Data*.

Senocak, A. U. G., Yilmaz, M. T., Kalkan, S., Yucel, I., & Amjad, M. (2023). An explainable two-stage machine learning approach for precipitation forecast. *Journal of Hydrology*, *627*. https://doi.org/10.1016/j.jhydrol.2023.130375

Shukla, S., & Wood, A. W. (2008). Use of a standardized runoff index for characterizing hydrologic drought. *Geophysical Research Letters*, *35*(2). https://doi.org/10.1029/2007GL032487

Singh, A., Reager, J. T., & Behrangi, A. (2021). Estimation of hydrological drought recovery based on precipitation and Gravity Recovery and Climate Experiment (GRACE) water storage deficit. *Hydrology and Earth System Sciences*, *25*(2), 511–526. https://doi.org/10.5194/hess-25-511-2021

Springer, A., Eicker, A., Bettge, A., Kusche, J., & Hense, A. (2017). Evaluation of the water cycle in the European COSMO-REA6 reanalysis using GRACE. *Water (Switzerland)*, *9*(4). https://doi.org/10.3390/w9040289

Sun, Q., Miao, C., Duan, Q., Ashouri, H., Sorooshian, S., & Hsu, K. L. (2018a). A Review of Global Precipitation Data Sets: Data Sources, Estimation, and

Intercomparisons. *Reviews of Geophysics*, *56*(1), 79–107. https://doi.org/10.1002/2017RG000574

Sun, Q., Miao, C., Duan, Q., Ashouri, H., Sorooshian, S., & Hsu, K. L. (2018b). A Review of Global Precipitation Data Sets: Data Sources, Estimation, and Intercomparisons. *Reviews of Geophysics*, *56*(1), 79–107. https://doi.org/10.1002/2017RG000574

Tangdamrongsub, N., Jasinski, M. F., & Shellito, P. J. (2021). Development and evaluation of 0.05g terrestrial water storage estimates using Community Atmosphere Biosphere Land Exchange (CABLE) land surface model and assimilation of GRACE data. *Hydrology and Earth System Sciences*, *25*(7), 4185–4208. https://doi.org/10.5194/hess-25-4185-2021

Thomas, A. C., Reager, J. T., Famiglietti, J. S., & Rodell, M. (2014). A GRACE-based water storage deficit approach for hydrological drought characterization. *Geophysical Research Letters*, *41*(5), 1537–1545. https://doi.org/10.1002/2014GL059323

Van Lanen, H. A. J., Wanders, N., Tallaksen, L. M., & Van Loon, A. F. (2013). Hydrological drought across the world: Impact of climate and physical catchment structure. *Hydrology and Earth System Sciences*, *17*(5), 1715–1732. https://doi.org/10.5194/hess-17-1715-2013

Vicente-Serrano, S. M., Beguería, S., López-Moreno, J. I., Angulo, M., & El Kenawy, A. (2010). A new global 0.5° gridded dataset (1901-2006) of a multiscalar drought index: Comparison with current drought index datasets based on the palmer drought severity index. *Journal of Hydrometeorology*, *11*(4), 1033–1043. https://doi.org/10.1175/2010JHM1224.1

Vicente-Serrano, S. M., López-Moreno, J. I., Beguería, S., Lorenzo-Lacruz, J., Azorin-Molina, C., & Morán-Tejeda, E. (2012). Accurate Computation of a Streamflow Drought Index. *Journal of Hydrologic Engineering*, *17*(2), 318–332. https://doi.org/10.1061/(asce)he.1943-5584.0000433

Wahr, J., Swenson, S., Zlotnicki, V., & Velicogna, I. (2004). Time-variable gravity from GRACE: First results. *Geophysical Research Letters, 31*(11). https://doi.org/10.1029/2004GL019779

Wang, Z., Zhong, R., & Lai, C. (2017). Evaluation and hydrologic validation of TMPA satellite precipitation product downstream of the Pearl River Basin, China. *Hydrological Processes, 31*(23), 4169–4182. https://doi.org/10.1002/hyp.11350

Watkins, M. M., Wiese, D. N., Yuan, D. N., Boening, C., & Landerer, F. W. (2015). Improved methods for observing Earth's time variable mass distribution with GRACE using spherical cap mascons. *Journal of Geophysical Research: Solid Earth, 120*(4), 2648–2671. https://doi.org/10.1002/2014JB011547

Wehbe, Y., Ghebreyesus, D., Temimi, M., Milewski, A., & Al Mandous, A. (2017). Assessment of the consistency among global precipitation products over the United Arab Emirates. *Journal of Hydrology: Regional Studies, 12,* 122–135. https://doi.org/10.1016/j.ejrh.2017.05.002

Wei, L., Jiang, S., Ren, L., Wang, M., Zhang, L., Liu, Y., Yuan, F., & Yang, X. (2021). Evaluation of seventeen satellite-, reanalysis-, and gauge-based precipitation products for drought monitoring across mainland China. *Atmospheric Research, 263*. https://doi.org/10.1016/j.atmosres.2021.105813

Wei, L., Jiang, S., Ren, L., Yuan, F., & Zhang, L. (2019). Performance of two long-term satellite-based and GPCC 8.0 precipitation products for drought monitoring over the Yellow River Basin in China. *Sustainability (Switzerland), 11*(18). https://doi.org/10.3390/su11184969

Wu, X., Feng, X., Wang, Z., Chen, Y., & Deng, Z. (2023). Multi-source precipitation products assessment on drought monitoring across global major river basins. *Atmospheric Research*, *295*. https://doi.org/10.1016/j.atmosres.2023.106982

Xu, K., Yang, D., Yang, H., Li, Z., Qin, Y., & Shen, Y. (2015). Spatio-temporal variation of drought in China during 1961-2012: A climatic perspective. *Journal of Hydrology*, *526*, 253–264. https://doi.org/10.1016/j.jhydrol.2014.09.047

APPENDICES

A. β1 Limit

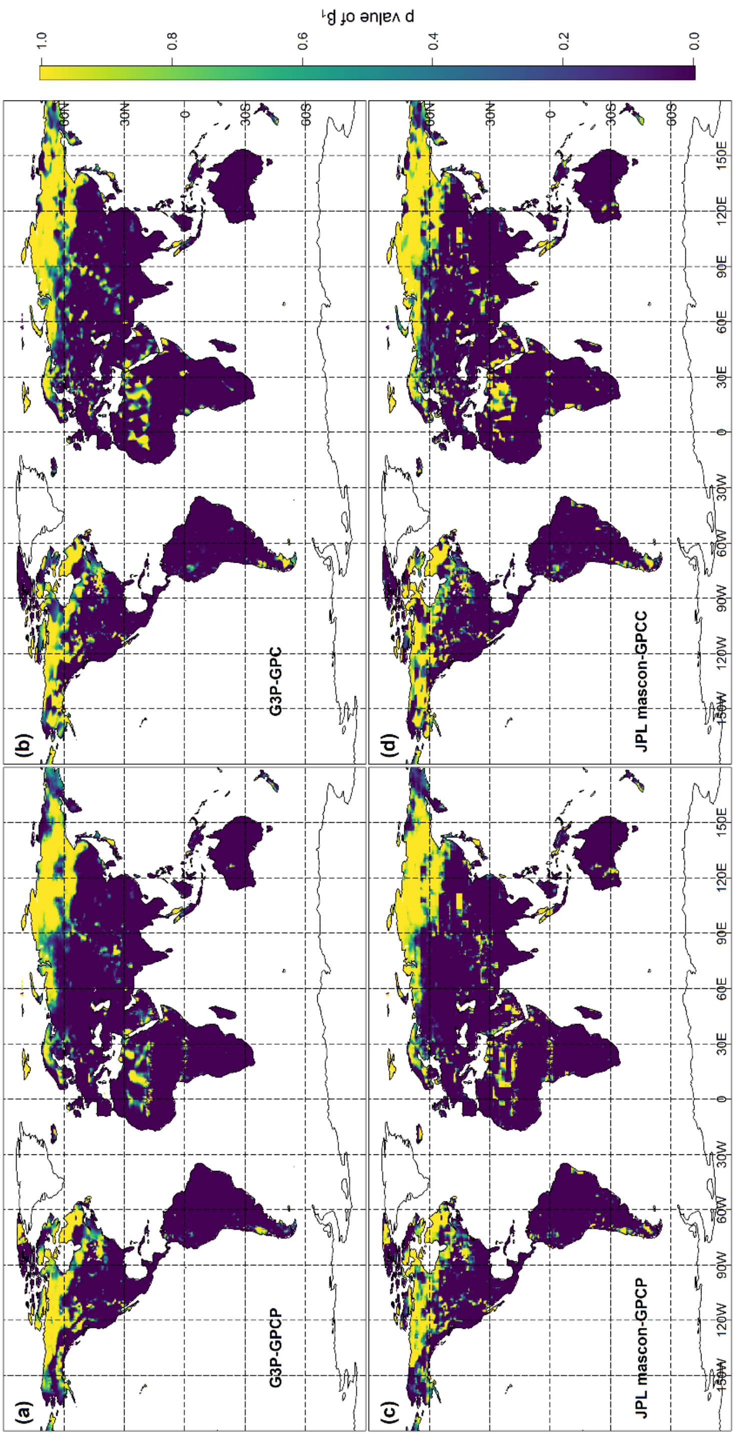

Figure A1. The spatial distributions of the p values of the β_1 obtained from all TWS-precipitation coupled products (a) G3P-GPCC, (b) G3P-GPCP, (c) JPL-GPCC, (d) JPL-GPCP.

B. Time Series of TWSA

The time series of the mean monthly TWSA dataset obtained from G3P and JPL are shown in Figures B1, B2, B3, B4, and B5 for Australia, South America, Southern Africa, Central Asia, and Northern Africa, respectively.

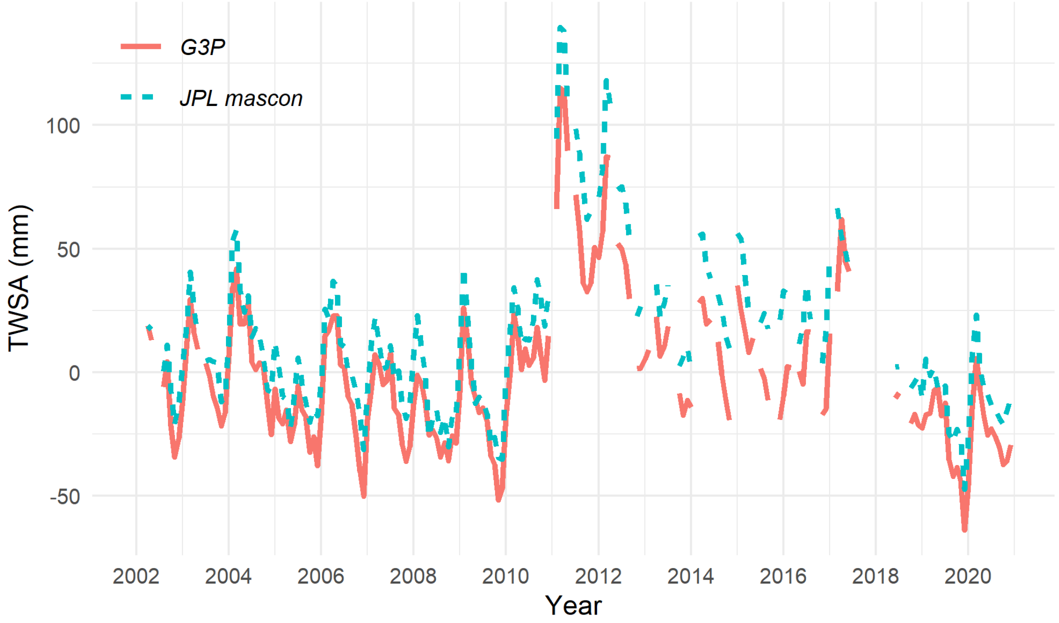

Figure B1. The time series of the mean monthly TWSA dataset obtained from G3P and JPL for Australia

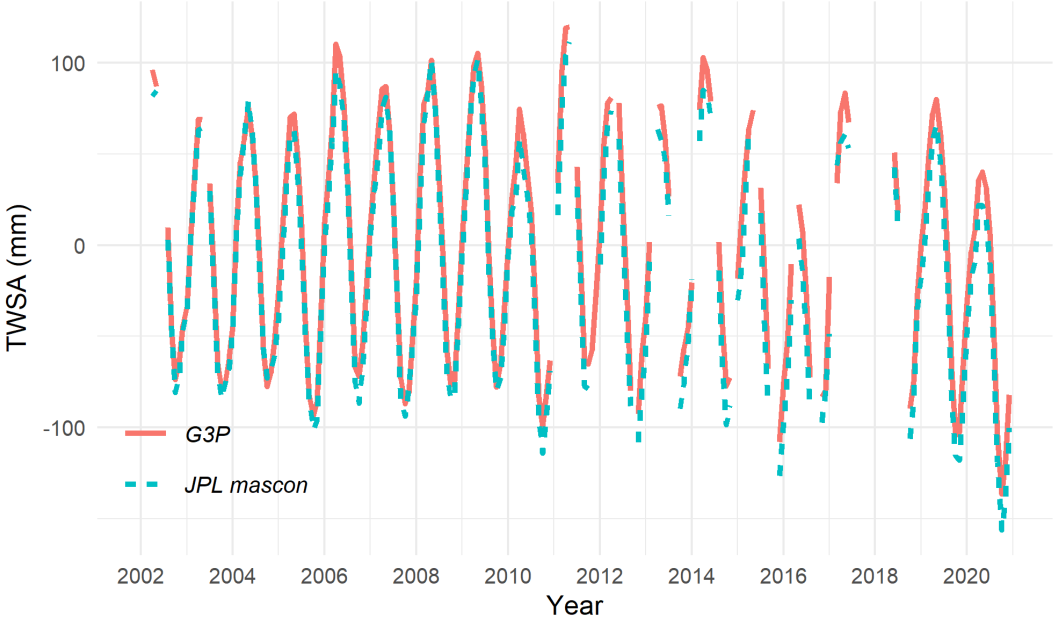

Figure B2. The time series of the mean monthly TWSA dataset obtained from G3P and JPL for South America

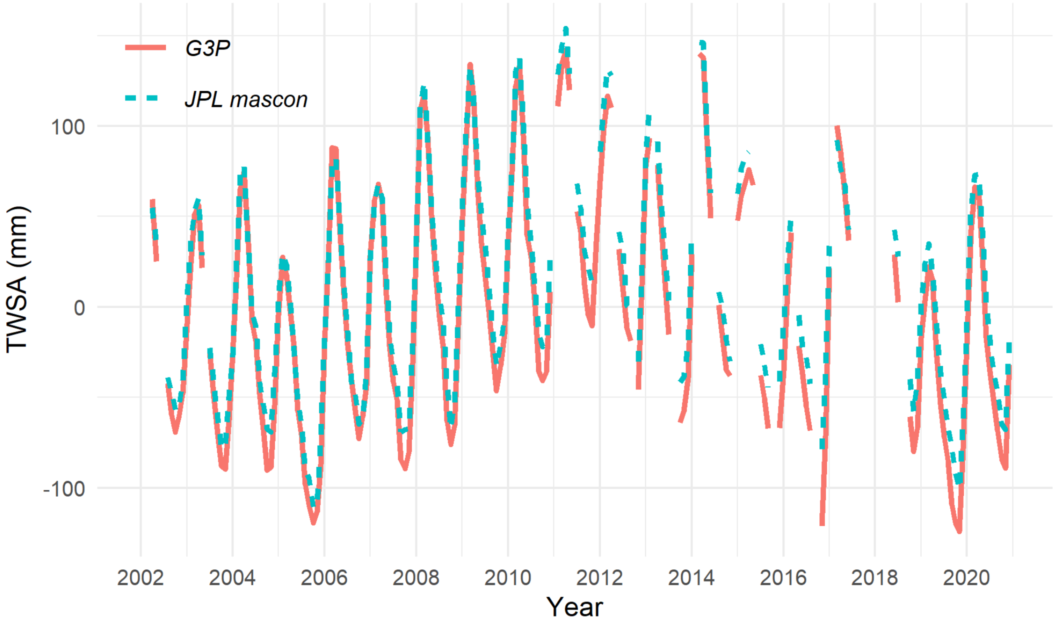

Figure B3. The time series of the mean monthly TWSA dataset obtained from G3P and JPL for Southern Africa

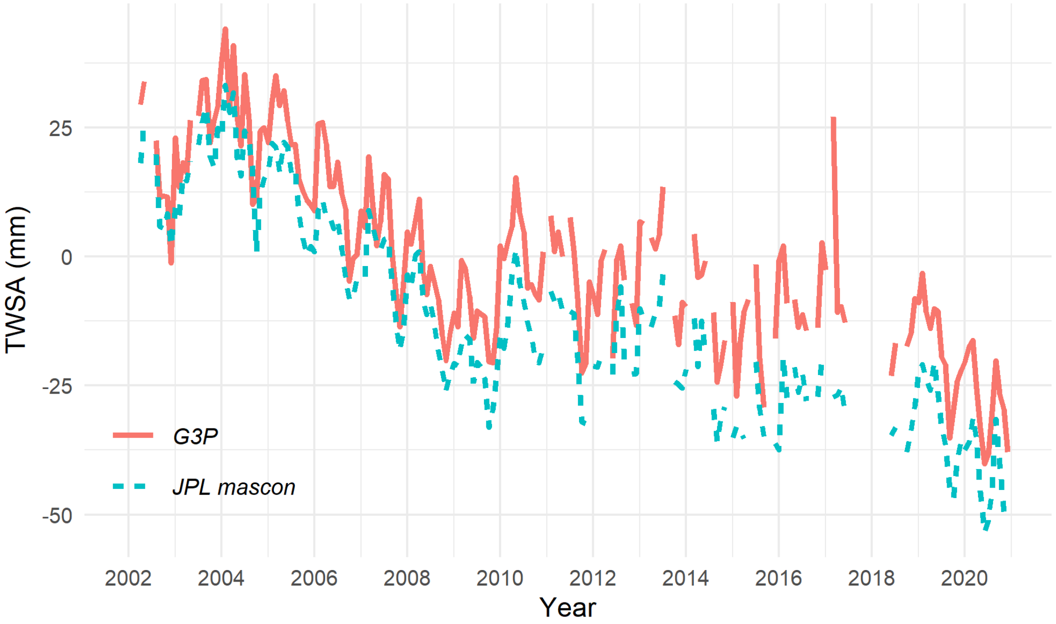

Figure B4. The time series of the mean monthly TWSA dataset obtained from G3P and JPL for Central Asia

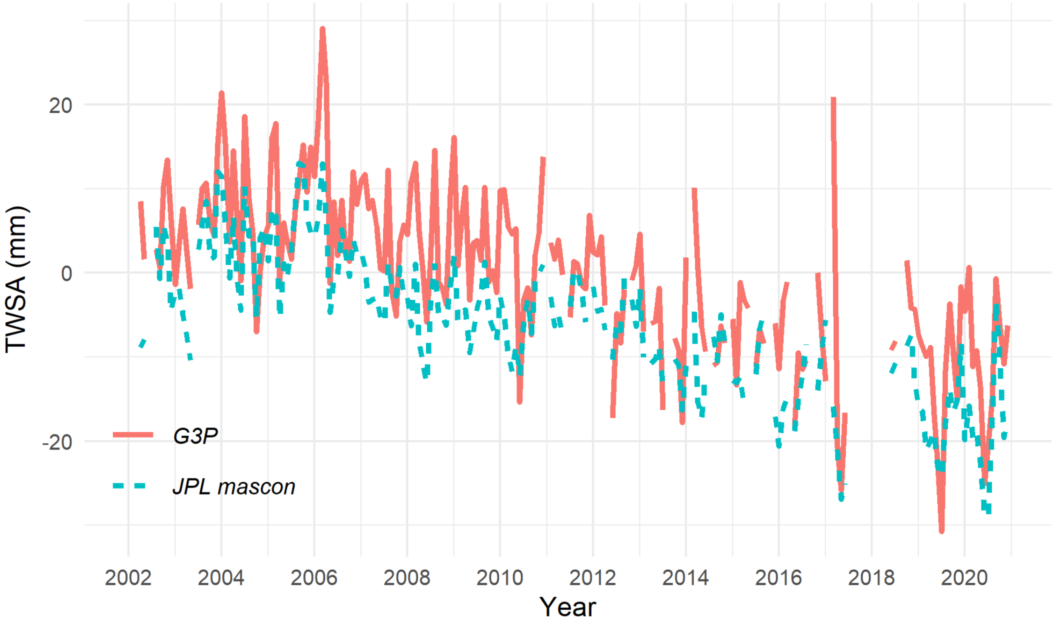

Figure B5. The time series of the mean monthly TWSA dataset obtained from G3P and JPL for Northern Africa

The time series of the mean monthly TWSA dataset obtained from G3P and JPL for arid and non-arid regions are shown in Figures B6a and B6b, respectively.

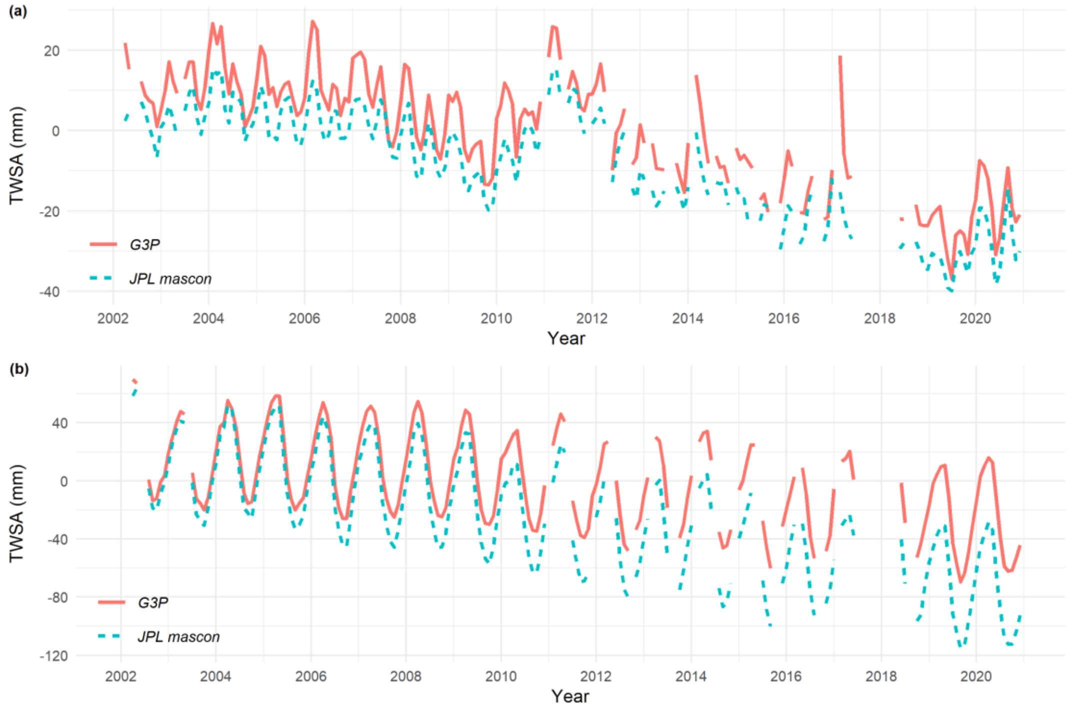

Figure B6. The time series of the mean monthly TWSA dataset obtained from G3P and JPL for (a) Arid and (b) non-arid regions

C. Spatial Distribution of the Precipitation Gauge

Figure C1 shows the spatial distribution of the average number of precipitation gauges from 2002 to 2020, as provided by the GPCC dataset.

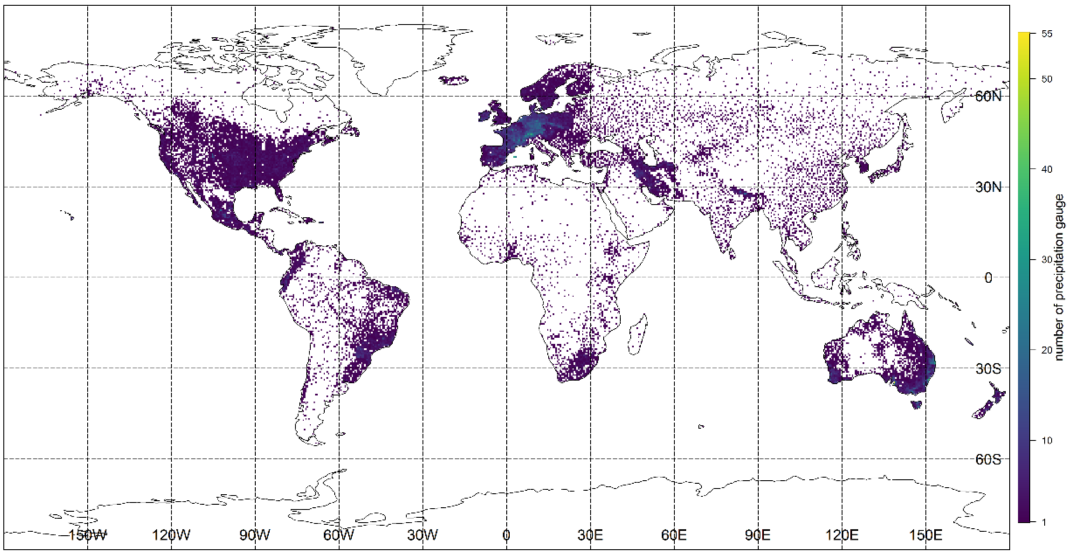

Figure C1. The spatial distribution of the average number of precipitation gauges from 2002 to 2020, as provided by the GPCC dataset.